

DISS. ETH NO. 29867

**A systematic analysis of the molecular patterns that  
define endothelial identities and states**

A thesis submitted to attain the degree of

DOCTOR OF SCIENCES

(Dr. sc. ETH Zurich)

presented by

**Stephan Paul Durot**

M.Sc. in Biology, ETH Zurich

born on 04.05.1992

accepted on the recommendation of

Prof. Dr. Nicola Zamboni

Prof. Dr. Uwe Sauer

Prof. Dr. Katrien De Bock

Prof. Dr. Tatiana Petrova

2024



## Table of contents

<b>Abstract</b>	3
<b>Zusammenfassung</b>	6
<b>General Introduction</b>	9
<b>Chapter 2</b>	37
Development of a multi-omics workflow to study the molecular patterns underlying proliferative and quiescent endothelial cells	
<b>Chapter 3</b>	61
Multi-omics analysis of endothelial cells reveals cell type-specific metabolic patterns governing cellular phenotypes	
<b>Chapter 4</b>	104
Systematic analysis of transcription factor activity patterns that underlie endothelial cell identities and states	
<b>Concluding Remarks</b>	129
<b>Acknowledgments</b>	148
<b>Curriculum Vitae</b>	150





## Abstract

Endothelial cells (ECs) form the inner linings of the vasculature, which consists of the cardiovascular and lymphatic systems. These two related yet distinct systems play a crucial role in maintaining tissue homeostasis. While quiescent in mature vasculature, ECs dynamically respond to external cues by migrating and proliferating to create new vessels. Importantly, dysregulation of the proliferation-quiescence balance disrupts vascular integrity and contributes to the progression of several cardiovascular and lymphatic diseases.

Development and maintenance of EC types and the vasculature are tightly controlled by the interplay of various transcription factors (TFs) and signaling pathways. Furthermore, studies in the last decades have highlighted the important role of metabolism in modulating differentiation into ECs as well as the formation and maintenance of a proliferative and quiescent state. Cellular metabolism orchestrates the chemical reactions within cells, converting nutrients into energy, building blocks for macromolecules, and facilitating waste elimination. This complex network integrates environmental and intracellular signals, influencing thereby cellular decisions crucial for differentiation and phenotypic formation. So far, studies often focused on specific pathways, relying on transcriptomics approaches, or used primarily human umbilical vein ECs (HUVECs). However, the previously demonstrated heterogeneity in metabolic protein transcript levels among ECs from different tissues emphasizes the need to explore tissue-specific cellular metabolic patterns, elucidating the extent of variance and its impact on diverse phenotypes and functions.

The use of untargeted, mass spectrometry-based measurements of proteins and metabolites enables a comprehensive investigation into the molecular lifestyles of cells across diverse growth states. This approach facilitates the identification of new molecular factors, such as metabolic pathways, that potentially mediate the formation and maintenance of cellular identities and growth states. The aim of this thesis was to explore the metabolic and proteomic diversity of ECs from different tissues and vascular beds by using untargeted proteomics and metabolomics and to examine the role of the cell type-specific molecular patterns in the formation and maintenance of EC identities and states.

To that end, in **chapter 2**, we established an experimental workflow to directly examine metabolite and protein levels of human dermal lymphatic ECs (HDLECs),

human intestinal lymphatic ECs (iLECs), human dermal blood ECs (HDBECs) and human umbilical vein ECs (HUVECs) in proliferation and quiescence through untargeted metabolomics and proteomics. Our experimental approach, which includes mitogen reduction and contact inhibition for quiescence induction, revealed a temporal transition from proliferation to quiescence, capturing conserved and cell type-specific metabolic and proteomic patterns. Data normalization effectively mitigated batch effects, paving the way for an in-depth exploration of molecular patterns defining EC phenotypes and the intricate landscape of EC metabolism.

In **chapter 3**, we conducted an in-depth analysis of the datasets from chapter 2 to uncover molecular patterns defining EC identities and states. Distinct proteomic and metabolic patterns in quiescence and proliferation were observed in each cell type, with some patterns aligning with known markers (e.g., PROX1 in lymphatic ECs). Consistent with previous studies, we found shared findings in EC types, such as the upregulation of fatty acid oxidation (FAO) in quiescent HUVECs, HDLECs, and iLECs or upregulation of branched-chain amino acid catabolism across all quiescent EC types. Functional studies in HUVECs and iLECs revealed diverse phenotypic alterations following enzyme inhibition, highlighting the importance of metabolic pathways for maintaining specific states in different endothelial cell types.

In **chapter 4**, we utilized the proteomics dataset to infer the activities of 263 TFs. The resulting TF activity patterns exhibited cell type- and state-specific behaviours, reflecting the unique characteristics and requirements of each cell type. Additionally, we identified TFs with distinct activities between blood endothelial cells (BECs) and lymphatic endothelial cells (LECs), including well-established markers of LEC and BEC identities. Furthermore, we conducted correlation analyses between TF activities and the expression patterns of 14 enzymes targeted for pharmacological inhibition. This analysis led to the identification of two new TFs that potentially regulate the expression of enzymes crucial for functional migration in both HUVECs and iLECs.

Overall, this thesis provides a comprehensive description of the unique molecular characteristics that define ECs from different tissues and vascular beds. Our validation efforts primarily focused on findings related to metabolism, and therefore, we believe that our multi-omics dataset holds the potential to uncover additional molecular factors involved in the formation and maintenance of specific EC identities and states and subsequently the cardiovascular and lymphatic systems.



## Zusammenfassung

Endothelzellen bilden die innere Auskleidung des Gefäßsystems, welches aus dem kardiovaskulären und lymphatischen System besteht. Diese beiden verwandten, aber trotzdem unterschiedlichen Systeme spielen eine entscheidende Rolle bei der Aufrechterhaltung der Gewebemöiostase. Endothelzellen befinden sich in ausgereiften Gefäßen im Ruhezustand, reagieren aber dynamisch auf externe Signale, indem sie migrieren und sich vermehren, um neue Gefäße zu bilden. Eine Dysregulation dieses Gleichgewichts zwischen Proliferation und Ruhezustand stört die Gefäßintegrität und trägt zur Entwicklung verschiedener kardiovaskulärer und lymphatischer Krankheiten bei.

Die Entwicklung und Aufrechterhaltung von verschiedenen Arten von Endothelzellen und des Gefäßsystems werden durch das komplexe Zusammenspiel verschiedener Transkriptionsfaktoren (TF) und Signalwege engmaschig gesteuert. Darüber hinaus haben Studien in den letzten Jahrzehnten die bedeutende Rolle des Stoffwechsels bei der Modulation der Differenzierung zu Endothelzellen sowie bei der Bildung und Aufrechterhaltung eines proliferativen und ruhenden Zustands hervorgehoben. Der zelluläre Stoffwechsel orchestriert die chemischen Reaktionen innerhalb von Zellen, wandelt Nährstoffe in Energie um, liefert Bausteine für Makromoleküle und ermöglicht die Ausscheidung von Abfallprodukten. Dieses komplexe Netzwerk integriert Umwelt- und intrazelluläre Signale und beeinflusst somit zelluläre Entscheidungen, die für Differenzierung und phänotypische Ausprägung entscheidend sind. Bisher konzentrierten sich Studien oft auf spezifische Stoffwechselwege, massen und verwendeten die Menge von Gentranskripten oder nutzten hauptsächlich humane Nabelschnurvenen-Endothelzellen (HUVECs). Die in Studien gezeigte Heterogenität in den Transkriptspiegeln von metabolischen Proteinen zwischen Endothelzellen aus verschiedenen Geweben betont jedoch die Notwendigkeit, gewebespezifische Zelluläre Stoffwechsellmuster zu erkunden, um den Umfang der Variabilität und deren Auswirkungen auf unterschiedliche Phänotypen und Funktionen zu verstehen.

Die Anwendung von nichtzielgerichteten, Massenspektrometrie-basierten Messungen von Proteinen und Metaboliten ermöglicht eine umfassende Untersuchung der molekularen Lebensweisen von Zellen in verschiedenen Wachstumszuständen. Diese Methode erleichtert die Identifizierung neuer molekularer Faktoren, wie

metabolischer Wege, die möglicherweise die Bildung und Aufrechterhaltung zellulärer Identitäten und Wachstumszustände vermitteln. Folglich war das Ziel dieser Arbeit, die metabolische und proteomische Vielfalt von Endothelzellen aus verschiedenen Geweben und Gefäßbetten zu erforschen und die Rolle der zelltypspezifischen molekularen Muster bei der Bildung und Aufrechterhaltung von Wachstumszuständen zu untersuchen.

Zu diesem Zweck haben wir in **Kapitel 2** einen experimentellen Aufbau etabliert, um direkt die Metabolit- und Proteinmengen von menschlichen dermalen lymphatischen Endothelzellen (HDLECs), menschlichen intestinalen lymphatischen Endothelzellen (iLECs), menschlichen dermalen Blutendothelzellen (HDBECs) und menschlichen Nabelschnurvenen-Endothelzellen (HUVECs) in Proliferation und Ruhezustand durch nichtzielgerichtete Metabolomik und Proteomik zu untersuchen. Unser experimenteller Aufbau, der Mitogenreduktion und Kontaktinhibition zur Ruhezustand-Induktion umfasst, zeigt einen zeitlichen Übergang von der Proliferation zur Ruhe über und erfasste konservierte sowie zelltypspezifische metabolische und proteomische Muster. Die Datennormalisierung behandelte Batch-Effekte effektiv und ebnete den Weg für eine eingehende Erforschung molekularer Muster, die Endothel-Phänotypen definieren, sowie die komplexe Landschaft des endotheligen Stoffwechsels.

In **Kapitel 3** führten wir eine eingehende Analyse der Datensätze aus Kapitel 2 durch, um die molekularen Muster zu identifizieren, die die Identitäten und Zustände von Endothelzellen definieren. Es wurden deutliche proteomische und metabolische Muster in Ruhezustand und Proliferation in jeder Zellart beobachtet, wobei einige Muster mit bekannten Markern übereinstimmten (z.B. PROX1 in lymphatischen Endothelzellen). Konsistent mit früheren Studien fanden wir gemeinsame Befunde in verschiedenen Endothelzelltypen, wie die Hochregulation der Fettsäureoxidation (FAO) in ruhenden HUVECs, HDLECs und iLECs oder die Hochregulation des Abbaus verzweigtkettiger Aminosäuren in allen ruhenden Endothelzelltypen. Funktionelle Studien in HUVECs und iLECs zeigten vielfältige phänotypische Veränderungen nach Enzyminhibition, was die Bedeutung metabolischer Wege für die Aufrechterhaltung spezifischer Zustände in verschiedenen Endothelzellen unterstreicht.

Im **Kapitel 4** nutzten wir den Proteom-Datensatz, um die Aktivitäten von 263 Transkriptionsfaktoren (TFs) zu erschließen. Die resultierenden TF-Aktivitätsmuster zeigten zelltyp- und zustandsspezifisches Verhalten, das die einzigartigen Merkmale

und Anforderungen jeder Zellart widerspiegelt. Zusätzlich identifizierten wir TFs mit unterschiedlichen Aktivitäten zwischen Blutendothelzellen (BEC) und lymphatischen Endothelzellen (LEC), einschließlich etablierter Marker für LEC- und BEC-Identitäten. Des Weiteren führten wir Korrelationsanalysen zwischen TF-Aktivitäten und den Expressionsmustern von 14 Enzymen durch, die Ziel pharmakologische Hemmung in den funktionellen Studienvorgesehen waren. Diese Analyse führte zur Identifikation von zwei neuen TFs, die möglicherweise die Expression von Enzymen regulieren, die für funktionelle Migration sowohl in HUVECs als auch in iLECs entscheidend sind.

Insgesamt bietet diese Arbeit eine umfassende Beschreibung der einzigartigen molekularen Merkmale, die Endothelzellen aus verschiedenen Geweben und Gefäßbetten definieren. Unsere Validierungsbemühungen konzentrierten sich hauptsächlich auf Ergebnisse im Zusammenhang mit dem Stoffwechsel, daher glauben wir, dass unser Multiomik-Datensatz das Potenzial hat, zusätzliche molekulare Faktoren aufzudecken, die an der Bildung und Aufrechterhaltung spezifischer endothelen Identitäten und Zustände und darauffolgend dem kardiovaskulären und lymphatischen System beteiligt sind.

# **Chapter 1**

## **General Introduction**

## Blood and lymphatic vasculature

The human body consists of approximately  $3 \times 10^{13}$  cells that are divided into around 200 different cell types, which are the basis of the four basic types of tissues<sup>1</sup>. The cardiovascular and lymphatic systems are parts of the connective tissue and are branched networks that run through the entire body and are found in every other tissue and organ<sup>2,3</sup>. These two related systems are both crucial for tissue homeostasis but have distinct physiological roles. The blind-ended lymphatic system is involved in fluid retention from tissues, immune response, and lipid absorption<sup>4-8</sup>, whereas the cardiovascular system is responsible for oxygen and nutrient transport, removal of waste, immune cell circulation, and thermoregulation<sup>9</sup>. Both blood and lymphatic systems are composed of capillaries and larger vessels, which are called collecting vessels in the lymphatic system<sup>8,9</sup>. Endothelial cells (ECs) line up these vessels in both networks and in the mature vasculature, ECs are quiescent most of their lifetime<sup>10-12</sup>. However, upon external stimulation through growth factors gradients or hypoxic conditions, in a process called (lymph)angiogenesis, ECs are activated and differentiate into migratory tip cells and proliferating stalk cells to form new vessels, for example to support wound healing or to provide tissues with nutrients and oxygen (Fig. 1A)<sup>13,14</sup>. Extensive signalling between tip and stalk cells, especially via Delta-like ligand 4 (DLL4) and Notch, ensures proper tip and stalk cell behaviour, partly through distinct regulation of metabolic activity, and ultimately facilitates vessel formation (Fig. 1B)<sup>10</sup>. Vessel formation is terminated once the tip cells encounter another tip cell or blood/lymphatic vessel, nutrient and oxygen levels meeting the demands of the tissues, or the decrease in proangiogenic factor levels, which all subsequently lead to re-establishment of quiescence in ECs<sup>13,15,16</sup>. ECs not only line up blood and lymphatic vessels as a simple monolayer, but they are also a critical component of vascular function. In the cardiovascular system, blood ECs (BECs) fulfil a myriad of functions: they regulate the vascular tone, coagulation and thrombosis formation, or recruit platelets and leukocytes after vascular injury<sup>17</sup>. And lymphatic ECs (LECs) are connected by intermittent cell-cell button junctions, which enables the entrance of lymph in an unidirectional way and of immune cells that travel through lymphatic vessels to lymph nodes for antigen presentation and activation of the immune response<sup>18</sup>.



## Development of blood and lymphatic vasculature

Development of the cardiovascular and lymphatic systems is a multi-step process starting in early embryos, in which mesodermal cells differentiate into angioblasts, the endothelial precursor cells (Fig. 1C)<sup>19</sup>. Angioblasts build the first primitive vascular structures, such as the primary plexus and aorta and cardinal veins, a process called vasculogenesis<sup>13,20</sup>. Subsequent formation of more complex vascular structures that include arteries, capillaries and veins is termed angiogenesis and is mediated through the interplay of different transcription factors (TFs), that control the transcription of a defined sets of genes, and signalling pathways<sup>13,20,21</sup>. The main drivers of arteriovenous development are vascular endothelial growth factor (VEGF-A) and Notch signalling<sup>22</sup>. Increased VEGF and Notch signalling initiates adoption of an arterial phenotype, while reduced activation of VEGF and COUP-TFII-mediated repression of Notch signalling leads to a venous phenotype<sup>22–25</sup>. Furthermore, distinct TFs define BEC identity and thereby support arterial and venous development<sup>26</sup>. The most prominent TFs are, besides COUP-TFII (NR2F2), GATA2, ETV2 and members of the HESR (Hey1, Hey2), FOX (FOXC1, FOXC2) and SOX (SOX7, SOX17, SOX18) family of transcription factors (Fig. 1B)<sup>20,21</sup>. Further maturation of blood vessels requires the formation of the basal lamina and the recruitment and association of pericytes and smooth muscle cells to the vessels, which results in quiescence of BECs<sup>27</sup>.

The last step in the development of the mature vasculature is lymphangiogenesis, in which venous BECs differentiate into lymphatic ECs (LECs) with subsequent lymphatic vasculature formation<sup>5,20,28–30</sup>. The differentiation is governed by SOX18, NR2F2 and the master regulator of LEC identity, PROX1 (Fig. 1D)<sup>5,20,30–33</sup>. PROX1 induces expression of LEC-specific markers, like VEGFR3 and integrin  $\alpha$ 9, that steer the migration of LECs along a VEGF-C gradient, the first step in lymphatic capillaries and vessels formation<sup>5,34</sup>. In contrast to VEGF receptor 1 and 2, which mainly regulate angiogenesis, lymphangiogenesis is mediated by the LEC-specific VEGF receptor 3 (VEGFR3)<sup>35</sup>. Further maturation of lymphatic vessels and the formation of lymphatic valves is controlled by the transcription factors GATA2, FOXC2 and NFATC1<sup>36,37</sup>. In addition to transcription factor binding, alternative mechanisms of transcriptional regulation, such as epigenetic signatures, partially mediated by long-noncoding RNAs,

have recently garnered increased attention in research. These mechanisms have been demonstrated to play a role in the formation of lymphatic endothelial cell identity<sup>38,39</sup>.

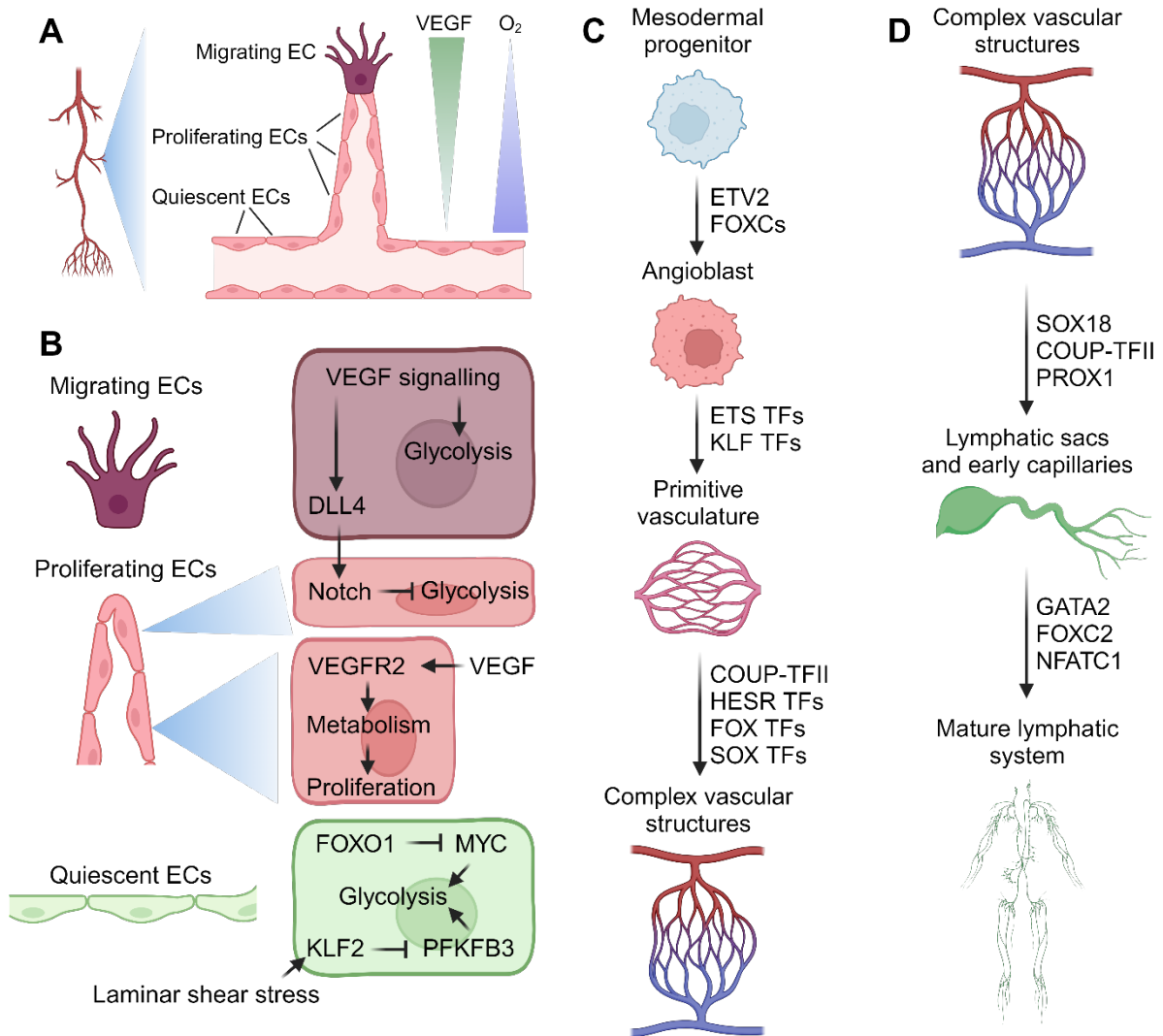


**Figure 1. Overview of vascular organization and development**

- (A) Scheme of the formation of novel blood vessels along a growth factor or hypoxia gradient.
- (B) Overview of some of the main regulators of migrating, proliferating and quiescent phenotypes, with special emphasis on glycolysis and its activation or repression in certain phenotypes. DLL4 = Delta-like ligand 4, VEGF = Vascular endothelial growth factor, VEGFR2 = VEGF receptor 2, FOXO1 = Forkhead box protein O1, MYC = MYC proto-oncogene, PFKFB3 = 6-phosphofructo-2-kinase/fructose-2,6-biphosphatase 3, KLF2 = Krüppel-like factor 2.
- (C) Development of the cardiovascular system from mesodermal progenitors. ETV2 = ETS variant transcription factor 2, FOXC = Forkhead box C, TFs = transcription factors, ETS = E26 transformation-specific, KLF = Krüppel-like factor, COUP-TFII = COUP transcription factor 2, HESR = Hairy and enhancer of split-related, FOX = Forkhead box, SOX = SRY-related HMG-box.
- (D) Development of the lymphatic system from venous vasculature. PROX1 = Prospero homeobox protein 1, GATA2 = GATA-binding factor 2, NFATC1 = Nuclear factor of activated T cells 1.

## **Diseases caused by dysfunctional vasculature**

Disturbances or alterations in these fine-tuned developmental and regulatory processes lead to endothelial dysfunction and consequently to various vasculature-related diseases<sup>17,40</sup>. Dysfunctional blood endothelium negatively impacts vascular tone, promoting the emergence of cardio- and cerebrovascular diseases such as hypertension, atherosclerosis, coronary artery disease and stroke<sup>17</sup>. Dysregulation of lymphatic homeostasis causes the development of various diseases throughout the body, for example lymphedema, inflammatory diseases of the skin (dermatitis) or inflammatory bowel disease<sup>8,41–43</sup>. Even though the mechanisms of EC development are well-understood, the causes of dysfunctional endothelial cells promoting disease progression are sometimes enigmatic and not just explainable through mutations in EC-shaping signalling molecules or TFs. Some diseases or disease-supporting dysfunctional vasculatures, however, can be caused by extrinsic factors or aberrant metabolism.

A classic example of a disease caused by mutations as well as extrinsic factors is lymphedema. It is a disease arising from impaired lymphatic drainage that leads to tissue swelling, inflammation and fibrosis, which substantially impairs function of the affected organ. The prevalence is high, it affects up to 250 million people worldwide<sup>41,42</sup>. Lymphedema is divided into two subgroups, primary and secondary lymphedema. Primary lymphedema is a hereditary disease caused by genetic mutations in genes like VEGFR3 or FOXC2 that drive lymphatic vessel development and maturation<sup>36,42</sup>. Primary lymphedema affects around 1 in 6'000 individuals. The vast majority of lymphedema cases, however, are secondary lymphedema cases, which are caused by extrinsic factors, such as filariasis, cancer-related treatments, traumas, surgery or obesity, which all damage or obstruct previously healthy lymphatic vessels<sup>42</sup>. The exact causes of secondary lymphedema are still being investigated, but a preliminary study showed that the synergistic interaction of specific single nucleotide polymorphisms (SNPs) in VEGFR3 and FOXC2 potentially supports the progression of secondary lymphedema<sup>44</sup>. Additionally, extensive research over the last years displays the pivotal role of metabolism to support normal EC functions and consequently suggests that metabolism and metabolic alterations are causative or supportive of vascular diseases, potentially also in secondary lymphedema<sup>45–47</sup>. Understanding the metabolic patterns that underlie health and diseased states in

endothelial cells is therefore beneficial for development of novel therapies. Indeed, Garcia-Caballero *et al.* demonstrated in a study that ketone bodies induce lymphangiogenesis and improve lymphatic vessel function in mice, alleviating symptoms of a human lymphedema-mimicking ablation of lymphatic vessels in mice tails<sup>48</sup>. The effect of aberrant metabolism in BECs is also demonstrated in a recent study by Zhang *et al.*<sup>49</sup>. They showed that enhanced serine biosynthesis in tumour BECs stimulates BEC overgrowth via increased glycolysis and nucleotide biosynthesis, leading to decreased perfusion of and lower oxygen levels in the tumour and reduced T cell infiltration, altogether promoting tumour growth<sup>49</sup>. Inhibition of serine biosynthesis prunes the vasculature, improves T cell infiltration, and consequently inhibits tumour growth.

## Endothelial cell metabolism

Endothelial cells exhibit high phenotypic plasticity, as they are mostly quiescent in their lifetime but can immediately switch to a proliferative state to form novel vessels. Recent studies attributed an essential role to metabolism to provide the bioenergetic and metabolic means of establishing and maintaining different growth states as well as lymphatic identity (Table 1)<sup>50–60</sup>. For example, PROX1 is the master regulator of LEC differentiation and accomplishes lymphatic identity formation and lymphangiogenesis through rewiring metabolism, specifically through upregulation of fatty acid  $\beta$ -oxidation (FAO), which then alters epigenetic regulation of lymphatic gene expression<sup>58</sup>. In brief, by increasing the expression of the mitochondrial fatty acid transporter CPT1 $\alpha$  and subsequent increased FAO, acetyl-CoA levels rise and serve as acetate source for enhanced histone acetylation of lymphatic genes by PROX1 and the histone acetyltransferase p300. The expression of lymphatic genes leads to differentiation into and proliferation of LECs, the first steps in lymphangiogenesis. As a consequence, CPT1 $\alpha$  knockdown impairs lymphangiogenesis through FAO inhibition, an effect that was shown to be reversible *in vitro* by acetate supplementation<sup>58</sup>. Besides this prime example of upregulated FAO for lymphangiogenesis, other metabolic pathways or reactions have been described to play a pivotal role in proliferating and quiescent ECs (Table 1). Many of the described pathways, such as glycolysis, tricarboxylic acid (TCA) cycle and pentose phosphate pathway (PPP), are part of central carbon metabolism (CCM), which is the most fundamental metabolic process in living cells to sustain

cellular bioenergetic balance and metabolic precursor levels needed for cellular survival and growth<sup>61</sup>.

## Glycolysis

Glycolysis is a highly conserved pathway in many different organisms that converts glucose into pyruvate, forming the energy-providing molecule adenosine triphosphate (ATP) and reduced nicotinamide adenine dinucleotide (NADH). ATP provides chemical energy and is thus essential for cells to run many biological processes. In glycolysis, for each molecule of glucose, 2 molecules of ATP are generated, compared to 36 molecules in aerobic respiration via oxidative phosphorylation (OXPHOS). Nevertheless, endothelial cells (blood and lymphatic) form most of their ATP via glycolysis<sup>50</sup>. This is even more surprising for BECs, because they have almost unlimited access to nutrients and oxygen from the blood. ATP generation via glycolysis offers three advantages, though: first, production of reactive oxygen species (ROS) is reduced, thereby decreasing the chances that excessive ROS levels damage proteins, lipids and nucleic acids<sup>62</sup>. Second, independence from oxygen to produce ATP enables BECs to sprout into tissues that have low oxygen levels. And third, larger amounts of oxygen can be transferred to surrounding tissue. Proliferating and quiescent ECs rely on glycolysis for ATP production, but it is less active in quiescence due to lower expression of glycolytic genes<sup>54,57</sup>. In detail, increase of glycolytic flux in proliferation is mediated by VEGF signalling, while higher activity of FOXO1, Notch signalling and Krüppel-like factor 2 (KLF2), a TF responding to laminar shear stress experienced by quiescent ECs in the mature vasculature, reduces glycolytic flux in quiescence<sup>50,53,54,63</sup>. FOXO1 suppresses glycolysis through inhibition of MYC, a known enhancer of glycolysis, while KLF2 reduces glycolysis partly by transcriptional repression of the glycolysis-activator 6-phosphofruco-2-kinase/fructose-2,6-biphosphatase 3 (PFKFB3) and the glycolysis enzymes hexokinase-2 (HK2) and phosphofructokinase 1 (PFK1)<sup>54,63</sup>. VEGF signalling on the other hand upregulates PFKFB3 expression which increases glycolytic flux. As a consequence, inhibition of PFKFB3 reduces growth and migration of ECs, while overexpression of PFKFB3 without additional angiogenic signalling enhances tip-cell behaviour and vessel sprouting, demonstrating the importance of metabolism to facilitate certain phenotypes and cellular functions<sup>50</sup>. Furthermore, under glucose-restricted conditions, for example during vascularization in nutrient-deprived tissues, glycolysis of migrating and proliferating ECs is fuelled by

degradation of internal glycogen storages that provides glucose<sup>64</sup>. Besides growth-state dependent global up- or downregulation of glycolytic flux in ECs, it was demonstrated that pyruvate kinase (PK), the enzyme that catalyses the conversion of phosphoenolpyruvate to pyruvate, supports the formation and maintenance of proliferation and quiescence as well<sup>65</sup>. The M2 isoform (PKM2) is almost exclusively expressed in ECs and plays a fundamental role in cell cycle progression and vascular integrity in a metabolism-independent way. PKM2 suppresses the cell cycle inhibitor p53 in proliferation and the NF- $\kappa$ B-induced expression of angiopoietin-2 in quiescence. This illustrates how enzymes in the central metabolic pathways of endothelial cells (ECs) contribute to the formation and maintenance of both blood and lymphatic vessels, revealing previously unknown mechanisms associated with these enzymes.

### **Pentose phosphate pathway**

Glycolysis is not only used to generate ATP, but it also contributes to the formation of a variety of different metabolites by fuelling other metabolic pathways, such as the PPP. Glycolysis-derived glucose 6-phosphate (G6P) is converted by glucose-6-phosphate dehydrogenase (G6PD) into 6-phospho-glucono-1,5-lactone, which is the first and rate-limiting step of the PPP. The PPP is mainly involved in the regeneration of the cofactor NADPH from its oxidized version NADP<sup>+</sup> and provides ribose for nucleotide biosynthesis. NADPH is needed to run anabolic and redox reactions and for the synthesis of nitric oxide (NO), a signalling molecule produced by endothelial nitric oxide synthases (eNOS) from arginine, that plays an important role in promoting migration and angiogenesis of BECs, but also in the regulation of the vascular tone<sup>66–69</sup>. Consequently, increased flux through the PPP has been shown to limit accumulation of ROS and provides building blocks for nucleotide biosynthesis needed by hyperproliferative ECs in cancer<sup>70,71</sup>.

### **TCA cycle and fatty acid $\beta$ -oxidation**

The TCA cycle is a set of oxidative reactions and a central hub for anabolic and catabolic reactions, redox regulation, signalling and energy production from carbon-containing molecules derived from various sources, such as pyruvate from glycolysis, acetyl-CoA from FAO, propionyl-CoA from branched chain amino acid breakdown or  $\alpha$ -ketoglutarate from glutaminolysis<sup>72</sup>. In proliferating ECs, the role of the TCA cycle is not primarily to contribute to energy generation or for redox homeostasis but for *de*

*novo* nucleotide synthesis for DNA replication through biosynthesis of the nucleotide precursor, aspartate, a process which is dependent on acetyl-CoA influx into TCA cycle from FAO<sup>51</sup>. In contrast, quiescent ECs use FAO and the TCA cycle to maintain redox homeostasis<sup>57</sup>. Quiescent BECs reside in a high-oxygen microenvironment and long-term exposure to ROS leads to cardiovascular dysfunction<sup>62</sup>. Nevertheless, a base level of ROS is crucial for migration and angiogenesis of BECs, through mediating the increased expression of VEGF<sup>73–75</sup>. Therefore, balanced redox control is crucial to avoid unwanted damage but still providing enough ROS to maintain proper cellular functions. In quiescent ECs, increased FAO through upregulation of fatty acyl transporter CPT1 $\alpha$  and other enzymes in FAO leads to higher levels of acetyl-CoA that enter the TCA cycle. Two of the TCA cycle intermediates, isocitrate and malate, are substrates of isocitrate dehydrogenase (IDH2) and malic enzyme (ME3), respectively, two enzymes that produce NADPH and that were shown to be higher expressed in quiescent ECs as well. NADPH is used by glutathione reductase to reduce glutathione, which in turn functions as substrate of glutathione peroxidase, an enzyme that clears intracellular ROS and thus protects quiescent ECs from excessive ROS levels<sup>57</sup>. Interestingly, EC quiescence is tightly connected to increased FAO, as it was demonstrated that overexpression of quiescence-inducing FOXO1 leads to an increase of FAO<sup>54,57</sup>. Furthermore, whether FAO is used for nucleotide production in proliferating ECs or redox homeostasis in quiescent ECs seems to be partly regulated through quiescence-promoting Notch<sup>57</sup>. A consequence of disturbed CPT1 $\alpha$  function *in vivo* is vascular leakage and hyperpermeability, which can be reversed through acetate treatment in mice<sup>57</sup>. CPT1 $\alpha$  is not only a key player in blood ECs but also in lymphatic ECs, where it facilitates the transition from venous BECs to LECs and sustains TCA intermediates for nucleotide biosynthesis in proliferation<sup>58</sup>. Intriguingly, lymphangiogenesis defects caused by inhibition of FAO can be rescued by acetate supplementation. Furthermore, besides FAO, also ketone body oxidation was shown to promote lymphangiogenesis<sup>48</sup>. Ketone bodies are metabolites produced in and secreted from the liver and yield a total of 22 ATPs per ketone body. They are an important energy source for different organs in times of low carbohydrate intake. Providing additional ketone bodies, thereby fuelling the TCA cycle through ketone body oxidation, increases LEC proliferation<sup>48</sup>. Even more surprising, feeding mice a ketogenic diet, which is a low-carbohydrate, high-fat diet resulting in increased circulating ketone bodies, promotes LEC proliferation and lymphangiogenesis.

**Table 1.** Overview of cell type- and state-dependent use of metabolic pathways in ECs. The upper table is mostly based on studies with blood endothelial cells, the lower table contains lymphatic endothelial cell-specific metabolic patterns that support phenotypes.

Phenotype	Pathway	Function
<b>Proliferating</b>	Glycolysis	<ul style="list-style-type: none"> <li>• ATP generation</li> </ul>
	Pentose phosphate pathway	<ul style="list-style-type: none"> <li>• Nucleotide precursors</li> <li>• Redox homeostasis through NADPH generation</li> </ul>
	TCA cycle	<ul style="list-style-type: none"> <li>• Nucleotide precursors</li> </ul>
	Fatty acid $\beta$ -oxidation	<ul style="list-style-type: none"> <li>• Anaplerosis through acetyl-CoA</li> <li>• Nucleotide precursors</li> </ul>
	Serine metabolism	<ul style="list-style-type: none"> <li>• Nucleotide precursors</li> <li>• Biosynthesis of essential co-factor heme</li> <li>• Mass balance in central carbon metabolism</li> </ul>
	Glutamine metabolism	<ul style="list-style-type: none"> <li>• Anaplerosis</li> <li>• Nucleotide precursor</li> <li>• Nitrogen source through transamination reactions</li> </ul>
	Electron transport chain	<ul style="list-style-type: none"> <li>• NAD<sup>+</sup> regeneration</li> <li>• Aspartate for nucleotide biosynthesis</li> </ul>
<b>Migrating</b>	Glycolysis	<ul style="list-style-type: none"> <li>• ATP generation</li> <li>• Actin remodeling needed for proper motility</li> </ul>
	Glutamine metabolism	<ul style="list-style-type: none"> <li>• Anaplerosis</li> <li>• Nitrogen source through transamination reactions</li> </ul>
	Proline metabolism	<ul style="list-style-type: none"> <li>• Collagen synthesis and modification</li> </ul>
	Lipid metabolism	<ul style="list-style-type: none"> <li>• Plasma membrane composition and fluidity</li> </ul>
<b>Quiescent</b>	Glycolysis	<ul style="list-style-type: none"> <li>• ATP generation</li> </ul>
	Pentose phosphate pathway	<ul style="list-style-type: none"> <li>• Redox homeostasis</li> </ul>
	TCA cycle	<ul style="list-style-type: none"> <li>• Redox homeostasis</li> </ul>
	Fatty acid $\beta$ -oxidation	<ul style="list-style-type: none"> <li>• Redox homeostasis</li> </ul>

Phenotype	Pathway	Function
<b>Differentiating</b>	Fatty acid $\beta$ -oxidation	<ul style="list-style-type: none"> <li>• Acetyl-CoA needed to establish LEC identity</li> </ul>
	Electron transport chain	<ul style="list-style-type: none"> <li>• Complex III regulates PROX1-VEGFR3 feedback loop and LEC identity</li> </ul>
<b>Proliferating</b>	Ketone body oxidation	<ul style="list-style-type: none"> <li>• Generates acetyl-CoA for anaplerosis which facilitates aspartate and nucleotide biosynthesis</li> </ul>



## Oxidative phosphorylation

In many cell types, OXPHOS is the predominant pathway to generate ATP. NADH is formed in glycolysis and the TCA cycle, and its electrons used by the electron transport chain (ETC), a series of complexes in the mitochondria, to generate a proton gradient that facilitates ATP synthesis via ATP synthase. Inhibition of OXPHOS impairs EC proliferation and vascular development<sup>76,77</sup>. However, the cause of the consequences that OXPHOS inhibition brings along in ECs is not a lack of ATP (most ATP is produced in glycolysis) but the diminished recycling of NADH to NAD<sup>+</sup>, which consequently impairs the flux in the TCA cycle<sup>76</sup>. Ectopic expression of NADH oxidases, that regenerate NAD<sup>+</sup>, rescues proliferation of ECs through increase of aspartate levels arising from normalized flux in the TCA cycle. Mitochondrial respiration does not only regulate BEC proliferation, but also LEC differentiation. Ma *et al.* demonstrated that deletion of complex III interferes with lymphatic vasculature development<sup>78</sup>. Specifically, deletion of complex III increases succinate, fumarate and 2-hydroxyglutarate levels, metabolites that inhibit  $\alpha$ -ketoglutarate-dependent dioxygenases in demethylase complexes. This leads to reduced epigenetic modifications and subsequent reduced expression of PROX1 and VEGFR3, demonstrating a feedback loop in which complex III activity, driven by differentiation and metabolic cues, regulates the expression of LEC identity-shaping factors.

## Lipid metabolism

Besides their contribution to EC proliferation and quiescence via FAO, lipids are part of some other processes that support proliferation and migration of ECs. Phospholipids are an integral part of the plasma membrane and their composition in the plasma membrane directly affects migration through altered membrane fluidity and subsequent capacity to form filopodia<sup>79</sup>. Phospholipids also function as signalling molecules, for example in the phosphatidylinositol 3-kinase (PI3K)/AKT/mTOR pathway<sup>80</sup>. This pathway has been shown to regulate the expression of angiogenic factors, like NO and angiopoietins, and contributes to the formation of blood vessels during development<sup>81,82</sup>. Proliferation of ECs is also reduced upon inhibition of fatty acid synthase (FASN)<sup>83</sup>. This is caused by elevated levels of malonyl-CoA, the substrate of FASN, which leads to malonylation and decreased activity of the mitogenic factor mTOR. Furthermore, FASN is needed for eNOS palmitoylation, which ensures

membrane localization into caveolae, where sources of arginine and tetrahydrobiopterine (BH4) are met to produce nitric oxide (NO)<sup>84</sup>.

## Amino acid metabolism

The two most studied amino acid pathways in ECs are serine and glycine biosynthesis and glutamine and asparagine metabolism. Glutamine is heavily consumed *in vitro* by ECs in order to replenish TCA cycle intermediates, a process called anaplerosis, which has been observed in many different cell types<sup>52,60,85</sup>. Glutamine plays a central role in different metabolic processes: through anaplerosis, it facilitates a functioning TCA cycle, and the resulting increased citrate levels drive *de novo* lipid biosynthesis<sup>86</sup>; it is essential for biosynthesis of nucleotides, non-essential amino acids (NEAA) and glutathione<sup>87</sup>; and glutamate, the product of glutamine hydrolysis, is a central hub for nitrogen and carbon needed for amino acid biosynthesis<sup>87</sup>. It has been shown that insufficient glutamine metabolism in BECs impairs anaplerosis, macromolecule production and redox homeostasis but not energy production, and consequently reduces proliferation but not migration<sup>52,60</sup>. Moreover, it was shown that asparagine synthetase, which converts glutamine and aspartate to asparagine and glutamate, is needed because of its role in biosynthesis of NEAA. The consequences of asparagine synthetase inhibition cannot be rescued through asparagine and glutamine supplementation and lead to impaired sprouting capacity. Glutamine is not only taken up from the environment but can be produced from glutamate by glutamine synthetase (GS). However, even in glutamine-scarce conditions, ECs only produce small amounts of glutamine<sup>59</sup>. GS is instead used as palmitoyl transferase in ECs, and as such, GS palmitoylates RhoJ, which is a Rho GTPase that regulates the assembly of cytoskeleton proteins and thus EC migration.

Phosphoglycerate dehydrogenase (PHGDH) is the first and rate-controlling step in *de novo* biosynthesis of serine and glycine, but it also maintains mass balance within central carbon metabolism<sup>88</sup>. It has been shown that serine biosynthesis through PHGDH is necessary for heme production, a co-factor in different metabolic complexes like, nitric oxide synthase, catalases and complex III and IV of the electron transport chain. Inhibition of PHGDH in BECs causes oxidative stress mainly through impaired ETC activity and partly through decreased glutathione and NADPH synthesis<sup>56</sup>. Yet, because serine supplementation does not rescue PHGDH inhibition, the cause of EC impairment could also be the disruption of the mass balance in central carbon

metabolism. Furthermore, a recent study attributed an important role of PHGDH in the formation of dysfunctional vasculature in glioblastoma, which leads to impaired perfusion and decreased oxygen levels and T cell infiltration<sup>49</sup>. Increased activity of PHGDH in tumour BECs enhances glycolysis and nucleotide biosynthesis, leading to BEC overgrowth. Reducing the activity of PHGDH through genetic or pharmacological measures prunes the vasculature and improves T cell infiltration and consequently CAR T-cell therapy. Both nucleotide and glycine synthesis from serine is routed through one-carbon (1C) metabolism. This suggests that 1C metabolism is an essential hub for EC proliferation and migration. Besides glutamine and serine metabolism, the relevant role of proline metabolism in endothelial migration has gotten some attention recently. Biosynthesis of proline and hydroxyproline, two major components of collagen, supports collagen biosynthesis and modification in the extracellular matrix. Decreased levels of proline and hydroxyproline were shown to impair EC migration through disturbed endothelial basal lamina deposition and mechanotransduction<sup>89,90</sup>. The role of arginine in the production of NO by eNOS, needed for migration, angiogenesis and regulation of vascular tone, should be mentioned as well<sup>91</sup>. However, besides the role of NO in endothelial homeostasis, the roles of the urea cycle itself and of arginine as substrate for NO production, have not gotten a lot of attention in research in recent years.

## **Missing pieces in EC metabolism research**

Over the past decades, extensive research revealed the diverse metabolic lifestyles underlying and shaping different EC identities and states. However, there are several shortcomings in these studies. First, most studies so far focused on the role of a handful of central metabolic pathways like glycolysis, FAO, OXPHOS or glutamine and serine metabolism, and their role in a specific growth state or cell type. Many studies are performed with human umbilical vein ECs (HUVECs), a model cell type for BECs, and the metabolic lifestyle of LECs remains understudied. The environment of LECs is, in comparison to BECs, low on oxygen and nutrients and high in lipids and lipoproteins, and therefore the metabolic patterns underlying LEC identities and states are likely diverging from the metabolic patterns in BECs. Indeed, recent transcriptomics studies of murine endothelial cells provided an overview of organ-specific transcriptomes of ECs, showing a heterogeneity in metabolic transcript levels between ECs from different tissues and between ECs from different vascular beds within a

single tissue<sup>89,92–95</sup>. Hence, an investigation that analyzes ECs from distinct vascular beds and tissues within the same experimental framework would be valuable for enhancing our understanding of the extent of metabolic variability among various EC types.

Second, most studies use either a targeted approach to study EC metabolism, e.g. measuring uptake and secretion rates of a couple of metabolites and abundances of metabolites in certain metabolic pathways, or they measure global transcript level changes (transcriptomics). Although transcriptomics is a widely applied and straightforward technique to determine transcript level changes, it is only a proxy for the actual abundances of proteins or the metabolic activity of cells. These limitations can be overcome by employing metabolomics and proteomics measurements, where the abundances of metabolites and proteins are directly assessed rather than inferred from transcriptomics data. Additionally, untargeted metabolomics and proteomics approaches nowadays result in measured abundances of thousands of metabolites and proteins, providing the foundation to generate a comprehensive picture of the metabolic lifestyle of mammalian cells, including endothelial cells. Untargeted proteomics data can be further used to infer activities of transcription factors, which is useful to study the transcriptional regulation that form the metabolic patterns in the different EC identities and states.

And lastly, most studies are static, i.e. they analyse proliferation or quiescence but do not contain information about the temporal heterogeneity in metabolism of different ECs when they transition from proliferation into quiescence or vice versa. For example, a study with non-malignant murine pro-B lymphocytes demonstrated diverse metabolic and proteomic patterns underlying the transition from quiescence to proliferation<sup>96</sup>. Considering the known growth state-specific metabolic patterns of ECs, we expect that the metabolic and proteomic patterns governing the transition between growth states in ECs can provide valuable insights into the establishment of a proliferative and quiescent state.

## **Methods to study metabolite levels**

The metabolome is the entirety of metabolites in a system, for example of all metabolites in a cell (intracellular metabolome), in the blood (blood metabolome) or in the environment of a cell (extracellular metabolome). Metabolomics is the study of the

metabolome and is commonly performed on mass spectrometry (MS) or nuclear magnetic resonance (NMR) platforms. Metabolomics measurements are divided into targeted and untargeted metabolomics. Targeted metabolomics is applied to determine the levels of specific metabolites in a sample, whereas untargeted metabolomics strives to determine the global metabolic profile of a sample<sup>97</sup>. Metabolomics measurements can either be quantitative or semi-quantitative. Quantitative analysis includes the use of dilution curves of specific metabolites, so-called standards, in order to quantify levels of these metabolites in a sample. Semi-quantitative analysis on the other hand does not include standards and aims to compare the measured levels of metabolites between two samples, resulting in relative changes between two samples, for example control vs. perturbation.

Targeted metabolomics is often applied to address very specific biological questions or hypotheses, thereby focusing on a handful of chemically well-characterized metabolites<sup>98</sup>. Most commonly, targeted metabolomics is performed by gas chromatography-coupled mass spectrometry (GC-MS) and liquid chromatography-coupled mass spectrometry (LC-MS), depending on the chemical type of the targets. For example, GC-MS is well suited for amino and organic acids, sugars and fatty acids. In contrast, LC-MS is a softer method that preserves molecular ions and is preferred in dynamic experiments<sup>99</sup>. Independent of the analytical platform used, the biggest advantage of targeted metabolomics is the quantification of the absolute concentrations of the targeted metabolites. By coupling MS to chromatography, it is as well able to distinguish between isomers. However, chromatography gradients are usually long and result in low sample throughput. Additionally, the targeted metabolites must be known beforehand, which limits coverage.

Untargeted metabolomics is the unbiased measurement of all metabolites present in a biological sample<sup>97,100</sup>. LC-MS is the most frequently used platform for untargeted metabolomics measurements. Another approach is flow injection analysis (FIA-MS), in which the chromatographic separation of metabolites is dropped and the samples directly injected into the mass spectrometer<sup>101</sup>. This technique enables a high throughput, yet still accurate, profiling of thousands of metabolites with concentrations over a range of 3 orders of magnitude in complex samples. Isomer identification and discrimination are the biggest limitations of FIA-MS. Nonetheless, FIA-MS provides valuable information on which metabolic processes are affected by a perturbation or

phenotype and thus supports the design of targeted follow-up measurements or validation experiments. In untargeted metabolomics measurements, accurate masses, isotopic patterns and retention times from LC-MS are compared with databases, such as the Kyoto Encyclopedia of Genes and Genomes (KEGG) or the Human Metabolome Database (HMDB), to annotate metabolites. Additional fragmentation of metabolites in a mass spectrometer (LC-MS/MS) can facilitate the identification of unknown metabolites, or metabolites that have similar masses and retention times. FIA-MS is a semi-quantitative approach when used without standards, therefore lacking the ability to quantify the absolute concentrations of metabolites. Another disadvantage of untargeted, high-throughput metabolomics is the introduction of unwanted variation in form of experimental variation, temporal drifts or batch effects. These effects must be removed through normalization techniques in order to ensure unbiased determination of biological variance<sup>102</sup>.

Altogether, metabolite levels can be measured in a targeted or untargeted way, and both approaches offer advantages, disadvantages and challenges. Targeted metabolomics is preferred for the quantification of a defined set of metabolites, while untargeted metabolomics provides the opportunity to measure the semi-quantitative abundance of thousands of metabolites simultaneously, thereby facilitating the comprehensive description of metabolic lifestyles of different biological systems.

## **Methods to study protein levels and transcription factor activities**

The proteome is the entirety of proteins in a biological system and proteomics is the study of the proteome. Like most metabolomics experiments, proteomics is performed on LC-MS platforms, enabling the quantification of either target proteins (targeted proteomics) or thousands of proteins simultaneously (untargeted proteomics)<sup>103,104</sup>. To generate a comprehensive description of the protein expression patterns that underlie cellular identities and states, untargeted proteomics is thus the preferred method. Nowadays, the most common untargeted proteomics methods use the so-called bottom-up approach, in which proteins are extracted and enzymatically digested before LC-MS/MS measurements. As a result, not the proteins themselves are measured in the mass spectrometer but protein-specific peptides<sup>105,106</sup>. Through mapping of the mass spectra of each peptide to *in silico* generated mass spectra, the identities and

relative abundances of proteins can be inferred<sup>104</sup>. The advantage of this method is the high coverage of the protein space, however, with the downside that low abundant proteins might not be measured, resulting in decreased sensitivity. Nonetheless, like in untargeted metabolomics, this is a powerful method to study the molecular processes underlying the formation and maintenance of specific phenotypes.

Many transcription factors are only present in low numbers in cells<sup>1</sup>. Their presence is often measured by quantitative polymerase chain reaction (qPCR) or RNA sequencing (RNAseq). These two techniques are very sensitive and identify already the presence of few TF transcripts in a biological sample. However, the sole presence of TF transcripts does not provide information whether the TFs are active in the cells. Since TFs regulate the expression of a defined set of genes, their activities can be inferred computationally from untargeted omics datasets, such as transcriptomics and untargeted proteomics. To that end, Garcia-Alonso *et al.* generated a collection of human TF-target interactions, which not only contains the interactions but also different confidence levels of the interactions, and whether it is an activating or repressing interaction<sup>107</sup>. The TF-target collection in combination with a transcriptomics or proteomics dataset lays the fundament of computational methods that infer TF activities<sup>108</sup>. These computational methods enable the identification of active TFs in a specific phenotype, without having to go through transcriptional or protein expression level changes manually. Yet, these methods are solely computational and may generate false positive results; thus, validation experiments are essential to evaluate the accuracy of TF activity inference.

## **Aims and outline of the thesis**

Recent advances in endothelial cell (EC) research highlight the significant role of metabolism in the formation and maintenance of EC identities and states, and consequently to support or impair healthy vasculature. We expect that the metabolic and proteomic patterns governing distinct EC identities and states are diverse and contingent on the roles and microenvironments of the respective EC types. To advance our understanding of the extend of metabolic variability across EC types, our goal was to generate a comprehensive description of the molecular patterns in four different EC types through direct measurements of metabolite and protein abundances. To that end, we set out to characterize the two BEC types human dermal BECs (HDBECs), human umbilical vein ECs (HUVECs) and the two LEC types human dermal LECs (HDLECs)

and intestinal LECs (iLECs), across proliferative and quiescent states by combining untargeted proteomics and metabolomics approaches. We then deployed the untargeted proteomics dataset to infer TF activities and used the TF activities dataset to determine the transcriptional regulatory networks that shape EC identities and states *in vitro*.

In **chapter 2**, we developed an experimental framework to study metabolite and protein levels of HDBECs, HUVECs, HDLECs and iLECs in proliferation, quiescence and the transition between the two states. We grew the four EC types for 10 days in similar conditions and determined the fraction of proliferating and quiescent cells by measuring *de novo* DNA synthesis. We could show that mitogen reduction in the growth medium and contact inhibition induces a strong quiescent state across the four EC types. We then performed untargeted measurements of extra- and intracellular metabolites and of intracellular proteins every 24 hours. Cell type-specific temporal metabolic and proteomic patterns are unchanged after data normalization and serve as a valuable resource for conducting further in-depth investigations into the molecular patterns that define EC identities and states.

In **chapter 3**, we used the datasets generated in chapter 2 and examined the molecular patterns that underlie EC identities and states. We observed distinct and general proteomic and metabolic patterns in quiescence and proliferation in each cell type. Some of these patterns recapitulate previous described markers or processes that are specific to a cell type or state. Additionally, we noted that certain findings from earlier studies at the transcript level and in specific cell types were consistent with our observations in the tested EC types. Furthermore, functional studies in HUVECs and iLECs exhibited diverse phenotypic alterations following inhibition of enzymes in metabolic pathways, such as heme biosynthesis, glutamate metabolism, fatty acid and nucleotide synthesis, indicating the diverging importance of certain metabolic pathways to maintain a specific state by different endothelial cell types.

In **chapter 4**, we used the proteomics dataset to infer the activities of 263 TFs. The resulting TF activity patterns show cell type- and state specific behaviour. However, we were also able to extract TFs whose activities are fundamentally different between BECs and LECs, including well-known markers of LEC and BEC identities. In addition, we correlated TF activities with expression patterns of 14 enzymes that were



targets of pharmacological inhibition and propose two new TFs that potentially regulate expression of enzymes necessary for functioning migration in HUVECs and iLECs.

## Additional projects

I contributed to the following, published projects, which are not a part of this thesis. The list is not definitive as it does not include unpublished work:

- Cherkaoui, S., **Durot S.** *et al.* A functional analysis of 180 cancer cell lines reveals conserved intrinsic metabolic programs. *Mol. Syst. Biol.* **18**, 1–15 (2022).

Contribution: Performed <sup>13</sup>C flux analysis and metabolomics/lipidomics measurements.

- González-Loyola, A. *et al.* FOXC2 controls adult lymphatic endothelial specialization, function, and gut lymphatic barrier preventing multiorgan failure. *Sci. Adv.* **7**, (2021).

Contribution: Metabolomics measurements of plasma samples, data analysis and visualisation.

- Bernier-Latmani, J. *et al.* ADAMTS18+ villus tip telocytes maintain a polarized VEGFA signaling domain and fenestrations in nutrient-absorbing intestinal blood vessels. *Nat. Commun.* **13**, 1–17 (2022).

Contribution: Metabolomics measurements of plasma samples, data analysis and visualisation.

- González-Loyola, A. *et al.* c-MAF coordinates enterocyte zonation and nutrient uptake transcriptional programs. *J. Exp. Med.* **219**, (2022).

Contribution: Metabolomics measurements of plasma samples, data analysis and visualisation.

## References

1. Milo, R., Jorgensen, P., Moran, U., Weber, G. & Springer, M. BioNumbers The database of key numbers in molecular and cell biology. *Nucleic Acids Res.* **38**, 750–753 (2009).
2. Carmeliet, P. Angiogenesis in health and disease. *Nat. Med.* **9**, 653–660 (2003).
3. Aspelund, A., Robciuc, M. R., Karaman, S., Makinen, T. & Alitalo, K. Lymphatic System in Cardiovascular Medicine. *Circ. Res.* **118**, 515–530 (2016).
4. Olszewski, W. L. The lymphatic system in body homeostasis: physiological conditions. *Lymphat. Res. Biol.* **1**, (2003).
5. Tammela, T. & Alitalo, K. Lymphangiogenesis: Molecular Mechanisms and Future Promise. *Cell* **140**, 460–476 (2010).
6. Randolph, G. J., Ivanov, S., Zinselmeyer, B. H. & Scallan, J. P. The lymphatic system: Integral roles in immunity. *Annu. Rev. Immunol.* **35**, 31–52 (2017).
7. Randolph, G. J. & Miller, N. E. Lymphatic transport of high-density lipoproteins and chylomicrons. *J. Clin. Invest.* **124**, 929–935 (2014).
8. Bernier-Latmani, J. & Petrova, T. V. Intestinal lymphatic vasculature: Structure, mechanisms and functions. *Nat. Rev. Gastroenterol. Hepatol.* **14**, 510–526 (2017).
9. Potente, M., Gerhardt, H. & Carmeliet, P. Basic and therapeutic aspects of angiogenesis. *Cell* **146**, 873–887 (2011).
10. Hellström, M. *et al.* Dll4 signalling through Notch1 regulates formation of tip cells during angiogenesis. *Nature* **445**, 776–780 (2007).
11. Ricard, N., Bailly, S., Guignabert, C. & Simons, M. The quiescent endothelium: signalling pathways regulating organ-specific endothelial normalcy. *Nat. Rev. Cardiol.* **18**, 565–580 (2021).
12. Izumi, N. *et al.* Fbxw7 controls angiogenesis by regulating endothelial notch activity. *PLoS One* **7**, (2012).
13. Adams, R. H. & Alitalo, K. Molecular regulation of angiogenesis and lymphangiogenesis. *Nat. Rev. Mol. Cell Biol.* **8**, 464–478 (2007).
14. De Bock, K., Georgiadou, M. & Carmeliet, P. Role of endothelial cell metabolism in vessel sprouting. *Cell Metab.* **18**, 634–647 (2013).
15. Potente, M. & Carmeliet, P. The Link Between Angiogenesis and Endothelial Metabolism. *Annu. Rev. Physiol.* **79**, 43–66 (2016).
16. Cao, R. *et al.* Collaborative interplay between FGF-2 and VEGF-C promotes lymphangiogenesis and metastasis. *Proc. Natl. Acad. Sci. U. S. A.* **109**, 15894–15899 (2012).

17. Rajendran, P. *et al.* The vascular endothelium and human diseases. *Int. J. Biol. Sci.* **9**, 1057–1069 (2013).
18. Baluk, P. *et al.* Functionally specialized junctions between endothelial cells of lymphatic vessels. *J. Exp. Med.* **204**, 2349–2362 (2007).
19. Cleaver, O. & Melton, D. A. Endothelial signaling during development. *Nat. Med.* **9**, 661–668 (2003).
20. Park, C., Kim, T. M. & Malik, A. B. Transcriptional regulation of endothelial cell and vascular development. *Circ. Res.* **112**, 1380–1400 (2013).
21. Trimm, E. & Red-Horse, K. Vascular endothelial cell development and diversity. *Nat. Rev. Cardiol.* **20**, 197–210 (2023).
22. Lawson, N. D., Vogel, A. M. & Weinstein, B. M. Sonic hedgehog and vascular endothelial growth factor act upstream of the Notch pathway during arterial endothelial differentiation. *Dev. Cell* **3**, 127–136 (2002).
23. You, L. R. *et al.* Suppression of Notch signalling by the COUP-TFII transcription factor regulates vein identity. *Nature* **435**, 98–104 (2005).
24. Phng, L. K. & Gerhardt, H. Angiogenesis: A Team Effort Coordinated by Notch. *Dev. Cell* **16**, 196–208 (2009).
25. Benedito, R. & Hellström, M. Notch as a hub for signaling in angiogenesis. *Exp. Cell Res.* **319**, 1281–1288 (2013).
26. Spitz, F. & Furlong, E. E. M. Transcription factors: From enhancer binding to developmental control. *Nat. Rev. Genet.* **13**, 613–626 (2012).
27. Armulik, A., Abramsson, A. & Betsholtz, C. Endothelial/pericyte interactions. *Circ. Res.* **97**, 512–523 (2005).
28. Tabrizi, Z. B., Ahmed, N. S., Horder, J. L., Storr, S. J. & Benest, A. V. Transcription Factor Control of Lymphatic Quiescence and Maturation of Lymphatic Neovessels in Development and Physiology. *Front. Physiol.* **12**, 1–12 (2021).
29. La, H. *et al.* Role of Transcriptional and Epigenetic Regulation in Lymphatic Endothelial Cell Development. *Cells* **11**, (2022).
30. Petrova, T. V. *et al.* Lymphatic endothelial reprogramming of vascular endothelial cells by the Prox-1 homeobox transcription factor. *EMBO J.* **21**, 4593–4599 (2002).
31. Ducoli, L. & Detmar, M. Beyond PROX1: transcriptional, epigenetic, and noncoding RNA regulation of lymphatic identity and function. *Dev. Cell* **56**, 406–426 (2021).
32. Wilting, J. *et al.* The transcription factor Prox1 is a marker for lymphatic endothelial cells in normal and diseased human tissues. *FASEB J.* **16**, 1271–1273 (2002).

33. Aranguren, X. L. *et al.* Transcription factor COUP-TFII is indispensable for venous and lymphatic development in zebrafish and *Xenopus laevis*. *Biochem. Biophys. Res. Commun.* **410**, 121–126 (2011).
34. Mishima, K. *et al.* Prox1 Induces Lymphatic Endothelial Differentiation via Integrin  $\alpha 9$  and Other Signaling Cascades. *Mol. Biol. Cell* **18**, 986–994 (2007).
35. Shibuya, M. Vascular Endothelial Growth Factor (VEGF) and Its Receptor (VEGFR) Signaling in Angiogenesis: A Crucial Target for Anti- and Pro-Angiogenic Therapies. *Genes and Cancer* **2**, 1097–1105 (2011).
36. Sabine, A. FOXC2 and fluid shear stress stabilize postnatal lymphatic vasculature. *J. Clin. Invest.* **125**, 3861–3877 (2015).
37. Kazenwadel, J. *et al.* GATA2 is required for lymphatic vessel valve development and maintenance. *J. Clin. Invest.* **125**, 2979–2994 (2015).
38. Tacconi, C., He, Y., Ducoli, L. & Detmar, M. Epigenetic regulation of the lineage specificity of primary human dermal lymphatic and blood vascular endothelial cells. *Angiogenesis* **24**, 67–82 (2021).
39. Ducoli, L. *et al.* LETR1 is a lymphatic endothelial-specific lncRNA governing cell proliferation and migration through KLF4 and SEMA3C. *Nat. Commun.* **12**, 1–22 (2021).
40. Schulte-Merker, S., Sabine, A. & Petrova, T. V. Lymphatic vascular morphogenesis in development, physiology, and disease. *J. Cell Biol.* **193**, 607–618 (2011).
41. Maclellan, R. A. & Greene, A. K. Seminars in Pediatric Surgery Lymphedema. **23**, 191–197 (2014).
42. Grada, A. A. & Phillips, T. J. Lymphedema: Pathophysiology and clinical manifestations. *J. Am. Acad. Dermatol.* **77**, 1009–1020 (2017).
43. Carlson, J. A. Lymphedema and subclinical lymphostasis (microlymphedema) facilitate cutaneous infection, inflammatory dermatoses, and neoplasia: A locus minoris resistentiae. *Clin. Dermatol.* **32**, 599–615 (2014).
44. Sheik, Y., Qureshi, S. F., Mohammed, B. & Nallari, P. FOXC2 and FLT4 Gene Variants in Lymphatic Filariasis. *Lymphat. Res. Biol.* **13**, 112–119 (2015).
45. Bierhansl, L., Conradi, L.-C., Treppe, L., Dewerchin, M. & Carmeliet, P. Central Role of Metabolism in Endothelial Cell Function and Vascular Disease. *Physiology* **32**, 126–140 (2017).
46. Rohlenova, K., Veys, K., Miranda-Santos, I., De Bock, K. & Carmeliet, P. Endothelial Cell Metabolism in Health and Disease. *Trends Cell Biol.* **28**, 224–236 (2018).
47. Falkenberg, K. D., Rohlenova, K., Luo, Y. & Carmeliet, P. The metabolic engine of endothelial cells. *Nat. Metab.* **1**, 937–946 (2019).

48. García-Caballero, M. *et al.* Role and therapeutic potential of dietary ketone bodies in lymph vessel growth. *Nat. Metab.* **1**, 666–675 (2019).
49. Zhang, D. *et al.* PHGDH-mediated endothelial metabolism drives glioblastoma resistance to chimeric antigen receptor T cell immunotherapy. *Cell Metab.* **35**, 517-534.e8 (2023).
50. De Bock, K. *et al.* Role of PFKFB3-driven glycolysis in vessel sprouting. *Cell* **154**, 651–663 (2013).
51. Schoors, S. *et al.* Fatty acid carbon is essential for dNTP synthesis in endothelial cells. *Nature* **520**, 192–197 (2015).
52. Huang, H. *et al.* Role of glutamine and interlinked asparagine metabolism in vessel formation. *EMBO J.* **36**, 2334–2352 (2017).
53. Yu, P. *et al.* FGF-dependent metabolic control of vascular development. *Nature* **545**, 224–241 (2017).
54. Wilhelm, K. *et al.* FOXO1 couples metabolic activity and growth state in the vascular endothelium. *Nature* **529**, 216–220 (2016).
55. Andrade, J. *et al.* Control of endothelial quiescence by FOXO-regulated metabolites. *Nat. Cell Biol.* **23**, 413–423 (2021).
56. Vandekerke, S. *et al.* Serine Synthesis via PHGDH Is Essential for Heme Production in Endothelial Cells. *Cell Metab.* **28**, 573-587.e13 (2018).
57. Kalucka, J. *et al.* Quiescent Endothelial Cells Upregulate Fatty Acid  $\beta$ -Oxidation for Vasculoprotection via Redox Homeostasis. *Cell Metab.* **28**, 881-894.e13 (2018).
58. Wong, B. W. *et al.* The role of fatty acid  $\beta$ -oxidation in lymphangiogenesis. *Nature* **542**, 49–54 (2017).
59. Eelen, G. *et al.* Role of glutamine synthetase in angiogenesis beyond glutamine synthesis. *Nature* vol. 561 (2018).
60. Kim, B., Li, J., Jang, C. & Arany, Z. Glutamine fuels proliferation but not migration of endothelial cells. *EMBO J.* **36**, 2321–2333 (2017).
61. Zou, W. & Al-Rubeai, M. Understanding central carbon metabolism of rapidly proliferating mammalian cells based on analysis of key enzymatic activities in GS-CHO cell lines. *Biotechnol. Appl. Biochem.* **63**, 642–651 (2016).
62. Brieger, K., Schiavone, S., Miller, F. J. & Krause, K. H. Reactive oxygen species: From health to disease. *Swiss Med. Wkly.* **142**, 1–14 (2012).
63. Doddaballapur, A. *et al.* Laminar shear stress inhibits endothelial cell metabolism via KLF2-mediated repression of PFKFB3. *Arterioscler. Thromb. Vasc. Biol.* **35**, 137–145 (2015).
64. Vizán, P. *et al.* Characterization of the metabolic changes underlying growth factor angiogenic

- activation: Identification of new potential therapeutic targets. *Carcinogenesis* **30**, 946–952 (2009).
65. Kim, B. *et al.* Endothelial pyruvate kinase M2 maintains vascular integrity. *J. Clin. Invest.* **128**, 4543–4556 (2018).
66. Murohara, T. *et al.* Endothelial Cell Migration. *Arter. Thromb Vasc Biol.* 1156–1161 (1999).
67. Cooke, J. P. & Losordo, D. W. Nitric oxide and angiogenesis. *Circulation* **105**, 2133–2135 (2002).
68. Förstermann, U. & Münzel, T. Endothelial nitric oxide synthase in vascular disease: From marvel to menace. *Circulation* **113**, 1708–1714 (2006).
69. Förstermann, U. & Sessa, W. C. Nitric oxide synthases: Regulation and function. *Eur. Heart J.* **33**, 829–837 (2012).
70. Leopold, J. A. *et al.* Glucose-6-phosphate dehydrogenase modulates vascular endothelial growth factor-mediated angiogenesis. *J. Biol. Chem.* **278**, 32100–32106 (2003).
71. Fessel, J. P. *et al.* Metabolomic analysis of bone morphogenetic protein receptor type 2 mutations in human pulmonary endothelium reveals widespread metabolic reprogramming. *Pulm. Circ.* **2**, 201–213 (2012).
72. Inigo, M., Deja, S. & Burgess, S. C. Ins and Outs of the TCA Cycle: The Central Role of Anaplerosis. *Annu. Rev. Nutr.* **41**, 19–47 (2021).
73. Taniyama, Y. & Griendling, K. K. Reactive Oxygen Species in the Vasculature: Molecular and Cellular Mechanisms. *Hypertension* **42**, 1075–1081 (2003).
74. Santoro, M. M. Fashioning blood vessels by ROS signalling and metabolism. *Semin. Cell Dev. Biol.* **80**, 35–42 (2018).
75. Kuroki, M. *et al.* Reactive oxygen intermediates increase vascular endothelial growth factor expression in vitro and in vivo. *J. Clin. Invest.* **98**, 1667–1675 (1996).
76. Diebold, L. P. *et al.* Mitochondrial complex III is necessary for endothelial cell proliferation during angiogenesis. *Nat. Metab.* **1**, 158–171 (2019).
77. Petit, M., Koziel, R., Etemad, S., Pircher, H. & Jansen-Dürr, P. Depletion of oxaloacetate decarboxylase FAHD1 inhibits mitochondrial electron transport and induces cellular senescence in human endothelial cells. *Exp. Gerontol.* **92**, 7–12 (2017).
78. Ma, W. *et al.* Mitochondrial respiration controls the Prox1-Vegfr3 feedback loop during lymphatic endothelial cell fate specification and maintenance. 1–17 (2021).
79. Glatzel, D. K. *et al.* Acetyl-CoA carboxylase 1 regulates endothelial cell migration by shifting the phospholipid composition. *J. Lipid Res.* **59**, 298–311 (2018).
80. Karar, J. & Maity, A. PI3K/AKT/mTOR Pathway in Angiogenesis. *Front. Mol. Neurosci.* **4**, 1–8

- (2011).
81. Kasuno, K. *et al.* Nitric Oxide Induces Hypoxia-inducible Factor 1 Activation That Is Dependent on MAPK and Phosphatidylinositol 3-Kinase Signaling. *J. Biol. Chem.* **279**, 2550–2558 (2004).
  82. Graupera, M. *et al.* Angiogenesis selectively requires the p110 $\alpha$  isoform of PI3K to control endothelial cell migration. *Nature* **453**, 662–666 (2008).
  83. Bruning, U. *et al.* Impairment of Angiogenesis by Fatty Acid Synthase Inhibition Involves mTOR Malonylation. *Cell Metab.* **28**, 866-880.e15 (2018).
  84. Wei, X. *et al.* De Novo lipogenesis maintains vascular homeostasis through endothelial nitric-oxide synthase (eNOS) palmitoylation. *J. Biol. Chem.* **286**, 2933–2945 (2011).
  85. Deberardinis, R. J. & Cheng, T. Q's next: The diverse functions of glutamine in metabolism, cell biology and cancer. *Oncogene* **29**, 313–324 (2010).
  86. Williams, N. C. & O'Neill, L. A. J. A role for the krebs cycle intermediate citrate in metabolic reprogramming in innate immunity and inflammation. *Front. Immunol.* **9**, 1–11 (2018).
  87. Yoo, H. C., Yu, Y. C., Sung, Y. & Han, J. M. Glutamine reliance in cell metabolism. *Exp. Mol. Med.* **52**, 1496–1516 (2020).
  88. Reid, M. A. *et al.* Serine synthesis through PHGDH coordinates nucleotide levels by maintaining central carbon metabolism. *Nat. Commun.* **9**, 1–11 (2018).
  89. Rohlenova, K. *et al.* Single-Cell RNA Sequencing Maps Endothelial Metabolic Plasticity in Pathological Angiogenesis. *Cell Metab.* **31**, 862-877.e14 (2020).
  90. Goveia, J. *et al.* An Integrated Gene Expression Landscape Profiling Approach to Identify Lung Tumor Endothelial Cell Heterogeneity and Angiogenic Candidates. *Cancer Cell* **37**, 21-36.e13 (2020).
  91. Gambardella, J. *et al.* Arginine and Endothelial Function. *Biomedicines* **8**, (2020).
  92. Kalucka, J. *et al.* Single-Cell Transcriptome Atlas of Murine Endothelial Cells. *Cell* **180**, 764-779.e20 (2020).
  93. Paik, D. T. *et al.* Single-Cell RNA Sequencing Unveils Unique Transcriptomic Signatures of Organ-Specific Endothelial Cells. *Circulation* **142**, 1848–1862 (2020).
  94. Dumas, S. J., García-Caballero, M. & Carmeliet, P. Metabolic Signatures of Distinct Endothelial Phenotypes. *Trends Endocrinol. Metab.* **31**, 580–595 (2020).
  95. Li, Q. *et al.* Single-cell transcriptome profiling reveals vascular endothelial cell heterogeneity in human skin. *Theranostics* **11**, 6461–6476 (2021).
  96. Lee, H. J. *et al.* Proteomic and Metabolomic Characterization of a Mammalian Cellular Transition from Quiescence to Proliferation. *Cell Rep.* **20**, 721–736 (2017).



97. Patti, G. J., Yanes, O. & Siuzdak, G. Metabolomics: the apogee of the omics trilogy. *Nat. Rev. Mol. Cell Biol.* **13**, 263–269 (2012).
98. Roberts, L. D., Souza, A. L., Gerszten, R. E. & Clish, C. B. Targeted metabolomics. *Curr. Protoc. Mol. Biol.* **1**, (2012).
99. Zamboni, N., Saghatelian, A. & Patti, G. J. Defining the Metabolome: Size, Flux, and Regulation. *Mol. Cell* **58**, 699–706 (2015).
100. Sévin, D. C., Kuehne, A., Zamboni, N. & Sauer, U. Biological insights through nontargeted metabolomics. *Curr. Opin. Biotechnol.* **34**, 1–8 (2015).
101. Fuhrer, T., Heer, D., Begemann, B. & Zamboni, N. High-Throughput, Accurate Mass Metabolome Profiling of Cellular Extracts by Flow Injection–Time-of-Flight Mass Spectrometry. *Anal. Chem.* **83**, 7074–7080 (2011).
102. Cuevas-Delgado, P., Dudzik, D., Miguel, V., Lamas, S. & Barbas, C. Data-dependent normalization strategies for untargeted metabolomics—a case study. *Anal. Bioanal. Chem.* **412**, 6391–6405 (2020).
103. Picotti, P. & Aebersold, R. Selected reaction monitoring-based proteomics: Workflows, potential, pitfalls and future directions. *Nat. Methods* **9**, 555–566 (2012).
104. Gillet, L. C., Leitner, A. & Aebersold, R. Mass Spectrometry Applied to Bottom-Up Proteomics: Entering the High-Throughput Era for Hypothesis Testing. *Annu. Rev. Anal. Chem.* **9**, 449–472 (2016).
105. Bhargava, M., Higgins, L., Wendt, C. H. & Ingbar, D. H. Application of clinical proteomics in acute respiratory distress syndrome. *Clin. Transl. Med.* **3**, 1–11 (2014).
106. Al Shweiki, M. H. D. R. *et al.* Assessment of Label-Free Quantification in Discovery Proteomics and Impact of Technological Factors and Natural Variability of Protein Abundance. *J. Proteome Res.* **16**, 1410–1424 (2017).
107. Garcia-Alonso, L., Holland, C. H., Ibrahim, M. M., Turei, D. & Saez-Rodriguez, J. Benchmark and integration of resources for the estimation of human transcription factor activities. *Genome Res.* **29**, 1363–1375 (2019).
108. Badia-I-Mompel, P. *et al.* decoupleR: ensemble of computational methods to infer biological activities from omics data. *Bioinforma. Adv.* **2**, 1–3 (2022).



## Chapter 2

### **Development of a multi-omics workflow to study the molecular patterns underlying proliferative and quiescent endothelial cells**

Stephan Durot<sup>1</sup>, Peter F. Doubleday<sup>1</sup>, Nicola Zamboni<sup>1</sup>

<sup>1</sup> Institute of Molecular Systems Biology, ETH Zürich, Otto-Stern-Weg 3, 8093 Zürich, Switzerland

Stephan Durot designed the study, conducted all the experiments, performed all data analyses, normalizations and visualizations and wrote the chapter. Peter F. Doubleday set up the LC-MS method for proteomics and supported proteomics sample preparation and data analysis and contributed to the writing. Nicola Zamboni helped designing the study, supervised and contributed to the writing.

## Abstract

The cardiovascular and lymphatic systems are networks of endothelial cells (ECs) and are crucial for tissue homeostasis. Mostly quiescent in the mature vasculature, ECs can proliferate again to form new vessels and disruptions in this process leads to vasculature-related diseases. Here, we aimed to develop a workflow that allows us to study and better understand the complexity and diversity of molecular patterns that underlie a proliferative and quiescent state. To that end, we developed an experimental workflow in which two blood and two lymphatic EC types proliferate and subsequently transition into quiescence. We performed untargeted extra- and intracellular metabolomics and proteomics with samples taken every 24 hours, allowing us to generate a comprehensive description of the dynamic molecular patterns in different proliferative states. We could show that with the applied normalization techniques for metabolomics and proteomics data, we conserve biological information like the expression of LEC- and BEC-specific marker proteins as well as markers of proliferation. Furthermore, we observed that metabolic pathway dynamics is inversed when quiescent cells are reseeded and proliferate again, confirming that we capture the relevant metabolic information in the transition from proliferation to quiescence and vice versa. Thus, the generated multi-omics datasets will be a valuable resource for data-driven analysis in the next chapters.

## Introduction

Endothelial cells (ECs) line up the cardiovascular and lymphatic systems, two systems that are crucial for tissue homeostasis<sup>1,2</sup>. ECs remain quiescent in the mature vasculature but migrate and proliferate in order to form new vessels upon external stimulation and subsequently become quiescent again<sup>3-5</sup>. Several diseases of the cardiovascular and lymphatic system emerge from malfunctioning ECs, for example if there is a disruption of the proliferation-quiescence balance<sup>6,7</sup>. In recent years, studies showed that metabolism plays a pivotal role in the formation and maintenance of a proliferating and quiescent state<sup>8-13</sup>. Moreover, there is a heterogeneity in metabolic proteins transcript levels between ECs from different tissues and vascular beds<sup>14,15</sup>. Therefore, it is important to study tissue- and vascular bed-dependent cellular

metabolic patterns in order to understand the extend of the metabolic variance between ECs and the impact of it on different phenotypes and cellular functions.

Cellular metabolism describes all the chemical reactions happening inside a cell that are needed to convert food into an available form of energy to run cellular processes, to provide building blocks for macromolecules and for waste elimination. Moreover, metabolism plays a major role in integrating environmental and intracellular signals and thus supporting cellular decision processes crucial for differentiation and formation of phenotypes of various mammalian cell types, including ECs<sup>8,13,16–19</sup>. There are different ways to measure or infer cellular metabolism. A technique that directly measures metabolite abundances is mass spectrometry-based untargeted metabolomics. It enables a comprehensive measurement of metabolite abundances in a sample, like intracellular metabolomes or supernatants of cell culture, and hence provides the opportunity to study the metabolic patterns that underlie cellular phenotypes<sup>20</sup>. With label-free quantitative (LFQ) proteomics, the quantities of thousands of proteins are determined simultaneously, including metabolic enzymes<sup>21</sup>. By mapping the quantities of enzymes on the metabolic network, one can infer which metabolic pathways play an important role in a certain phenotype. However, activities of metabolic fluxes are not only dependent on enzyme quantities but also on enzyme activities and regulation, limiting the interpretability of proteomics results. A very similar approach with the same limitation is transcriptomics, in which the abundances of gene transcripts are determined and subsequently as well mapped onto the metabolic network to infer usage of metabolic pathways.

The limitations of most studies on EC metabolism so far are that they either focus on very few specific metabolic pathways, especially in central carbon metabolism, and that they use transcriptomics approaches to infer metabolic activities or that they are done only on human umbilical vein ECs (HUVECs). These limitations confine the understanding of the true complexity of metabolic variability between different EC types and states. So, our goal was to obtain an experimental setup to study metabolism of ECs from different tissues and vascular beds in a proliferating and quiescent state directly through untargeted metabolomics and proteomics. To that end, we used contact inhibition and mitogen reduction to induce quiescence, measured the fraction of quiescent cells and performed extra- and intracellular untargeted metabolomics and proteomics every 24 hours. In our experimental setup, most cells are proliferating after 2 days and undergo transition into quiescence, thereafter,

reaching a mostly quiescent state on day 5. We applied data normalization on metabolomics and proteomics data to account for batch effects and could show that cell-specific temporal metabolic and proteomic patterns are conserved. With this dataset at hand, we will be able to study molecular patterns that define EC phenotypes and to examine the complexity of EC metabolism.

## Results

### Contact inhibition and mitogen reduction induces a strong quiescent state in endothelial cells

We aimed to develop a workflow that enables us to study the molecular patterns that underlie a proliferative and quiescent state of representable endothelial cell (EC) types. We chose the four endothelial cell types human umbilical vein endothelial cells (HUVEC), human dermal blood endothelial cells (HDBEC), human dermal lymphatic endothelial cells (HDLEC) and intestinal lymphatic endothelial cells (iLEC). Using these four cell types, we can study the fundamental differences between blood and lymphatic vessel derived ECs, as well as the difference between ECs from the same vascular beds but from different tissues.

The first goal was to identify conditions that allow to obtain populations of either quiescent or proliferating cells. Quiescence can be induced *in vitro* by growing cells to full confluence (Fig. 1A)<sup>13,22</sup>. Additionally, we tested two different growth media to assess whether the amount of specific growth factors (GF) influences growth and quiescence induction. One medium was the standard growth medium for endothelial cells, endothelial growth medium 2 (EGM-2), the other medium was a 1/1 (v/v) mix of EGM-2 with medium 199 (M199). In the EGM-2/M199 growth medium, fibroblast GF (FGF), vascular endothelial GF (VEGF), epidermal GF (EGF) and insulin-like GF (IGF) that are part of EGM-2, are thus reduced by 50%. We first seeded HUVECs at a density of 20'000 cells/cm<sup>2</sup> with either of the two growth media and assessed growth dynamics with automated time-lapse microscopy. We found no significant effect of the two media on growth (Fig. 1B). Next, we wanted to determine the fraction of proliferating cells after each day of growing the cells for 10 days in the same plate. To that end, we added 10µM of the DNA synthesis monitoring probe ethynyl-2'-deoxyuridine (EdU) 24 hours before each time point and measured the fraction of EdU-positive cells, a proxy for

proliferation, on a cell analyzer<sup>23</sup>. We observed a significant increase of EdU-negative, thus quiescent cells, at day 4 to day 10 for HUVECs that grew in EGM-2/M199 medium compared to EGM-2 medium only (Fig. 1C).

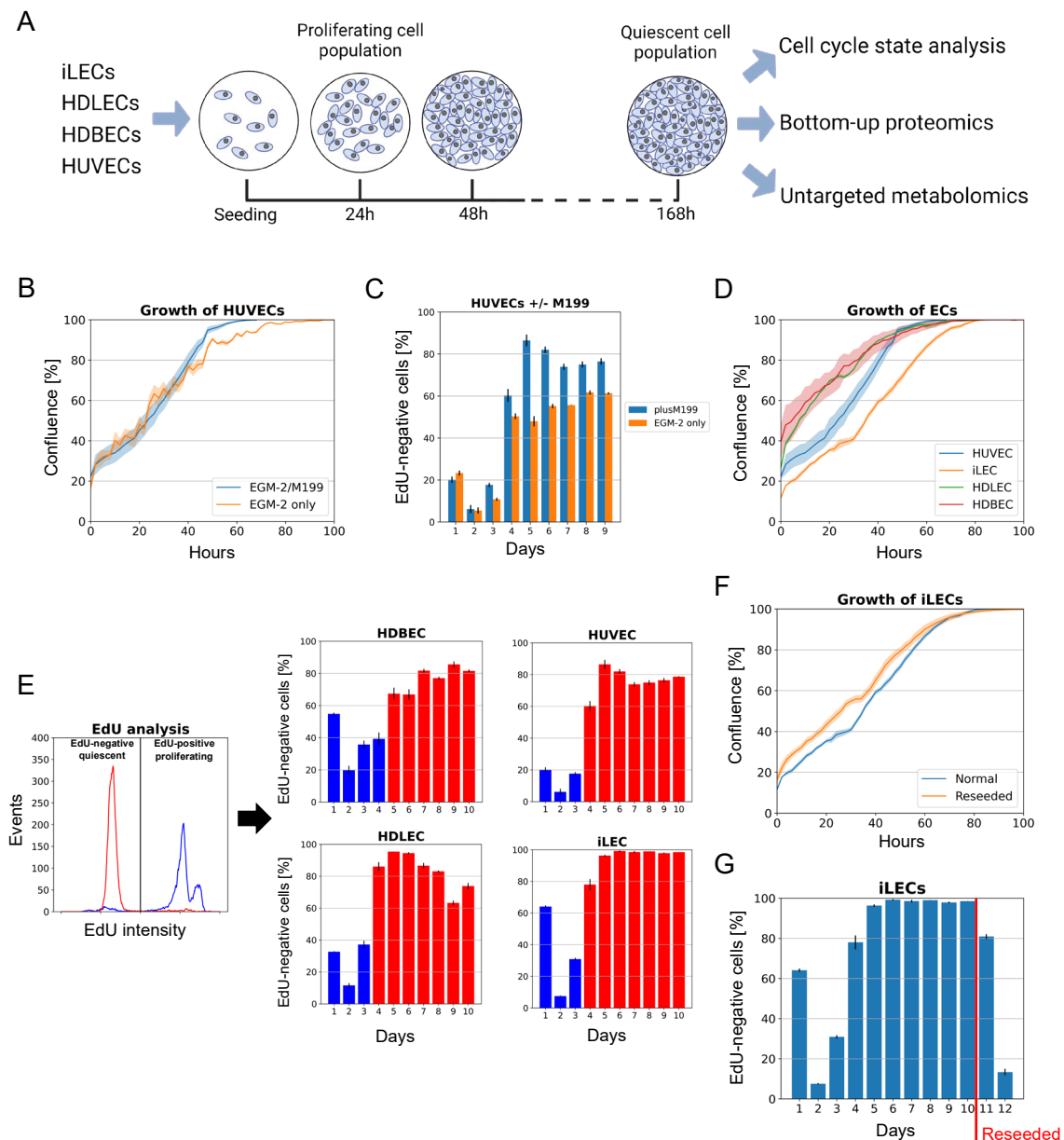


**Figure 1. Contact inhibition and mitogen reduction induces a strong quiescent state in endothelial cells.**

- (A) Experimental setup.  $n = 3$  replicates per day and cell line for each measurement.  
 (B) Growth curves of HUVECs in EGM-2 only or EGM-2/M199 medium.  
 (C) Fraction of EdU-negative, quiescent HUVECs grown in EGM-2 only or EGM-2/M199 medium.  
 (D) Growth curves of all EC types in EGM-2/M199 medium.  
 (E) Fraction of EdU-negative, quiescent cells in all EC types grown in EGM-2/M199 medium.  
 (F) Growth curves of iLECs in the normal setup and when reseeded after 10 days grown in the same vessel.  
 (G) Fraction of EdU-negative, quiescent iLECs in the normal setup as well as 24 and 48 hours after reseeding.

We performed the same growth measurements and EdU incorporation assay with EGM-2/M199 medium with the other three cell types. Due to different sizes of the cell types and some variations in the segmentation of the microscopy pictures, the starting confluence varied between 15% for iLECs and 40% for HDBECs (Fig. 1D). All cell types reached full confluence after 60 to 80 hours. The fraction of quiescent cells increased in all four cell types after day 2, the strongest in iLECs and HDLECs, in which more than 95% of cells were quiescent after day 5 (Fig. 1E). The effect was less prominent in HDBECs, but they still reached 67% quiescent cells after 5 days. One reason for the slightly lower fraction of quiescent cells in HDBECs, and to a lesser extent in HUVECs, is that they started to grow in 3D (Suppl. Fig. 1). Taken together, contact inhibition and a reduction of specific growth factors leads to strong induction of quiescence in all four cell types.

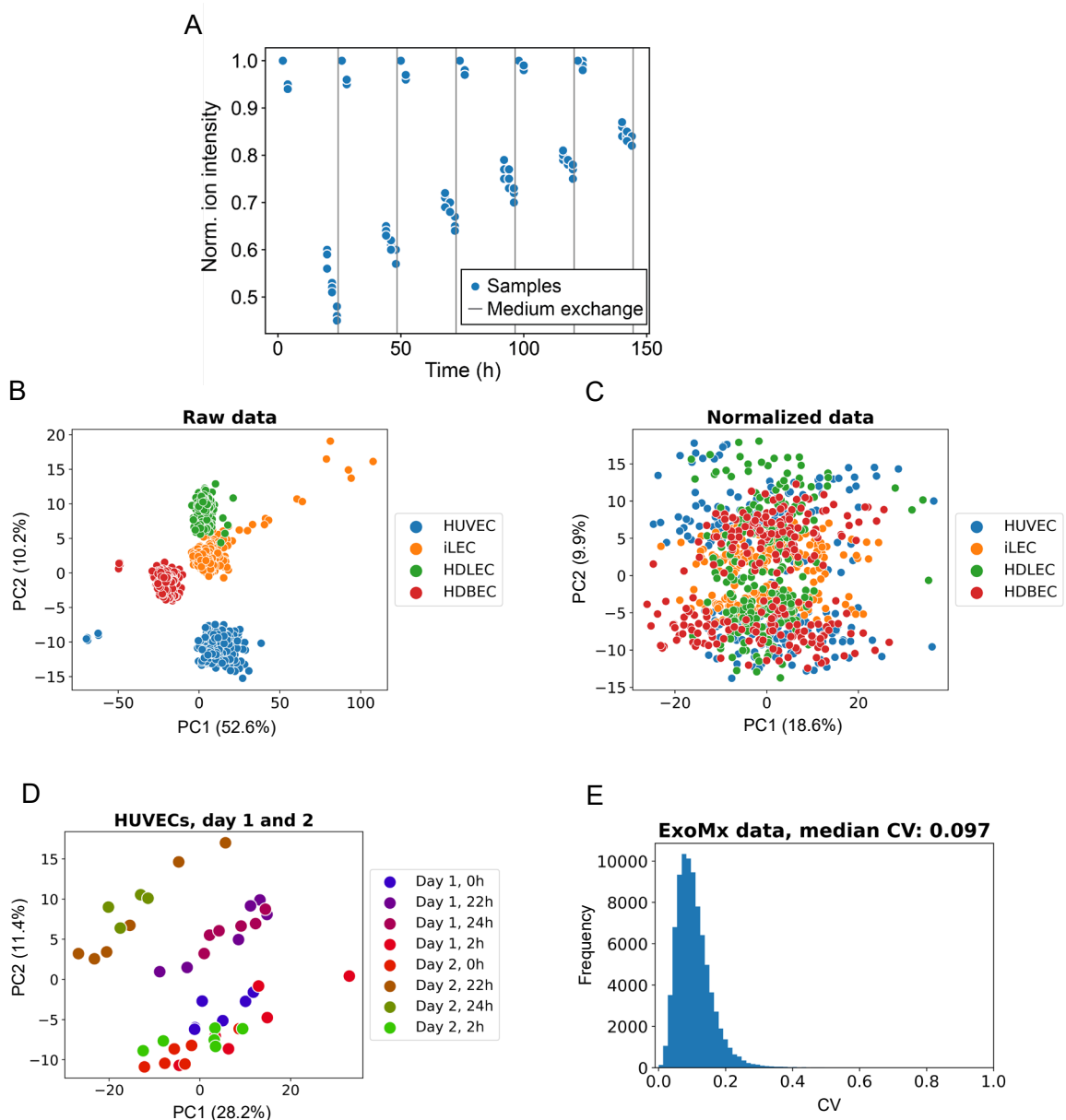
Given that almost 100% of iLECs were quiescent after 10 days, we wondered whether the cells were indeed only quiescent and would therefore start growing again when seeded at a lower confluence. Upon reseeded of cells grown for 10 days in the same plate, we observed an immediate resumption of growth (Fig. 1F). Furthermore, the fraction of quiescent cells of reseeded iLECs reduced from almost 100% to around 15% 48 hours post-reseeding, indicating that these cells have the capacity to proliferate again even when kept in quiescence for as long as 10 days (Fig. 1G).

## **An experimental setup to measure uptake and secretion rates of extracellular metabolites**

Extracellular metabolomics is a useful tool to infer general metabolic activity of cells. We developed a setup in which supernatant samples are taken over 24 hours and can be used in a linear regression to determine uptake and secretion rates of metabolites (Fig. 2A). To that end, we exchanged growth medium every 24 hours, took samples of cellular supernatants between each medium exchange (0 hours, 2 hours, 22 hours and 24 hours after exchange) and conducted mass spectrometry-based, untargeted metabolomics measurements, resulting in the annotation of 521 metabolites in all samples (Fig. 2A)<sup>24</sup>. Mass spectrometry-based metabolomics is a very sensitive technique and underlies temporal variation that leads to batch effects. Such temporal batch effects were observed in our extracellular metabolomics dataset because the



samples from the different EC types were analyzed at different days (Fig. 2B). We applied a moving median-based temporal drift normalization to remove batch effects, making sure that the temporal metabolic diversity within a cell type is not affected (Fig. 2C, 2D). High reproducibility between biological replicates after normalization was highlighted by the median coefficient of variation of 9.7% between biological replicates (Fig. 2E). The presented workflow for extracellular metabolomics provides dynamic uptake and secretion data with high intra-sample reproducibility, and preliminary results showed that we are indeed able to capture cell state- and type-specific uptake and secretion patterns (Fig. 2C, 2D).



(legend on next page)

**Figure 2. An experimental setup to systematically study uptake and secretion rates of extracellular metabolites.**

- (A) Experimental setup to determine uptake and secretion rates of metabolites.  $n = 6$ , 3 biological and 2 technical replicates per day and cell line for each measurement.
- (B) Principal component analysis (PCA) of the raw extracellular metabolomics data.
- (C) PCA of the data after moving median normalization to correct for temporal batch effects.
- (D) PCA of day 1 and day 2 HUVEC samples illustrates the cell-specific temporal variability in the data.
- (E) Distribution of coefficients of variations between the three biological replicates.

## **ECs exhibit state-dependent, reversible intracellular metabolic patterns**

On top of the general metabolic activity of cells, we aimed to analyse intracellular metabolomes to deepen our understanding of which metabolic features support the transition into and maintenance of EC quiescence. Therefore, we performed mass spectrometry-based, untargeted metabolomics of intracellular metabolites that were extracted every 24 hours in all four cell types<sup>24</sup>. By using an untargeted measurement, we were able to annotate 1413 metabolites across all cell types. Just as in the extracellular metabolomics experiments, intracellular metabolomics data exhibited temporal batch effects because these samples were also measured at different days (Fig. 3A). We applied again a moving median-based temporal drift normalization to remove temporal trends, followed by a mean normalization to account for biomass differences at the time of metabolite extraction. The resulting dataset did not show batch effects anymore (Fig. 3B). Moreover, the temporal metabolic patterns within a cell type were still conserved, and the variance between biological replicates is minimal (median CV = 3.1%) (Fig. 3C, 3D).

While iLECs that transit from proliferation to quiescence exhibited various temporal metabolic patterns, it remained unclear when and what kind of metabolic patterns would appear when cells go from quiescence to proliferation. Thus, we conducted metabolomics measurements of iLECs that were grown to quiescence for 10 days and reseeded at 20'000 cells/cm<sup>2</sup>. Briefly, we reseeded iLECs and extracted intracellular metabolites every 2 hours from seeding to 12 hours post-seeding and every 6 hours after that until 48 hours post-seeding and analyzed the extracted metabolomes as in the time-series experiments. While there was no clear metabolic distinction of samples between 2 up to 18 hours in the principal component analysis, later time point samples started to distinguish themselves from the early samples (Fig. 3E). We then performed a differential analysis between all samples and the 2 hours samples with subsequent pathway enrichment analysis to infer the metabolic pathway

usage over time and compared it with the normal time-series experiment. Interestingly, reseeded iLECs showed inversed metabolic profiles to the time-series experiment, which means that the same metabolic pathways play an important, yet inversed role in supporting transition into and out of quiescence, respectively (Suppl. Fig. 2). To summarize, untargeted metabolomics measurements with subsequent data normalization resulted in a comprehensive dataset that allows us to study metabolic patterns in proliferating, quiescent and transiting ECs.

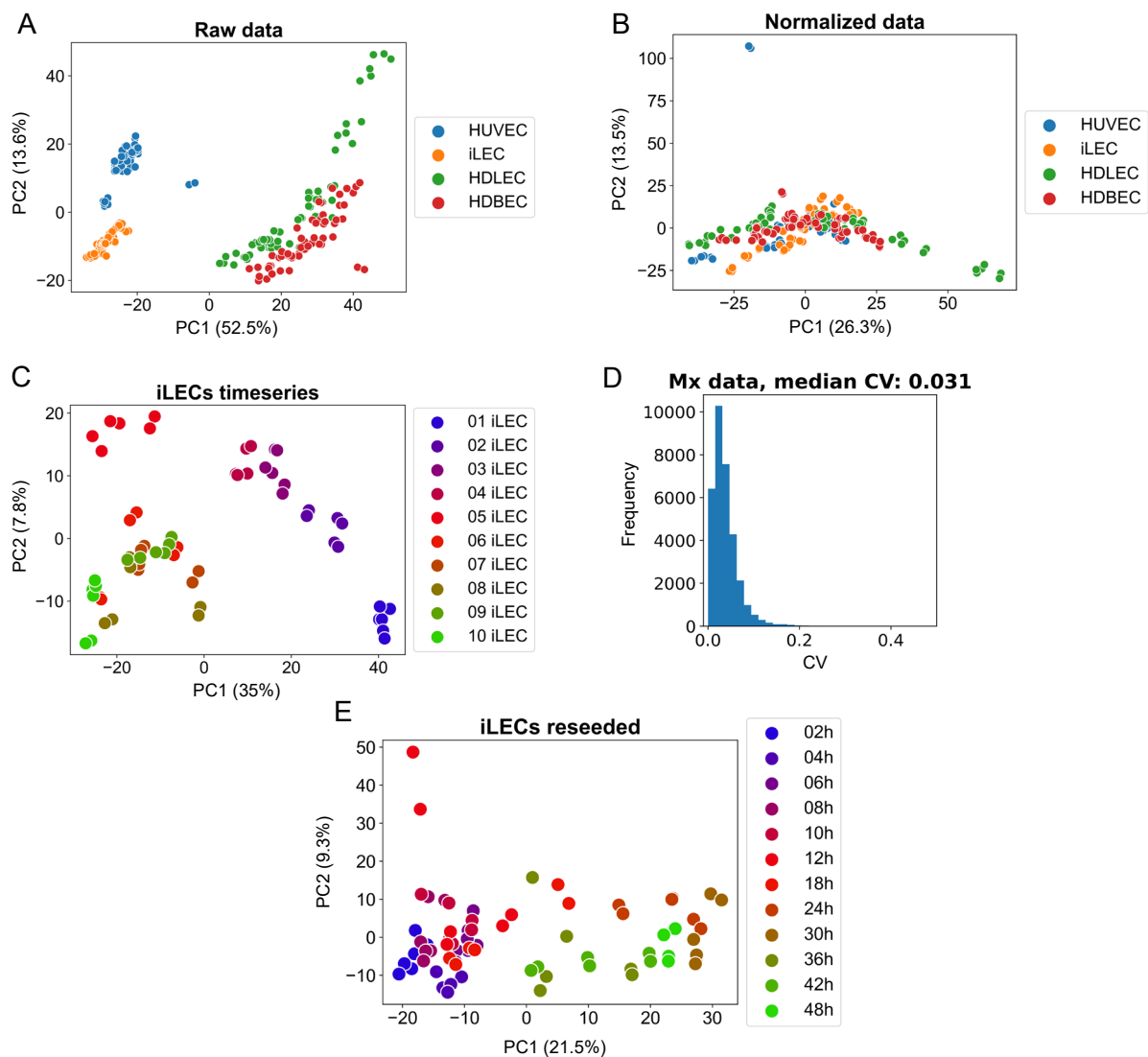


**Figure 3. ECs exhibit state-dependent, reversible intracellular metabolic patterns.**

- (A) PCA of the raw intracellular metabolomics data.  $n = 6$ , 3 biological and 2 technical replicates per day and cell line for each measurement.
- (B) PCA of the data after moving median normalization to correct for temporal batch effects and mean normalization to correct for biomass differences at the time of sampling.
- (C) PCA of iLECs samples illustrates the cell-specific temporal variability in the data.
- (D) Distribution of coefficients of variations between the three biological replicates.
- (E) PCA of reseeded iLECs.

## **Label-free quantitative proteomics workflow to study protein expression patterns in different cell types and states**

Label-free quantitative proteomics is a technique to measure the quantities of thousands of proteins simultaneously. Hence, it is a convenient tool to study the proteomic patterns that define cell type identities and states in our screen. We performed label-free quantitative proteomics on all cell types at each day between day 2 and day 7, when cells undergo the transition from proliferation to quiescence. To that end, we seeded the cells at a density of 20'000 cells/cm<sup>2</sup>, lysed them in 8M urea buffer with subsequent sonication, reduced and alkylated the proteins and trypsinized and desalted them (Fig. 4A)<sup>25,26</sup>. The resulting peptides were measured by LC-MS/MS, in which the peptides were first separated by a 90 minutes gradient on a C18 column and subsequently analyzed on an orbitrap mass spectrometer using a data-independent analysis (DIA) approach (Fig. 4A)<sup>27</sup>. The resulting raw files were converted to mzML files via MSConvert and were subjected to a neural network-based DIA processing software called DIA-NN, which enabled the identification and quantification of proteins in our samples (Fig. 4A)<sup>28,29</sup>. Finally, protein intensities were normalized using the normalization procedure maxLFQ<sup>21</sup>. This is an important step as it ensures comparable quantities of proteins between the cell types and days and within biological replicates (Fig. 4B, 4C).

The final dataset contained 7894 protein groups that were discovered at a 1% protein group-level false discovery rate cut-off. Principal component analysis of all samples showed distinction between blood and lymphatic endothelial cells after normalization (Fig. 4D). Moreover, we checked if cell type and state specific marker proteins showed an expected expression pattern. Indeed, the LEC- and BEC-specific markers LYVE1 and STAT6, respectively, had clear expression patterns in either cell types (Fig. 4E)<sup>30,31</sup>. Furthermore, Marker Of Proliferation Ki-67 (MKI67) and proliferating cell nuclear antigen (PCNA), two markers of proliferation, were consistently lower expressed in quiescent cells (Fig. 4F)<sup>32,33</sup>.

In our full dataset, 3333 proteins were detected in all samples. It is common to perform data imputation for missing values in gene expression or sequencing experiments. We wondered whether data imputation might help to fill missing values in our dataset. Thus, we applied a random forest-based imputation method to fill the missing intensities in the remaining 4561 proteins for which the measured data was

incomplete<sup>34</sup>. Generally, the imputed values were on the lower scale of intensities (Suppl. Fig. 3A). However, when looking at cell type-specific markers, for example PROX1 for LECs and STAT6 for BECs, data imputation created intensity values for these proteins, even though they are most likely not expressed in the respective cell types (Suppl. Fig. 3B, 3C). We therefore moved on with the original dataset without imputation. Taken together, these results show that with the applied measurement and data processing steps, we were able to create a comprehensive protein expression dataset enabling us to compare expression patterns within and between cell types and states.

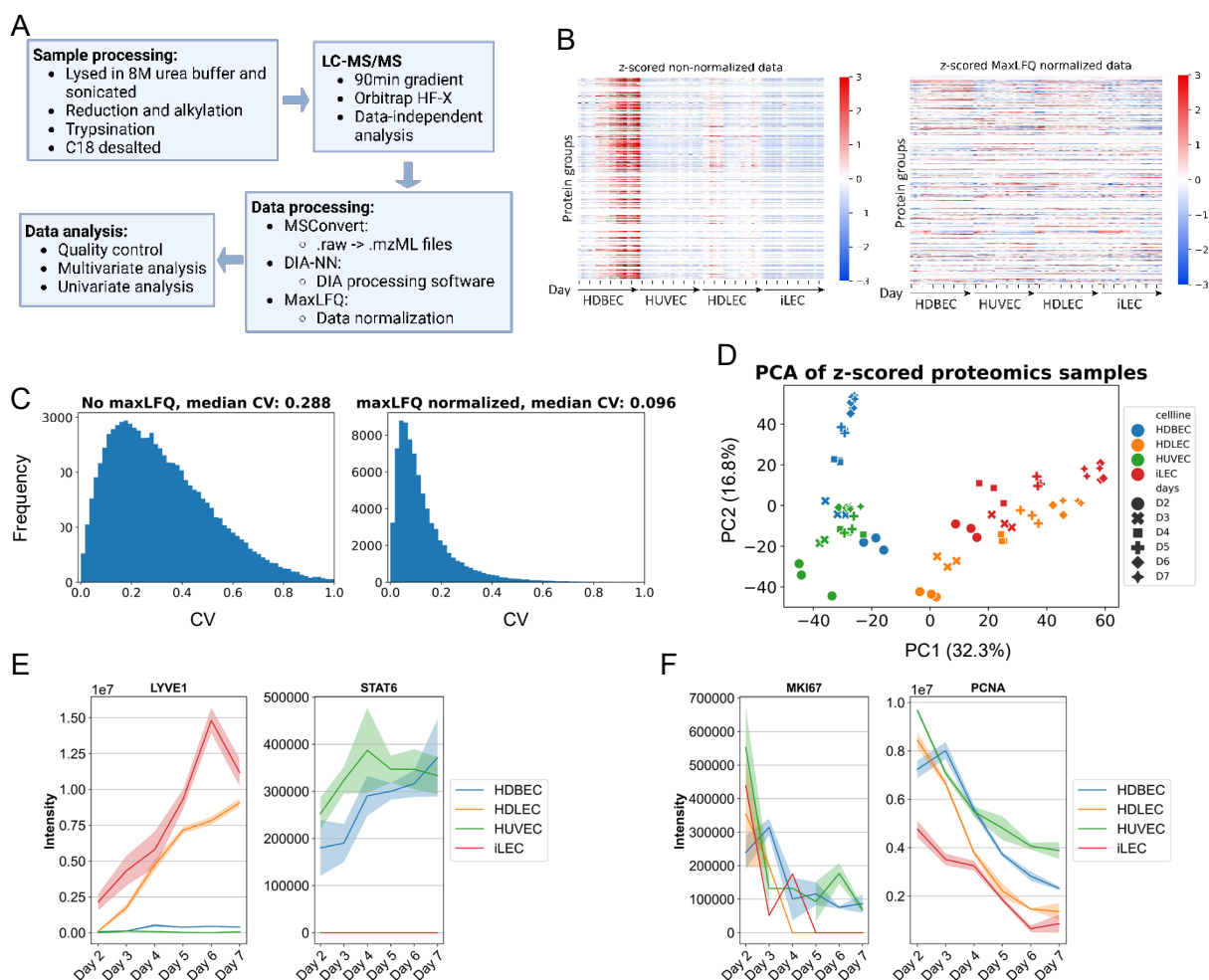


**Figure 4. Label-free quantitative proteomics workflow to study protein expression patterns in different cell types and states.**

- (A) Workflow of label-free quantitative proteomics.  $n = 3$  biological replicates per day and cell line for each measurement.
- (B) Z-scored intensities of protein groups before (left panel) and after (right panel) maxLFQ normalization.
- (C) Distribution of coefficients of variations between the three biological replicates before (left panel) and after (right panel) maxLFQ normalization.
- (D) PCA of z-scored proteomics dataset.
- (E) Intensities of the LEC marker LYVE1 and BEC marker STAT6.
- (F) Intensities of the proliferation markers MKI67 and PCNA.

## Discussion

The presented experimental workflow allows us to study the molecular patterns that define endothelial cell types and states. Using the exact same experimental setup for four endothelial cell types and subsequent normalization techniques applied on the metabolomics and proteomics data, we generated a further resource that enables us to not only study the molecular patterns in each cell type individually but make them comparable between the cell types to distill cell type-specific molecular peculiarities. This is a further step towards understanding EC biology and helps us to assess the diversity of metabolism and protein levels among endothelial cells from different tissues and vascular beds.

Although all cell types were mostly proliferating at day 2 and quiescent at day 5 in our screen, induction of quiescence seemed to be a bit stronger in LECs compared to BECs, which was also reflected in the slightly higher expression of the proliferation markers MKI67 and PCNA in BECs after day 5. However, the dynamics of the transition from proliferation into quiescence followed the same pattern in the four cell types and therefore the experimental setup proved to be useful, nevertheless. In vivo, upon activation, quiescent endothelial cells start to migrate and proliferate and build new vessels <sup>35</sup>. It is consequently important to examine the phenotype and molecular patterns when quiescent cells start to proliferate again. From all ECs, iLECs have the highest fraction of quiescent cells throughout day 5 to day 10 and are most suitable to study the phenotype and metabolic patterns when reseeded. We found that they immediately started to grow again, resulting in a high fraction of proliferating cells 48 hours post-seeding and metabolic patterns that were inverse to the contact inhibition setup. This result showed us that either setup can be used to study proliferation and quiescence of endothelial cells.

Batch effects in metabolomics measurements are a common problem and can have multiple reasons <sup>36</sup>. The extra- and intracellular metabolomics samples in our screen showed batch effects. Since we used the exact experimental setup for each cell type, these batch effects are most likely due to temporal reasons. The applied moving median-based normalization approach is a simple and gentle, yet effective method to correct for temporal batch effects. Additionally, we performed a mean normalization on intracellular metabolomics samples. This is again a gentle normalization method to account for biomass differences. By using these two

normalization methods, we made sure that the temporal metabolic variance within a cell type was conserved, which was indeed the case and important for further data analysis.

Compared to metabolomics, sample preparation in proteomics is more complex and includes many more steps that are prone for errors. Even though we normalized for protein concentrations before trypsination, we observed batch effects in the proteomics samples, likely arising from the last steps of sample preparation (C18 desalting), from the LC-MS/MS measurements and biological origin (biomass differences). By applying maxLFQ normalization, we could diminish these effects and improve reproducibility between biological replicates. As with the metabolomics samples, temporal proteomic variance within cell types was still conserved, both at the global level, as seen in the PCA, and for expected individual proteins, such as the proliferation markers MKI67 and PCNA. MaxLFQ normalization also conserved cell type-specific information, like LEC-specific LYVE1 and BEC-specific STAT6 expression. Interestingly, LYVE1 expression increased in LECs over time. LYVE1 is a characteristic molecular feature of capillary LECs<sup>30</sup>. Hence, increased expression of LYVE1 suggests that LECs that are grown *in vitro* acquire a capillary-like molecular phenotype only after transition into quiescence. Accordingly, for *in vitro* experiments with LECs that should have capillary-like molecular patterns, it might be advisable to perform experiments on LECs that have been in culture for at least 4 days.

There are several limitations that must be kept in mind using this experimental setup. Although we observed metabolic and proteomic diversity between the cell types, growing ECs in monoculture in a defined medium *ex vivo* mitigates the true molecular complexity that is most likely also influenced by their microenvironment, such as shear stresses from blood and lymph flow, interaction with other cell types, nutrient and oxygen availability or the presence of tissue-specific signals. Further experiments with microfluidic devices to imitate blood and lymph flow or co-cultures for cell-cell interactions could add an additional, *in vivo*-like layer to the molecular description of various EC types<sup>37-39</sup>. Also, we assumed that the lack of DNA synthesis is a proxy of quiescence; however, we do not know exactly at which cell cycle state the cells stopped, it could be either G0, G1 or even G2/M. One possibility to assess the exact cell cycle state in the future would be staining and measurement of DNA and RNA content because cells in G0 are assumed to have the same amount of DNA as in G1, but less RNA<sup>22</sup>.

## Materials and Methods

### Cell culture

Human umbilical vein endothelial cells were purchased from Lonza (cat. no. C2519A), human dermal blood endothelial cells (cat. no. C-12211) and human dermal lymphatic endothelial cells (cat. no. C-12216) from PromoCell. Intestinal lymphatic endothelial cells are a kind gift from Tatiana Petrova from the University of Lausanne. All endothelial cells were cultured in T-75 cell culture flasks (Thermo Fisher Scientific, cat. no. 156472) in Endothelial Cell Growth Medium-2 (EGM-2) (BulletKit, Lonza, cat. no. CC-3162). EGM2 was made from Endothelial Cell Basal Medium-2 (EBM2), with added endothelial supplements including 2% fetal bovine serum (FBS) (v/v), hydrocortisone, VEGF, human FGF, R3-IGF-1, ascorbic acid, human EGF, glutaraldehyde GA-1000, and heparin. Additionally, we added 10mg/ml ciprofloxacin (Sigma-Aldrich, cat. no. 17850). After the first passage, regular FBS in the culture medium was replaced by dialyzed FBS (dFBS, Sigma-Aldrich, cat. no. F0392). Experiments were performed until passage six. For metabolomics, proteomics and phenotype experiments, cells were seeded at a density of 20'000 cells/cm<sup>2</sup> in a mixed medium (MM). MM consists of 50% EGM2 (with dFBS) and 50% Medium 199 (Gibco, cat. no. 22340020) supplemented with 20% dFBS, 1% penicillin/streptomycin (P/S, Gibco, cat. no. 15140122), 2mM glutamine (Gibco, cat. no. 25030081) and 0.4% (v/v) endothelial cell growth supplement (PromoCell, cat. no. C-39215).

### Quiescence induction and cell cycle analysis

ECs were grown for 10 days to assess fractions of proliferating and quiescent cells at each day. The fraction was determined by EdU incorporation into DNA using the EdU Flow Cytometry Kit 488 from baseclick (Sigma-Aldrich, cat. no. BCK-FC488-100)<sup>23</sup>. Briefly, EdU was added at a concentration of 10µM 24 hours prior to trypsinization and cell fixation with 4% PFA to label the cells. Using a click-it reaction, 6-FAM was attached to EdU and EdU incorporation analysed using a BD LSRFortessa Cell Analyzer with a 488nm laser for excitation and a 530/30 emission filter. Flow cytometry data was analysed with Flowing Software 2.5.1 from Turku Bioscience.

### Intracellular metabolomics



Cells were grown in 1.5ml mixed medium in 6-well plates as described above. Every 24 hours, the medium was removed from the wells and cells were washed with pre-warmed wash buffer, made of freshly prepared 75 mM ammonium carbonate in nanopure water, adjusted to pH 7.4 using 10% acetic acid. After washing the cells, metabolites were extracted with ice-cold extraction buffer, containing 40% (v/v) methanol, 40% (v/v) acetonitrile and 20% (v/v) nanopure water for 1 hour at -20°C. Cells were detached from the wells using a cell lifter, transferred into tubes and centrifuged. Supernatants (metabolic extracts) were stored at -80°C until measurement. Untargeted metabolomics of metabolic extracts was performed by flow injection analysis–time-of-flight mass spectrometry on an Agilent 6550 Q-TOF mass-spectrometer as previously described<sup>24</sup>. Measurements were performed in negative ionization mode, and spectra were recorded from a mass/charge ratio of 50 to 1000. Ions were annotated based on their measured mass using reference compounds from the Human Metabolome Database (HMDB 4.0), with a tolerance of 1 mDa. Data analysis was performed with an in-house developed pipeline based on Matlab (The MathWorks). Samples were normalized within each cell-type by normalization of the mean ion intensity to account for the cell number differences at sampling. Differential analysis was performed using a Student's t test and significance was corrected for multiple hypothesis testing with the Benjamini-Hochberg method, and an adjusted p-value < 0.05 was considered significant. Metabolic pathway enrichment was done using pathway definitions from HMDB, using a p-value cut-off of 0.05 and a log<sub>2</sub>(fold-change (FC)) cut-off of 0.25. Significance of enrichments was corrected for multiple hypothesis testing by the Benjamini-Hochberg method, and an adjusted p-value of < 0.05 was considered significant.

### **Extracellular metabolomics**

Cells were grown in 1.5ml mixed medium in 6-well plates as described above. Every 24 hours, the medium was replaced with fresh medium. Supernatant samples were taken 0 hours, 2 hours, 22 hours and 24 hours after medium exchange. Supernatant samples were diluted 1:50 with nanopure water before metabolomics measurement. Untargeted metabolomics of supernatant samples was performed by flow injection analysis–time-of-flight mass spectrometry on an Agilent 6520 Q-TOF mass-spectrometer as described above. Ions were annotated based on their measured mass using reference compounds from the Human Metabolome Database (HMDB 4.0), with

a tolerance of 3 mDa. Within each day, samples were normalized to the first time point and linear regression applied to determine the uptake or secretion rate in normalized ion intensity per hour.

## Proteomics

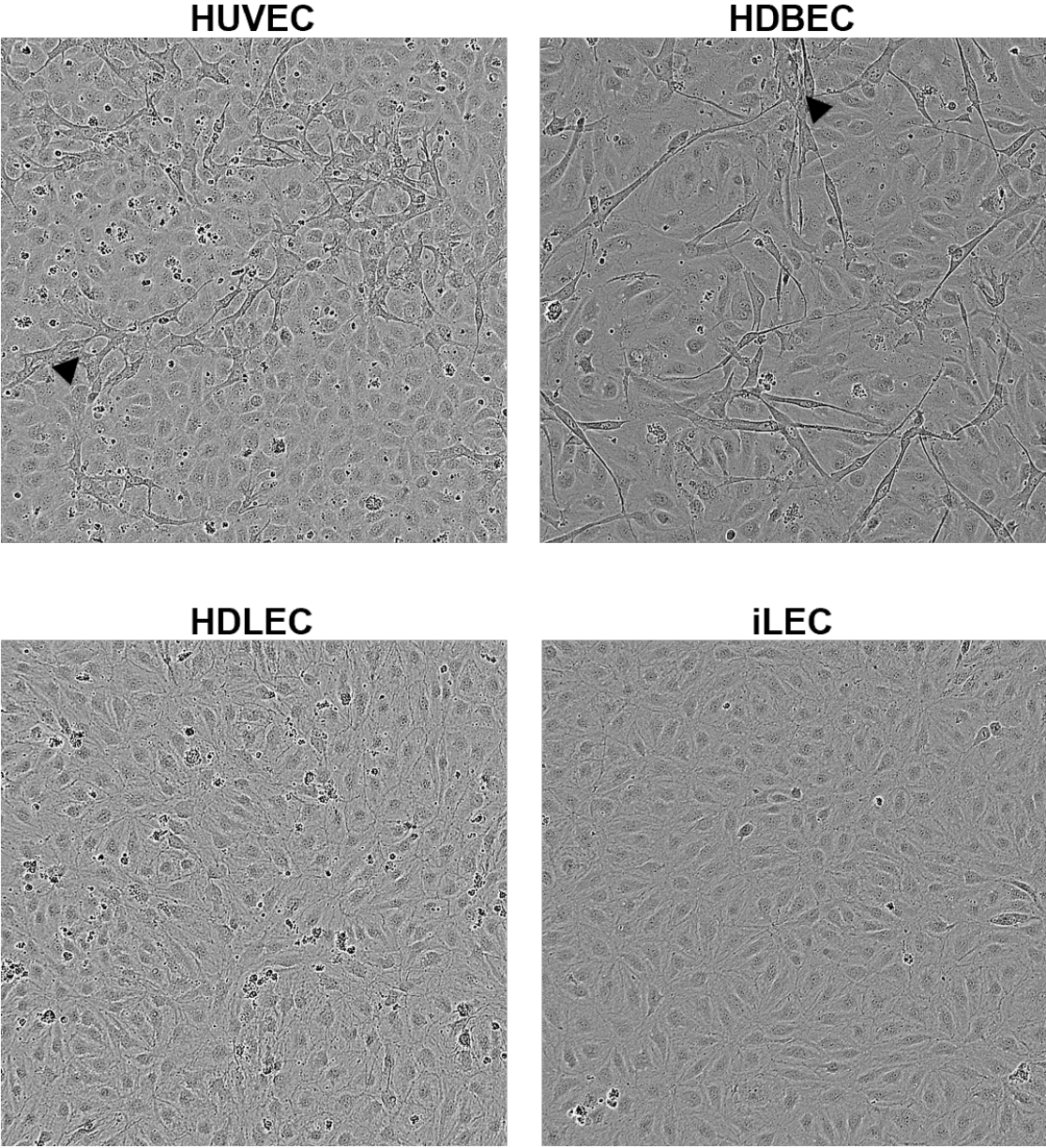
Proteomics sample preparation protocol was adapted from <sup>25</sup> and <sup>26</sup>. In brief, cells were grown in 1.5ml mixed medium in 6-well plates as described above. After removal of medium and washing of cells with PBS, cells were lysed in lysis buffer (8M urea buffer) and subsequently sonicated, centrifuged and supernatants transferred into fresh tubes for protein reduction with DTT and alkylation with iodoacetamide. Supernatants were incubated for 25min at 50°C with 5mM DTT and after cooling down to room temperature, iodoacetamide to 15mM final concentration was added and the mixture incubated for 30min at RT in the dark. An additional 5mM DTT was used to quench unreacted iodoacetamide for 15min at RT in the dark. Protein concentration was determined by BCA assay. Samples were then diluted 1:8 with 100mM HEPES, pH 8.5, to reduce the concentration of urea to 1M. Trypsin was added to the diluted samples to reach a 100:1 sample:trypsin (w/w) ratio and the mix incubated at 37°C overnight on a thermomixer. To stop trypsin digestion, samples were acidified with TFA to 0.4% (vol/vol) to reach a pH around 3. Before MS measurements, samples were desalted using Pierce C18 spin columns (Thermo Scientific, cat. no. 89870).

Peptides were analyzed online by liquid chromatography-tandem mass spectrometry (LC-MS/MS). Online reversed phase chromatography was performed using a Vanquish Neo UPLC system (Thermo Scientific, Sunnyvale) equipped with a heated column compartment set to 50 °C. Mobile Phase A consisted of 0.1% formic acid (FA) in water, while Mobile Phase B was 80% acetonitrile in water and 0.1% FA. Peptides (~1 µg) were loaded onto a C18 analytical column (500 mm, 75 µm inner diameter), packed in-house with 1.8 µm ReproSil-Pur C18 beads (Dr. Maisch, Ammerbuch, Germany) fritted with Kasil, keeping constant pressure of 600 bar or a maximum flow rate of 1 µl/min. After sample loading, the chromatographic gradient was run at 0.3 µl/min and consisted of a ramp from 0 to 43% Mobile Phase B in 70 min, followed by a wash at 100% Solution B in 9 min total, and a final re-equilibration step of 3 column volumes (total run time 90 min).

Peptides from each sample were analysed on an Orbitrap HF-X mass spectrometer (Thermo Fisher Scientific, San Jose, CA) using an overlapping window data-independent analysis (DIA) pattern described by Searle et al <sup>27</sup>, consisting of a precursor scan followed by DIA windows. Briefly, precursor scans were recorded over a 390-1010 m/z window, using a resolution setting of 120,000, an automatic gain control (AGC) target of 1e6 and a maximum injection time of 60 ms. The RF of the ion funnel was set at 40% of maximum. A total of 150 DIA windows were quadrupole selected with a 8 m/z isolation window from 400.43 m/z to 1000.7 m/z and fragmented by higher-energy collisional dissociation, HCD, (NCE=30, AGC target of 1e6, maximum injection time 60 ms), with data recorded in centroid mode. Data was collected using a resolution setting of 15,000, a loop count of 75 and a default precursor charge state of +3. Peptides were introduced into the mass spectrometer through a 10  $\mu$ m tapered pulled tip emitter (Fossil Ion Tech) via a custom nano-electrospray ionization source, supplied with a spray voltage of 1.6 kV. The instrument transfer capillary temperature was held at 275 °C.

All Thermo RAW files were converted to mzML format using the ProteoWizard package <sup>28</sup> (version 3.0.2315). Vendor-specific peak picking was selected as the first filter and demultiplexing with a 10 ppm window was used for handling the overlapping data collection window scheme. Processed mzML files were then searched using DIA-NN <sup>29</sup> (version 1.8) and the UniProt Homo sapiens proteome (UP000005640, June 15 2021) as the FASTA file for a “library-free” deep neural network-based search approach. Data was searched using deep learning-based spectra and retention time as described by Demichev et al, with trypsin as the protease, and allowing for 2 missed cleavages, with N-terminal methionine cleavage, and cysteine carbamidomethylation. Peptide length was allowed to range from 7-30 amino acids with a precursor charge state range from +1 to +4, a precursor range of 300-1800 m/z and a fragment ion range of 200-1800 m/z. Data was processed to a 1% precursor-level false discovery rate (FDR) with mass accuracy, MS1 accuracy, and match between runs set to the software default settings. A single-pass mode neural network classifier was used with protein groups inferred from the input Homo sapiens FASTA file. Protein quantities were normalized by delayed normalization and maximal peptide ratio extraction (maxLFQ)<sup>21</sup>.

# Supplementary Material

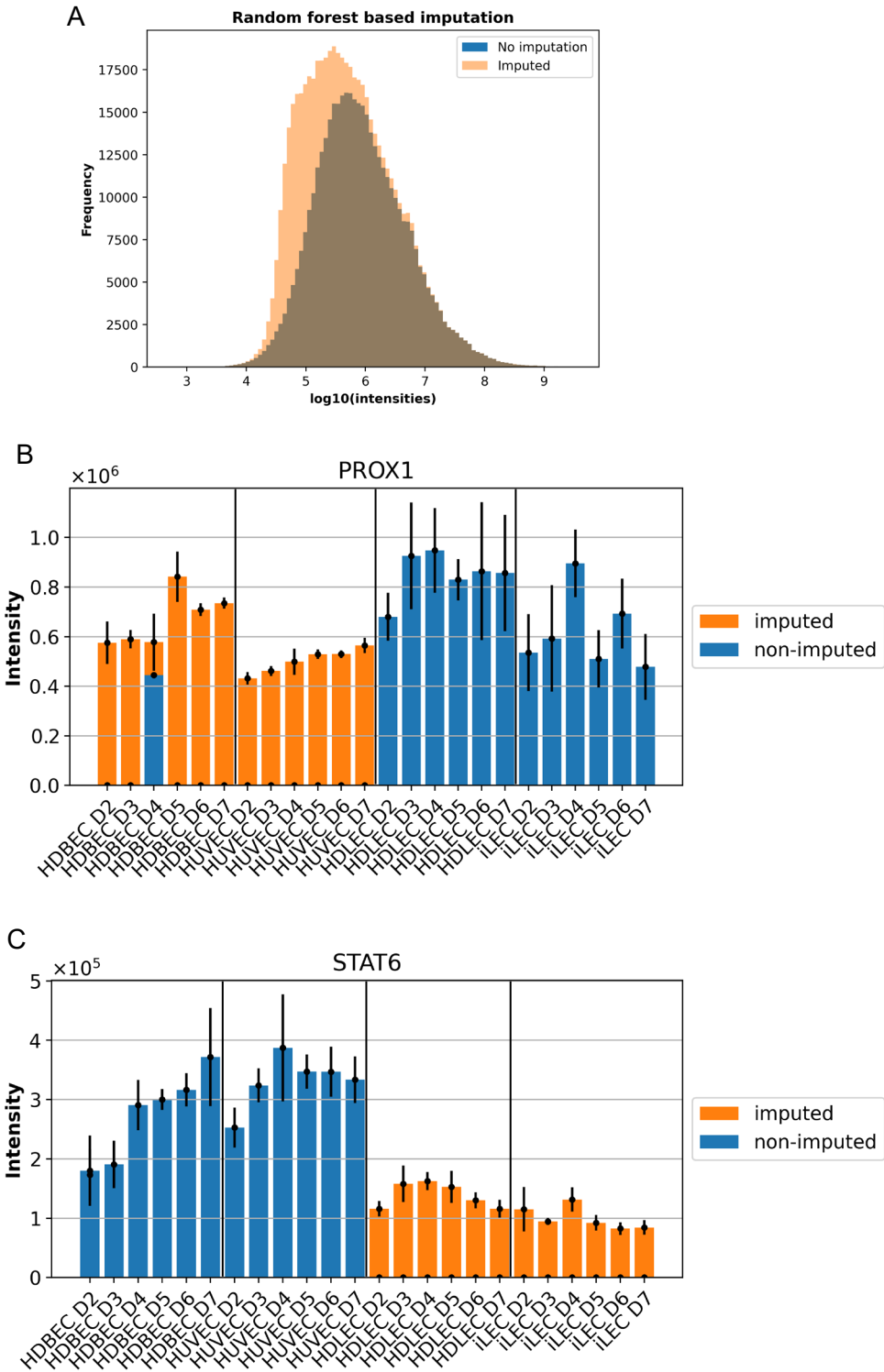


**Supplementary Figure 1. Morphology of quiescent ECs**  
Microscopy pictures of the four ECs after 5 days in culture. Most cells are quiescent at that stage, but the arrows in the HUVEC and HDBEC pictures show that these cells can grow into 3D.



**Supplementary Figure 2. Pathway enrichment analysis of iLECs in the normal setup (top panel) and reseeded setup (lower panel).**

In the normal setup, samples are compared to day 2, in the reseeded setup with the 2 hours post-reseeding timepoint. The colors depict the adj. p-value of the enrichments, calculated with a hypergeometric test. The signs of the enrichments are based on the direction of the enrichment. Hence, a negative sign means lower abundance of intermediates in the pathway, a positive sign higher abundance of intermediates. The color bars of the two panels are inverted.



Supplementary Figure 3. Random forest-based imputation of proteomics data.

- (A) Distribution of log<sub>10</sub>-transformed intensities before and after imputation.
- (B) Intensities of LEC marker PROX1 before and after imputation.
- (C) Intensities of BEC marker STAT6 before and after imputation.

## References

1. Carmeliet, P. Angiogenesis in health and disease. *Nat. Med.* **9**, 653–660 (2003).
2. Aspelund, A., Robciuc, M. R., Karaman, S., Makinen, T. & Alitalo, K. Lymphatic System in Cardiovascular Medicine. *Circ. Res.* **118**, 515–530 (2016).
3. Adams, R. H. & Alitalo, K. Molecular regulation of angiogenesis and lymphangiogenesis. *Nat. Rev. Mol. Cell Biol.* **8**, 464–478 (2007).
4. De Bock, K., Georgiadou, M. & Carmeliet, P. Role of endothelial cell metabolism in vessel sprouting. *Cell Metab.* **18**, 634–647 (2013).
5. Cao, R. *et al.* Collaborative interplay between FGF-2 and VEGF-C promotes lymphangiogenesis and metastasis. *Proc. Natl. Acad. Sci. U. S. A.* **109**, 15894–15899 (2012).
6. Eelen, G. *et al.* Endothelial Cell Metabolism. *Physiol. Rev.* **98**, 3–58 (2017).
7. Morfousse, F. & Noel, A. Lymphatic and blood systems: Identical or fraternal twins? *Int. J. Biochem. Cell Biol.* **114**, 105562 (2019).
8. Yu, P. *et al.* FGF-dependent metabolic control of vascular development. *Nature* **545**, 224–241 (2017).
9. Wilhelm, K. *et al.* FOXO1 couples metabolic activity and growth state in the vascular endothelium. *Nature* **529**, 216–220 (2016).
10. García-Caballero, M. *et al.* Role and therapeutic potential of dietary ketone bodies in lymph vessel growth. *Nat. Metab.* **1**, 666–675 (2019).
11. Ricard, N., Bailly, S., Guignabert, C. & Simons, M. The quiescent endothelium: signalling pathways regulating organ-specific endothelial normalcy. *Nat. Rev. Cardiol.* **18**, 565–580 (2021).
12. Wong, B. W. *et al.* The role of fatty acid  $\beta$ -oxidation in lymphangiogenesis. *Nature* **542**, 49–54 (2017).
13. Kalucka, J. *et al.* Quiescent Endothelial Cells Upregulate Fatty Acid  $\beta$ -Oxidation for Vasculoprotection via Redox Homeostasis. *Cell Metab.* **28**, 881-894.e13 (2018).
14. Kalucka, J. *et al.* Single-Cell Transcriptome Atlas of Murine Endothelial Cells. *Cell* **180**, 764-779.e20 (2020).
15. Paik, D. T. *et al.* Single-Cell RNA Sequencing Unveils Unique Transcriptomic Signatures of Organ-Specific Endothelial Cells. *Circulation* **142**, 1848–1862 (2020).
16. Geiger, R. *et al.* L-Arginine Modulates T Cell Metabolism and Enhances Survival and Anti-tumor Activity. *Cell* **167**, 829-842.e13 (2016).
17. Ludikhuizen, M. C. & Rodríguez Colman, M. J. Metabolic Regulation of Stem Cells and

- Differentiation: A Forkhead Box O Transcription Factor Perspective. *Antioxidants Redox Signal.* **34**, 1004–1024 (2021).
18. Almeida, L., Lochner, M., Berod, L. & Sparwasser, T. Metabolic pathways in T cell activation and lineage differentiation. *Semin. Immunol.* **28**, 514–524 (2016).
  19. Teuwen, L. A., Geldhof, V. & Carmeliet, P. How glucose, glutamine and fatty acid metabolism shape blood and lymph vessel development. *Dev. Biol.* **447**, 90–102 (2019).
  20. Sévin, D. C., Kuehne, A., Zamboni, N. & Sauer, U. Biological insights through nontargeted metabolomics. *Curr. Opin. Biotechnol.* **34**, 1–8 (2015).
  21. Cox, J. *et al.* Accurate proteome-wide label-free quantification by delayed normalization and maximal peptide ratio extraction, termed MaxLFQ. *Mol. Cell. Proteomics* **13**, 2513–2526 (2014).
  22. Lemons, J. M. S. *et al.* Quiescent fibroblasts exhibit high metabolic activity. *PLoS Biol.* **8**, (2010).
  23. Salic, A. & Mitchison, T. J. A chemical method for fast and sensitive detection of DNA synthesis in vivo. *Proc. Natl. Acad. Sci. U. S. A.* **105**, 2415–2420 (2008).
  24. Fuhrer, T., Heer, D., Begemann, B. & Zamboni, N. High-Throughput, Accurate Mass Metabolome Profiling of Cellular Extracts by Flow Injection–Time-of-Flight Mass Spectrometry. *Anal. Chem.* **83**, 7074–7080 (2011).
  25. Weekes, M. P. *et al.* Quantitative temporal viromics: An approach to investigate host-pathogen interaction. *Cell* **157**, 1460–1472 (2014).
  26. Villén, J. & Gygi, S. P. The SCX\_IMAC enrichment approach for global phosphorylation. *Nat. Protoc.* **3**, 1630–1638 (2008).
  27. Searle, B. C. *et al.* Chromatogram libraries improve peptide detection and quantification by data independent acquisition mass spectrometry. *Nat. Commun.* **9**, (2018).
  28. Chambers, M. C. *et al.* A cross-platform toolkit for mass spectrometry and proteomics. *Nat. Biotechnol.* **30**, 918–920 (2012).
  29. Demichev, V., Messner, C. B., Vernardis, S. I., Lilley, K. S. & Ralser, M. DIA-NN: neural networks and interference correction enable deep proteome coverage in high throughput. *Nat. Methods* **17**, 41–44 (2020).
  30. Podgrabinska, S. *et al.* Molecular characterization of lymphatic endothelial cells. *Proc. Natl. Acad. Sci. U. S. A.* **99**, 16069–16074 (2002).
  31. Gao, P., Ren, G., Liang, J. & Liu, J. STAT6 Upregulates NRP1 Expression in Endothelial Cells and Promotes Angiogenesis. *Front. Oncol.* **12**, 1–13 (2022).
  32. Gerdes, J., Schwab, U., Lemke, H. & Stein, H. Production of a mouse monoclonal antibody



- (B1N) reactive with a human nuclear antigen associated with cell proliferation. *Int. J. Cancer* **31**, 13–20 (1983).
33. Kelman, Z. PCNA: Structure, functions and interactions. *Oncogene* **14**, 629–640 (1997).
34. Stekhoven, D. J. & Bühlmann, P. Missforest-Non-parametric missing value imputation for mixed-type data. *Bioinformatics* **28**, 112–118 (2012).
35. Potente, M. & Carmeliet, P. The Link Between Angiogenesis and Endothelial Metabolism. *Annu. Rev. Physiol.* **79**, 43–66 (2016).
36. Alseekh, S. *et al.* Mass spectrometry-based metabolomics: a guide for annotation, quantification and best reporting practices. *Nat. Methods* **18**, 747–756 (2021).
37. Sabine, A., Saygili Demir, C. & Petrova, T. V. Endothelial Cell Responses to Biomechanical Forces in Lymphatic Vessels. *Antioxid. Redox Signal.* **25**, 451–465 (2016).
38. Goers, L., Freemont, P. & Polizzi, K. M. Co-culture systems and technologies: Taking synthetic biology to the next level. *J. R. Soc. Interface* **11**, (2014).
39. Casbas-Hernandez, P., Fleming, J. M. & Troester, M. A. Gene expression analysis of in vitro cocultures to study interactions between breast epithelium and stroma. *J. Biomed. Biotechnol.* **2011**, (2011).



## Chapter 3

### **Multi-omics analysis of endothelial cells reveals cell type-specific metabolic patterns governing cellular phenotypes**

Stephan Durot<sup>1</sup>, Peter F. Doubleday<sup>1</sup>, Lydia Schulla<sup>1</sup>, Nicola Zamboni<sup>1</sup>

<sup>1</sup> Institute of Molecular Systems Biology, ETH Zürich, Otto-Stern-Weg 3, 8093 Zürich, Switzerland

Stephan Durot designed the study, measured and analysed the multi-omics data, planned and conducted the follow-up experiments and wrote the chapter. Peter F. Doubleday set up the LC-MS method for proteomics and supported proteomics sample preparation and data analysis and contributed to the writing. Lydia Schulla planned and conducted the follow-up experiments and contributed to the writing. Nicola Zamboni helped designing the study, supervised and contributed to the writing.

## Abstract

Endothelial cells (ECs), lining up the inner layer of the vascular system, are mostly quiescent but switch to a proliferative state to form new vessels. The formation and maintenance of EC identities and states are supported by various factors, including metabolic pathways. Using untargeted proteomics and metabolomics, we created a comprehensive description of the molecular patterns underlying the identities and states of two blood and two lymphatic EC types. We observed distinct and general metabolic patterns in quiescence and proliferation in each cell type, for example a HUVEC-specific decrease of porphyrin biosynthesis intermediates or upregulation of BCAA catabolism across all cell types in quiescence. Further functional studies exhibit diverse phenotypic alterations after enzyme inhibition of pathways such as heme biosynthesis, glutamate metabolism, fatty acid and nucleotide synthesis, indicating the diverging importance of certain metabolic pathways to maintain a specific state by different endothelial cell types.

## Introduction

The cardiovascular and lymphatic systems are branched networks that run through the entire body and are found in every tissue and organ<sup>1,2</sup>. Both networks are lined by endothelial cells (ECs), and in the mature vasculature, ECs that have left mitotic cell division remain quiescent for most of their lifetime. However, to support wound healing or to provide tissues with nutrients and oxygen, ECs are stimulated and differentiate into migratory tip cells and proliferating stalk cells to form new vessels<sup>3,4</sup>. After the formation of new vessels, quiescence is re-established to maintain proper architecture and homeostatic function<sup>3,5</sup>.

This process is critically important, as a number of cardiovascular and lymphatic system diseases originate from malfunctioning ECs, when the induction or exit from quiescence goes awry<sup>6,7</sup>. Indeed, primary lymphatic diseases, such as lymphedema, are induced by mutations in various genes responsible for lymphangiogenesis or maintenance of quiescence and lead to proliferation of normally quiescent cells and disruption of cell-cell junctions with subsequent flow of lymph into the interstitium<sup>8</sup>. However, outside of these primary, genetic causes of lymphedema, secondary

lymphedema is not fully characterized by genetic mutations<sup>8</sup>. Instead, of critical interest, recent studies have attributed an essential role to metabolism in establishing and maintaining a quiescent or proliferating state as well as for differentiation, migration and angiogenesis of blood as well as lymphatic ECs<sup>9-21</sup>. Alterations in metabolic activity of ECs might therefore induce or support the formation and progression of cardiovascular and lymphatic diseases at the cellular level.

Recent transcriptomics studies of murine endothelial cells provided an overview of organ-specific mRNA expression in ECs, showing a heterogeneity in metabolic transcript levels between ECs from different tissues and between ECs from different vascular beds within a single tissue<sup>22-24</sup>. However, to date most studies on EC metabolism have focused on a handful of specific metabolic pathways using transcriptomics approaches, or only use human umbilical vein ECs (HUVECs) as a model for all ECs. Thus, extrapolating results to other EC niches from distinct tissues or different vascular beds may not be representative of endothelial cell biology in its true complexity.

Therefore, here, we characterized the metabolism of four different EC types — two from the cardiovascular system and two from the lymphatic system — across proliferative and quiescent states by combining untargeted quantitative proteomics and metabolomics approaches. In support of previous studies performed at the transcript-level, our multi-omics approach creates a further resource towards understanding EC biology. Furthermore, we found that the four EC types are phenotypically similar but metabolically distinct, and through functional studies, we observed that the cells reorganize metabolism in different phenotypes in a cell type-specific manner to support altered cellular demands. Indeed, specifically examining HUVECs and intestinal LECs (iLECs) through pharmacological perturbations to assess the physiological relevance of metabolic pathways identified that HUVECs but not iLECs rely on sufficient heme levels for NO production to promote migration and sprouting. On the other hand, iLECs are more sensitive to disturbances in the glutamate –  $\alpha$ -ketoglutarate balance, resulting in migration defects.

## Results

### Endothelial cell lines identities and states are defined by distinct proteomic signatures

In the previous chapter, we developed an experimental workflow that allows us to study the molecular patterns that define identities and states in four endothelial cell types: human umbilical vein endothelial cells (HUVECs); human dermal blood endothelial cells (HDBECs); human dermal lymphatic endothelial cells (HDLECs); and intestinal lymphatic endothelial cells (iLECs) (Fig. 1A). All EC lines had a fraction of EdU-negative, quiescent cells two days after seeding with HUVECs being the lowest at 5% and HDBECs the highest at 20%. After 5 days in continuous culture, more than 80% of HUVECs, HDLECs and iLECs and more than 70% of HDBECs were EdU-negative, and therefore quiescent.

To understand the molecular mechanisms that underlie EC identities and states, we performed label-free quantitative proteomics of all four cell lines from day 2 to day 7 post-seeding. Overall, we identified 7,894 protein groups at a 1% protein group-level false discovery rate cut-off. First, we used this dataset for partial least squares discriminant analysis (PLS-DA) in order to determine the proteins whose expression levels are associated with either lymphatic (iLECs and HDLECs) or blood endothelial cells (HDBECs and HUVECs) (Fig. 1B, Suppl. Table 1). The grouping of individual cell types and inclusion of all states enabled us to study the general, state-independent proteomic patterns that underlie LEC and BEC identity. The weights of all proteins on the first component of the PLS-DA, discriminating BECs and LECs, were subject of a permutation approach to generate LEC- and BEC-associated protein lists. Using a 10% cut-off, these two lists contained 424 and 1,873 proteins for LECs and BECs, respectively, including markers of LECs (PROX1, LYVE1) and BECs (STAT6, NRP1) (Fig. 1C, Suppl. Fig. 1A, B)<sup>25–27</sup>. We next conducted a pathway enrichment analysis with the proteins in the two lists using the Reactome pathway database<sup>28</sup> to examine the cellular processes that underlie EC identities. We found enrichments of BEC-associated proteins in 153 pathways and of LEC-associated proteins in 78 pathways (FDR < 0.05) (Suppl. Table 1). Interestingly, metabolic pathways were among the top enriched pathways in LECs but not in BECs. For example, fatty acid  $\beta$ -oxidation and TCA cycle and the respiratory electron transport chain were the two most enriched

pathways in LECs, reflecting their known, crucial role in lymphangiogenesis and LEC specification and maintenance (Fig. 1D)<sup>16,29</sup>. Furthermore, metabolism itself (FDR = 0.004), glyoxylate metabolism and glycine degradation (FDR = 0.005) and lysine (FDR = 0.02) and BCAA catabolism (FDR = 0.02) were enriched in LECs, but not in BECs (Suppl. Table 1).

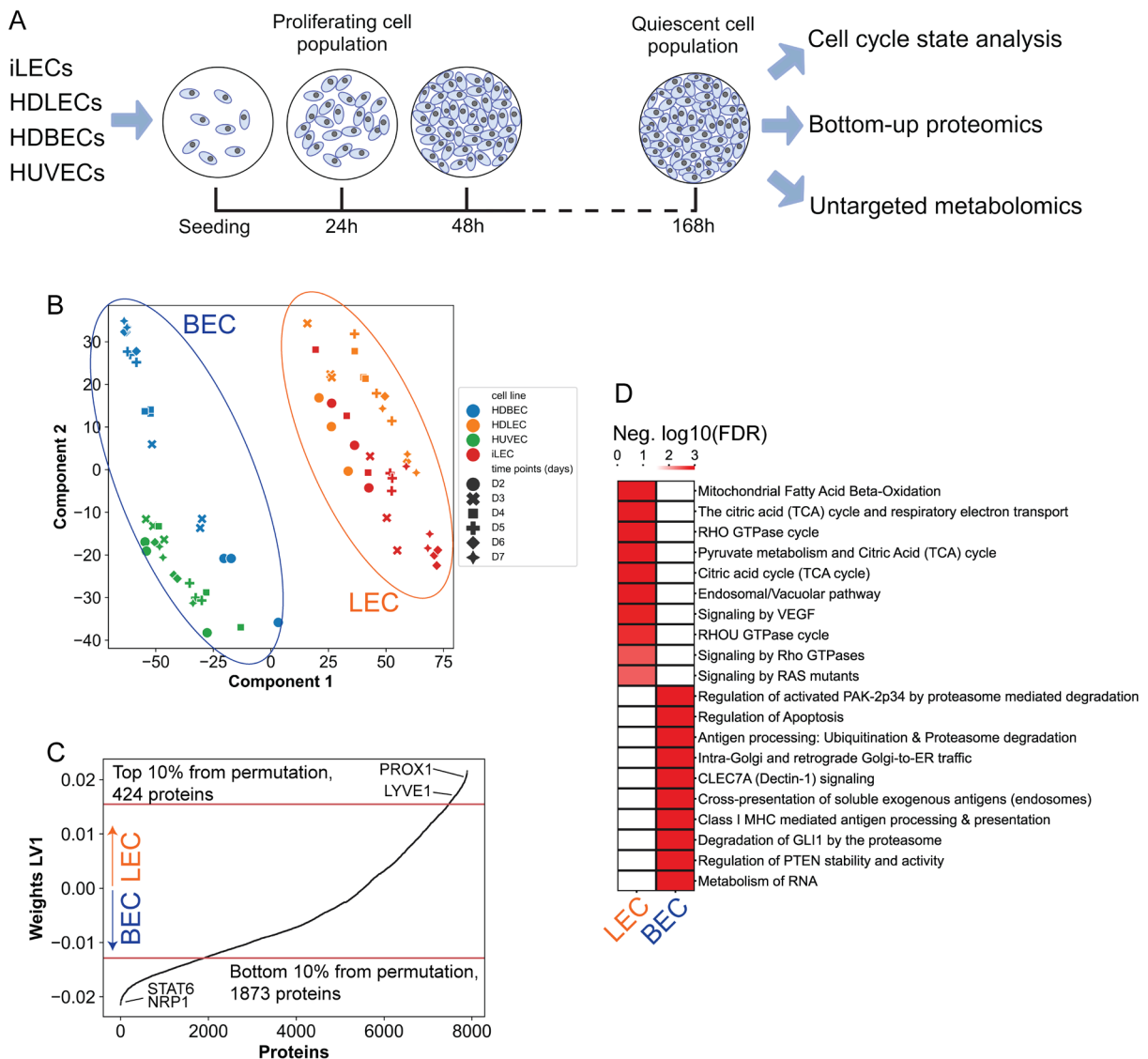


**Figure 1. Endothelial cell lines identities and states are defined by distinct proteomic signatures.**

- Experimental setup.  $n = 3$  replicates per day and cell line for each measurement.
- Partial least squares discriminant analysis (PLS-DA) of day 2 to day 7 proteomics samples showing the discrimination between LECs and BECs among component 1.
- Weights of the first component of the PLS-DA. Each protein has a weight that corresponds to its cell type-related information. A permutation approach was applied to determine the 10% and 90% percentile, associated with BEC and LEC identity, respectively.
- Pathway enrichment analysis of LEC- and BEC-associated proteins, showing the top 10 enriched pathways for both cell types.

To further explore proteomic patterns underlying cellular identity and quiescence induction across the EC types, we moved forward with day 2 and day 5 post-seeding time points given the similar growth kinetics that were observed across cell lines. These time points represent the most distinct states of proliferation and quiescence, respectively, across all time points. Differential analysis between day 5 (quiescent) and day 2 (proliferating) samples identified an expected, core proteomic signature related to cell cycle in quiescent ECs. For example, proteins involved in DNA replication, translation or cell cycle, such as CDK1, MCM2, MCM3, MCM7, LARP4 were downregulated in quiescent cells (Suppl. Fig. 1B)<sup>30–34</sup>. We also identified significant differential expression of proteins known to participate in vessel formation, maintenance and cellular quiescence<sup>35–44</sup>. Indeed, proteins related to extracellular matrix organisation and adhesion (CCN1, NID1), platelet activation and coagulation (VWF, MMRN1, TFPI), autophagy (ACP2, LIPA, GAA, TPP1) or inflammation and senescence inhibition (NTN4) were all upregulated above 2-fold during quiescence (Suppl. Fig. 1B).

Beyond core differences in protein expression, principal component analysis and Spearman's correlation also identified different proteomic patterns dependent on cell types and proliferative states (Suppl. Fig. 1C, 1D). While proliferating ECs exhibited diverse proteomic patterns, in quiescence, ECs from the same vascular beds had similar proteomic patterns. We hypothesized that proteomic distinctions might reflect the distinct physiological roles of quiescent lymphatic and blood ECs in maintaining tissue homeostasis. To determine which pathways govern these distinct physiological roles, we performed pathway enrichment analysis using the Reactome pathway database<sup>28</sup> with proteins that had an  $\text{abs}(\log_2(\text{FC})) > 0.5$  between day 5 and day 2 samples and a q-value of less than 0.05. In total, 105 pathways had positive enrichments and 186 had negative enrichments ( $\text{FDR} < 0.05$ ) in at least one cell line (Suppl. Table 2). Among the top negative enriched pathways in quiescence were, not surprisingly, pathways involved in cell cycle or metabolism of nucleotides, but also pathways involved in rRNA processing, translation, seleno-amino acid metabolism or metabolism of amino acids and derivatives, which includes all pathways responsible for biosynthesis and degradation of amino acids (Suppl. Table 2). Positive enrichments in quiescence are more diverse in the different ECs. For example, the strongest enriched pathways in HDBECs are involved in membrane trafficking, vesicle-mediated transport or asparagine N-linked glycosylation (Suppl. Table 2). On the other hand, the



top five positively enriched pathways in HDLECs are associated to TCA cycle, electron transport chain and Complex I biogenesis (Suppl. Table 2). Interestingly, metabolism is positively enriched in all four cell lines in quiescence, showing the important role of metabolic pathways in the induction and maintenance of quiescence (Suppl. Fig. 1E). To further understand which parts of the metabolic network are important for quiescence, we focused on the 36 metabolic pathways that were enriched in at least one cell line (FDR < 0.05) (Suppl. Fig. 1E). In total, 8 out of the 36 metabolic pathways had a negative enrichment, including nucleotide biosynthesis, metabolism of amino acids and derivatives and seleno-amino acid metabolism (Suppl. Fig. 1E). Positive enrichments include TCA cycle, the electron transport chain, branched-chain amino acid (BCAA) catabolism, glycosphingolipid and sphingolipid metabolism, carbohydrate metabolism and  $\beta$ -oxidation of fatty acids (Suppl. Fig. 1E). These pathway-level findings are supported by previous work, although done at the transcript-level. Indeed, mitochondrial fatty acid  $\beta$ -oxidation has been shown to be upregulated in quiescent HUVECs for vasculoprotection via redox homeostasis<sup>15</sup>. We observed a similar magnitude of positive enrichments in quiescent iLECs, HDLECs and HUVECs but not in HDBECs. Quiescent HDBECs generally have weaker enrichments of metabolic pathways, and, besides metabolism (FDR = 0.003), only metabolism of carbohydrates (FDR = 0.035), glucose (FDR = 0.035) and fatty acids (FDR = 0.038) are significantly enriched. However, in all quiescent ECs, there is an enrichment of proteins in branched-chain amino acid catabolism (FDR < 0.01 in HUVECs, HDLECs and iLECs, FDR = 0.052 in HDBECs). It was previously shown that promoting BCAA catabolism by the PPM1K phosphatase maintains glycolysis and quiescence in hematopoietic stem cells<sup>45</sup>. Increase of BCAA catabolism in all quiescent ECs might hint at an important role of BCAA catabolism to maintain quiescence in endothelial cells, similar to hematopoietic stem cells. In line with the previous pathway enrichments of LEC-associated proteins results, iLECs and HDLECs have a stronger enrichment in TCA cycle and electron transport chain-associated pathways (FDR <  $10^{-6}$  in iLECs and HDLECs compared to FDR of 0.028 in HUVECs and 0.16 in HDBECs), suggesting that these two pathways are specifically critical for lymphatic ECs to maintain a quiescent state. Taken together, ECs exhibit cell type and state-dependent expression patterns of proteins in metabolic pathways, particularly in fatty acid  $\beta$ -oxidation, TCA cycle, electron transport chain and BCAA catabolism.

## **Distinct metabolic programs underlie quiescence induction and maintenance processes across different cell lines**

While our analysis of protein expression patterns identified distinctions in metabolic pathways between EC types, it remained unclear what these patterns mean for metabolite levels and the metabolic activity of the four endothelial cell types. Thus, we examined the general metabolic activity of the four cell lines by determining the uptake and secretion rates of extracellular metabolites. Specifically, we exchanged the growth medium every 24 hours, sampled cellular supernatants between each medium exchange and measured the supernatants in an untargeted manner using time-of-flight mass spectrometry (Suppl. Fig. 2A, Suppl. Table 3)<sup>46</sup>. In total, we annotated 521 extracellular metabolite and quantified uptake and secretion rates by linear regression of ion intensities between two medium exchanges.

For all cell types, uptake of ascorbate and pyruvate from the medium, and secretion of lactate remain a core metabolic feature (Fig. 2A). However, in contrast to the similar patterns of cell proliferation and quiescence across cell lines, generally, the metabolite uptake and secretion patterns vary in the different ECs, likely reflecting diverse metabolic activities across cell types and states (Fig. 2A, 2B, Suppl. Fig. 2B, 2C and 2D). Proliferating HUVECs take up 50% of glucose in the supernatant over 24h and have the highest glucose uptake among the cell lines tested. They also have a 2-fold increased lactate secretion in proliferation compared to quiescence, indicating a highly glycolytic proliferative stage. Additionally, proliferating and quiescent HUVECs consume amino acids at higher levels than the other cell types, especially cysteine (-30% in 24h) and methionine (-20% in 24h) during proliferation and glutamine (-10% in 24h) in quiescence. On the other hand, levels of amino acids and lactate in the supernatant increase by 10-20% and 72%, respectively, in quiescent and proliferating HDBECs over 24h. Surprisingly, in contrast to the previously described glycolysis-driven proliferative state of BECs, they only start to consume glucose when they become quiescent, decreasing glucose levels by 22% in 24h (Fig. 2A, 2B)<sup>47</sup>. The two lymphatic endothelial cell types (iLECs and HDLECs) show more similar uptake and secretion patterns compared to HDBECs and HUVECs (Suppl. Fig. 2B), but they vary in the amplitude of glucose and glutamine uptake and lactate secretion. HDLECs have a 35% increased uptake of glucose and secretion of lactate when they are quiescent, whereas glucose consumption and lactate secretion decrease in quiescent iLECs by

85% and 17%, respectively. Interestingly, iLECs and HDLECs start to secrete certain amino acids (alanine, proline and aspartate) as they transition into quiescence.

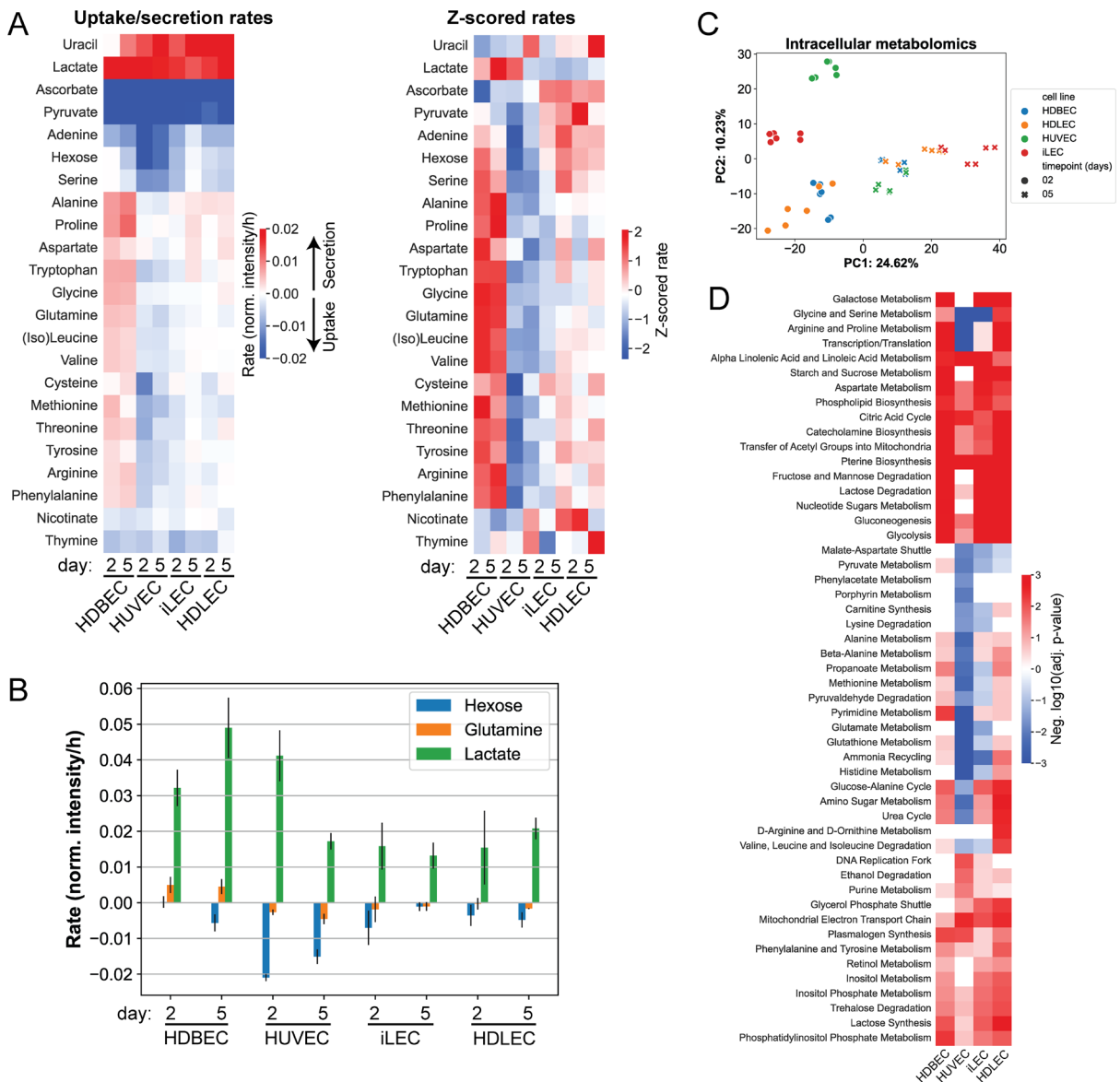


**Figure 2. Distinct metabolic programs underlie quiescence induction and maintenance processes across different cell lines.**

- (A) Left: normalized ion intensity change per hour for detected amino acids and growth media components. Negative rate corresponds to uptake, positive rates to secretion of metabolites. Right: z-scored uptake/secretion rates. z-scoring was performed over metabolites to illustrate relative changes between cell lines.
- (B) Normalized ion intensity change per hour for hexose, lactate, glutamine and pyruvate in proliferating (2D) and quiescent (5D) cells. Negative rate corresponds to taken up metabolites, positive rates to secreted metabolites.
- (C) PCA of intracellular metabolites of each cell line in proliferation and quiescence.
- (D) Metabolite PEA of quiescence vs proliferation samples, hierarchically clustered. Negative values correspond to increased enrichments in proliferation, positive values to increased enrichments in quiescence.

In short, phenotypes of ECs are similar in terms of the increased fraction of quiescent cells upon contact inhibition and the metabolic programs underlying proliferation and quiescence seem to be even more diverse than what would be expected from the proteomics data. Moreover, these data do not support the case for a general decrease of metabolic activity in quiescent ECs, but in contrast, a reorganization of metabolism to meet and support cell type-specific demands, similar to previous results in fibroblasts and epithelial cells<sup>48,49</sup>. Indeed, the distinct high metabolic activity of EC cell lines is clearly reflected in the magnitude of uptake and secretion rates between the cell types.

To deepen our understanding of how metabolism supports the transition into and maintenance of EC quiescence, we also performed untargeted metabolomics on intracellular metabolite pools<sup>46</sup>. In total, we identified 1,413 metabolites across all cell lines (Suppl. Table 4). In accordance with the uptake and secretion patterns, intracellular metabolomes vary depending on cell type and state (Fig. 2C, Suppl. Fig. 3A). Clustering by principal component analysis and Spearman's correlation show that the metabolomes of HDBECs and HDLECs are more similar in proliferation compared to quiescence, in which the metabolome of HDLECs rather resembles the metabolome of iLECs (Fig. 2C, Suppl. Fig. 3A). Next, we performed a differential analysis between samples collected at day 2 (proliferation) and day 5 (quiescence). A total of 63 metabolites changed significantly at our statistical cut-offs (absolute of the log<sub>2</sub>-transformed fold-change of day 5 vs day 2 samples ( $\text{abs}(\log_2(\text{FC})) > 0.5$ , adj. p-value  $< 0.05$ ) in at least one of the cell types (Suppl. Fig. 3B, Suppl. Table 4). 75% of these metabolites have larger pool sizes in quiescence, such as ascorbate, that is taken up from the medium, and some fatty acids or building blocks of phospholipids (e.g. CDP-ethanolamine), likely reflecting the decreased need of quiescent cells to build new plasma membrane elements. Glutamine levels are significantly decreased only in quiescent HUVECs by 35%, even though quiescent HUVECs have the highest uptake rate of glutamine, potentially pointing towards increased glutamine dependence of quiescent HUVECs compared to the other cell types. Proline levels are decreased in quiescent HUVECs by 39% and are slightly but significantly increased in quiescent HDBECs ( $\log_2(\text{FC}) = 0.28$ , adj. p-value = 0.0003) and HDLECs ( $\log_2(\text{FC}) = 0.2$ , adj. p-value = 0.003), although these cell lines secrete proline in quiescence.

Given the small, yet significant changes in metabolite abundances, we next conducted a pathway enrichment analysis with all metabolites that had an  $\text{abs}(\log_2(\text{FC})) > 0.25$  and a p-value of less than 0.05. The abundances of intermediates in 51 metabolic pathways changed significantly in at least one cell line (Fig. 2D, Suppl. Table 4). 29 pathways are positively enriched in quiescent HDBECs and HDLECs, exhibiting a high degree of metabolic similarity between HDBECs and HDLECs. As opposed to this, quiescent HUVECs show negative enrichment in 12 amino acid and related metabolic pathways, such as glycine and serine metabolism, arginine and proline metabolism, glutamate metabolism, valine, leucine and isoleucine degradation, amino sugar metabolism and glutathione metabolism. Some of these negative enrichments are also observed in quiescent iLECs (e.g. glutamate metabolism, glycine and serine metabolism). In short, intracellular metabolomics results, on a metabolite and pathway level, show that different endothelial cell types have distinct metabolic patterns in proliferation and quiescence. Additionally, intracellular metabolic patterns can only be explained to some extent by altered expression of proteins involved in these pathways, indicating that these patterns are regulated not only by changing protein expression levels, but also through allosteric regulation, post-translational modifications or other mechanisms.

### **Pharmacological inhibitors identify HUVEC- and iLEC-specific metabolic program susceptibilities underlying different cellular states and functions**

From our previous multi-omics results, we hypothesized that distinct endothelial cell types may rely on different metabolic pathways to support cellular programs related to quiescence. To validate the multi-omics results and to assess how metabolism may define or differentiate cellular responses, we examined the effect of 14 metabolic drugs on growth, migration, and sprouting capacity of iLECs and HUVECs, specifically, as representatives from lymphatic and blood ECs, respectively (Table 1, Suppl. Fig. 4A). We chose inhibitory drugs targeting pathways that are differentially or similarly enriched on the proteome or metabolome level across the four cell lines. These include compounds to target enzymes in central carbon metabolism (oxidative phosphorylation (OXPHOS), TCA cycle, pentose phosphate pathway (PPP)) as well as amino acid (glutamate, serine), nucleotide, heme, glutathione, biopterine and fatty acid biosynthesis metabolism (Table 1). Based on our metabolomics and proteomics

analysis, we expected to see various phenotypic consequences upon pharmacological inhibition, such as an iLEC-dependent sensitivity to perturbations in OXPHOS and TCA cycle or a higher sensitivity of HUVECs to perturbations in heme biosynthesis.

**Table 1. Compounds and concentrations used for pharmacological perturbation in validation experiments.**

Compound name	Concentration	Target gene	Pathway
UK5099	40 $\mu$ M	MPC	TCA cycle
G6PDi-1	0.07 $\mu$ M	G6PD	Pentose phosphate pathway
Rotenone	0.5 $\mu$ M	Complex I	Electron transport chain
CB-839	23nM	GLS	Glutamate metabolism
R162	23 $\mu$ M	GLUD1	Glutamate metabolism
Succinyl acetone	18 $\mu$ M	ALAD	Heme biosynthesis
Dihydroxypyrimidine	300 $\mu$ M	GCH1	Biopterine biosynthesis
Buthionine sulfoximine	2 $\mu$ M	GCLC	Glutathione biosynthesis
ABH hydrochloride	0.14 $\mu$ M	ARG	Urea cycle
Methotrexate	100 $\mu$ M	DHFR	Nucleotide biosynthesis
C75	35 $\mu$ M	FASN	Fatty acid synthesis
Dimethyl fumarate	25 $\mu$ M	PHGDH	Serine biosynthesis
Pemetrexed	200nM	DHFR/GARFT/TS	Nucleotide biosynthesis
Fluorouracil	10 $\mu$ M	TS	Nucleotide biosynthesis

Overall, HUVECs and iLECs exhibit a wide range of growth and migration rate changes upon treatment with the 14 drugs (Fig. 3A). 5-Fluorouracil (5-FU), Pemetrexed and Methotrexate inhibit growth by targeting key enzymes in nucleotide biosynthesis and folate metabolism: 5-FU and Pemetrexed target thymidylate synthase (TYMS), Methotrexate and Pemetrexed target dihydrofolate reductase (DHFR). We expected these drugs to have similar growth and migration effects on HUVECs and iLECs. We find that Methotrexate and 5-FU, but not Pemetrexed, inhibit growth in HUVECs by 98% and 61%, respectively. Surprisingly, we further observe a decreased growth of 55% and 72% of Methotrexate- and Pemetrexed-treated iLECs, respectively, but no effect of 5-FU on growth of iLECs (Fig. 3B). Migration, a normal cellular function of ECs, is determined by a scratch assay that measures the time it takes cells to close the scratch<sup>50</sup>. Cells were either treated with drugs 5 days prior to and after the scratch assay to study the long-term effects of metabolic perturbations or only after the scratch assay to study the short-term effects. 5-FU reduces migration rate of HUVECs by 23% and of iLECs by 75%, Pemetrexed the migration rate of HUVECs and iLECs by 48% and 100%, respectively, and Methotrexate the migration rate of HUVECs by 48% and of iLECs by 100% after 5 days of treatment prior to the scratch assay (Fig. 3C).

Pemetrexed also reduces migration by 68% of iLECs that were treated after the scratch was made (Fig. 3C). We hypothesize that some of these results could be explained by the differential expression of the target enzymes TYMS and DHFR. For example, expression levels of TYMS is around 6 times higher in proliferating HUVECs than iLECs, possibly reflecting a higher dependence of proliferating HUVECs to TYMS and a higher susceptibility upon inhibition with 5-FU (Fig. 3D). In contrast, expression of DHFR is 50% higher in proliferating HUVECs compared to iLECs, implying that higher sensitivity of iLECs to DHFR inhibition is linked to lower levels of DHFR (Fig. 3D).

Fatty acid synthase (FASN) has previously been reported to be critical for angiogenesis of HUVECs<sup>51</sup>. FASN expression is 1.5 and 2.5-fold increased in proliferating HUVECs and iLECs, respectively, relative to quiescent cells (Fig. 3D). FASN inhibitor C75 stops growth of HUVECs and reduces their migration rate by 52% after long-term and 94% after short-term treatment. C75 also stops growth of iLECs and diminishes migration rate by 100% after long-term and 54% after short-term treatment (Fig. 3E, 3F). FASN inhibition was shown to increase levels of malonyl-CoA in HUVECs, which leads to mTOR malonylation, decreased mTORC1 kinase activity and subsequent decreased proliferation<sup>51</sup>. According to our data, this mechanism may be conserved among different EC types.

Proteomics identified the upregulation of TCA cycle enzymes in quiescent HUVECs (FDR = 0.05) and iLECs (FDR = 0.001) (Suppl. Fig. 2E). Therefore, we hypothesized that MPC inhibition would likely impair cellular functions of ECs. Indeed, growth of HUVECs, but not iLECs, was slightly but significantly decreased by 15% upon treatment with UK5099, an inhibitor of mitochondrial pyruvate carrier (Fig. 3A, 3E). Additionally, UK5099 reduces migration rate in long- and short-term treated HUVECs by 27% and 31%, respectively, and strongly, but with weak statistical significance in long-term treated iLECs (-68%, p-value = 0.08) (Fig. 3F). This indicates that HUVECs but not iLECs rely more on TCA cycle to potentially provide building blocks for proliferation and that reduction of pyruvate flux into TCA cycle impairs a normal quiescent state of HUVECs and iLECs and eventually the ability to migrate<sup>52</sup>. A recent study showed that upregulation of the mitochondrial pyruvate carrier (MPC) in adult neural stem cells is necessary to maintain quiescence by sustaining TCA cycle and OXPHOS, a mechanism that is potentially also crucial for HUVECs and iLECs<sup>53</sup>.

Expression levels of TCA cycle proteins are linked to and generally higher in LECs and might lead to a higher tolerance of LECs to perturbations in TCA cycle (Fig. 1E).

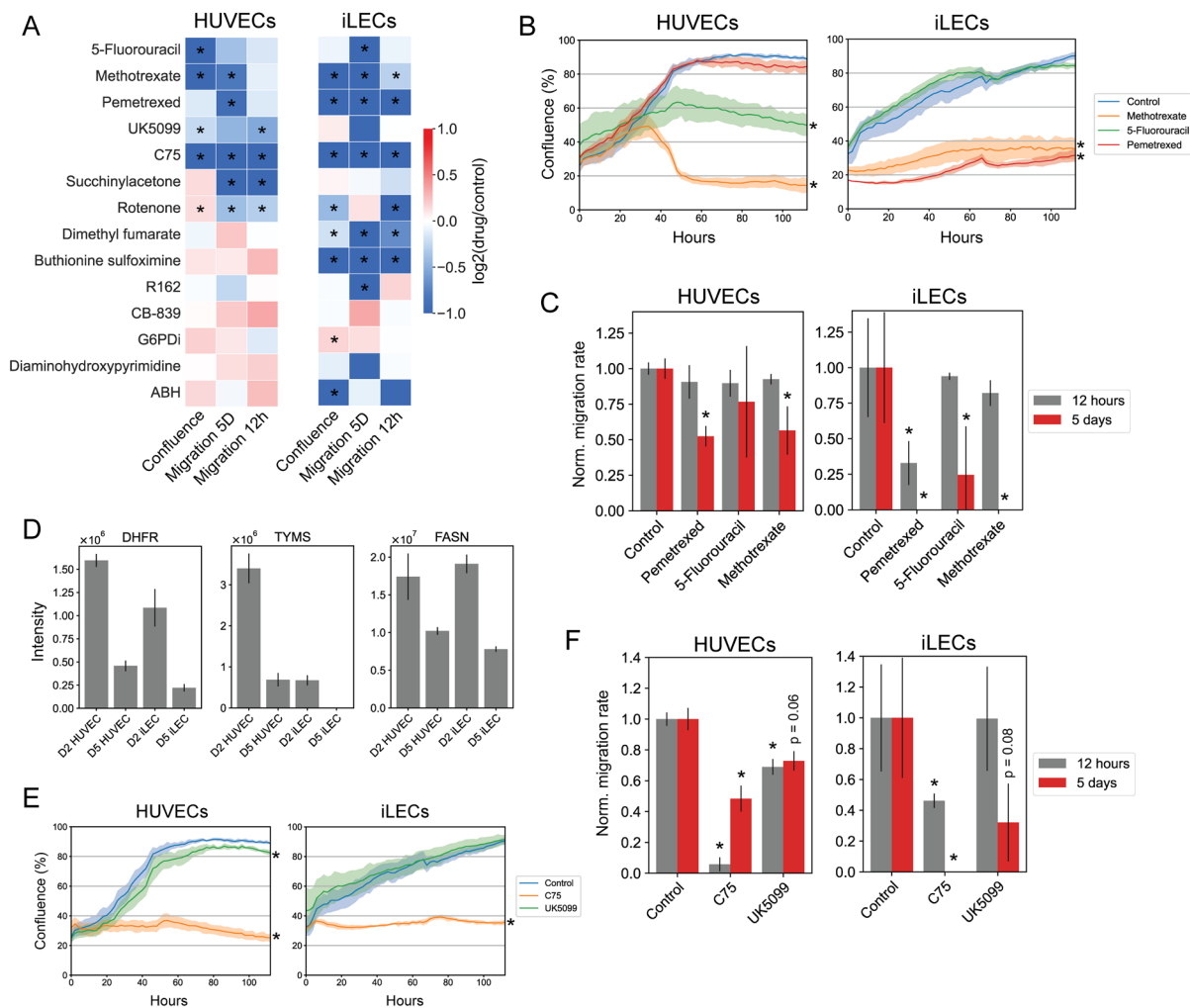


**Figure 3. HUVEC- and iLEC-specific metabolic programs are susceptibilities during quiescence induction.**

- (A) Overview of the phenotypic consequences after treatment with the 14 drugs. Migration 5D refers to the migration rate after 5 days of drug treatment and migration 12h to the migration rate without prior drug treatment.  $n = 3$  replicates for each perturbation and cell line in all measurements.  $p$ -values were determined using a two-tailed Student's  $t$ -test. \* =  $p$ -value < 0.05.
- (B) Growth curves of HUVECs and iLECs treated with anti-proliferative drugs.
- (C) Migration rates of HUVECs and iLECs treated with anti-proliferative drugs, normalized to the respective control. 5 days corresponds to samples that were already treated with drugs 5 days prior to the scratch assay, 12 hours to samples that were treated with drugs only right after scratch generation. Error bars denote standard deviation.  $n = 3$  replicates.  $p$ -values were determined using a two-tailed Student's  $t$ -test. \* =  $p$ -value < 0.05.
- (D) Expression levels of TYMS, DHFR and FASN.
- (E) Growth curves of HUVECs and iLECs treated with C75 and UK5099.
- (F) Migration rates of HUVECs and iLECs treated with C75 and UK5099, normalized to the respective control. 5 days corresponds to samples that were already treated with drugs 5 days prior to the scratch assay, 12 hours to samples that were treated with drugs only right after scratch generation. Error bars denote standard deviation.  $n = 3$  replicates.  $p$ -values were determined using a two-tailed Student's  $t$ -test. \* =  $p$ -value < 0.05.



## HUVECs and iLECs have divergent dependencies to nitric oxide and ROS metabolic pathways for migration and sprouting

Five drugs in our screen directly or indirectly interfere with reactive oxygen species (ROS) and nitric oxide metabolism as part of their mechanism of action (Fig. 4A)<sup>54–58</sup>. The key cardiovascular signalling molecule nitric oxide (NO) plays an important role in promoting migration and angiogenesis of blood endothelial cells and is produced by endothelial nitric oxide synthases (eNOS)<sup>59,60</sup>. Soluble ROS emerge as products of oxidative metabolism in cells and one of its members, superoxide ( $O_2^-$ ), reacts with NO, leading to decreased intracellular NO levels<sup>61–63</sup>. Long-term exposure to ROS leads to cardiovascular dysfunction, however, lower ROS levels are crucial for migration and angiogenesis of HUVECs, through increasing expression of vascular endothelial growth factors<sup>61,64–66</sup>.

Dimethyl fumarate (DF) is an inhibitor of phosphoglycerate dehydrogenase (PHGDH), the enzyme involved in the committing step for *de novo* serine biosynthesis<sup>54,67</sup>. Serine is required for the biosynthesis of heme, a co-factor of ROS-clearing catalases and eNOS. Succinylacetone (SA) depletes heme levels as well, but through inhibition of aminolevulinic acid dehydratase (ALAD), an enzyme involved in heme/porphyrin biosynthesis<sup>55</sup>. Butathione sulfoximine (BS) inhibits *de novo* biosynthesis of the antioxidant glutathione by blocking glutamate cysteine ligase (GCL)<sup>56</sup>. Rotenone blocks Complex I (NADH Coenzyme Q oxidoreductase) of the mitochondrial electron transport chain, leading to elevated ROS levels<sup>57</sup>. G6PDi-1 depletes NADPH levels by decreasing flux into PPP, a major source of NADPH production crucial for detoxification of ROS<sup>68</sup>.

Interestingly, we found that none of these five drugs affects the growth of HUVECs (Fig. 4B). On the other hand, growth of iLECs is decreased by 18% through DF, by 26% through Rotenone and by 57% through BS, indicating that proliferating iLECs are more sensitive than HUVECs to disturbances in ROS metabolism (Fig. 4B). Even though the five drugs do not affect proliferating HUVECs, Rotenone and SA decrease migration rate of HUVECs by around 20% and 80%, respectively, after long- and short-term treatment (Fig. 4C). Rotenone decreases migration of iLECs by 65% only when the drug is added right after the scratch assay (Fig. 4C). SA has no effect on iLEC migration, while DF decreases migration of iLECs up to 90% after long-term treatment

(Fig. 4C). BS and G6PDi do not affect migration of HUVECs (Fig. 4C). G6PDi does not influence migration of iLECs and migration of BS-treated iLECs could not be measured due to premature cell death (Fig. 4C).

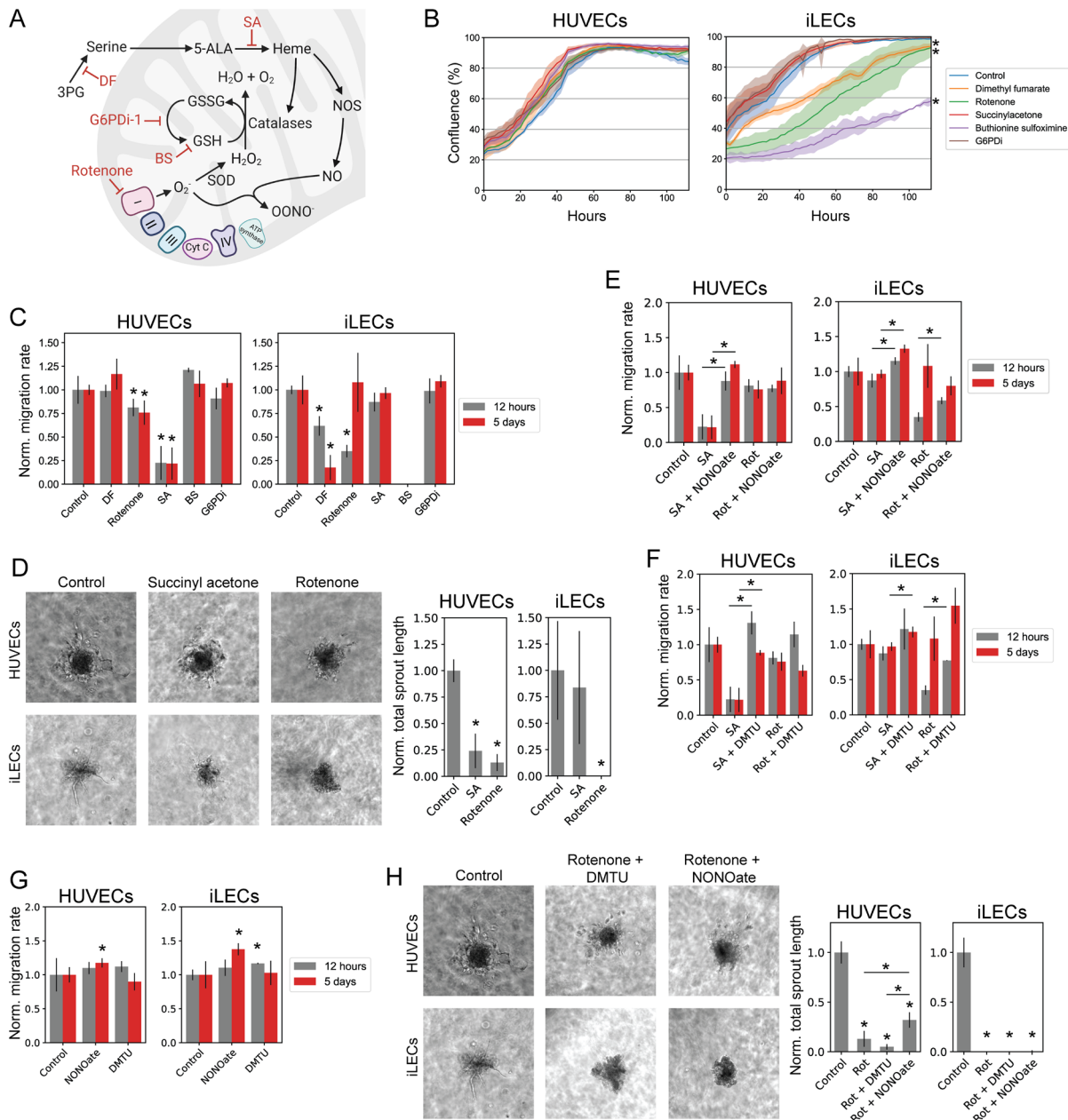


**Figure 4. HUVECs and iLECs have divergent dependencies to nitric oxide and ROS metabolic pathways for migration and sprouting.**

- (A) Schematic overview of the targets of the 5 drugs targeting ROS and NO metabolism. SA = succinyl acetone, DF = dimethyl fumarate, G6PDi = G6PD inhibitor, BS = buthionine sulfoximine.  
 (B) Growth curves of HUVECs and iLECs treated with ROS and NO metabolism targeting drugs.  
 (C) Migration rates of HUVECs and iLECs treated with ROS and NO metabolism targeting drugs, normalized to the respective control. 5 days corresponds to samples that were already treated with drugs 5 days prior to the scratch assay, 12 hours to samples that were treated with drugs only right after scratch generation.

Error bars denote standard deviation. n = 3 replicates. p-values were determined using a two-tailed Student's t-test. \* = p-value < 0.05.

- (D) Representative pictures of vessel sprouting assay and total sprout length normalized to the respective control of HUVECs and iLECs treated with SA and rotenone. Error bars denote standard deviation. n = 3 replicates. p-values were determined using a two-tailed Student's t-test. \* = p-value < 0.05.
- (E) Migration rates of SA- and rotenone-treated HUVECs and iLECs supplemented with NONOate.
- (F) Migration rates of SA- and rotenone-treated HUVECs and iLECs supplemented with DMTU.
- (G) Migration rates of HUVECs and iLECs treated with NONOate or DMTU.
- (H) Representative pictures of vessel sprouting assay and total sprout length normalized to the respective control of HUVECs and iLECs treated with rotenone and supplemented with either NONOate or DMTU. Error bars denote standard deviation. n = 3 replicates. p-values were determined using a two-tailed Student's t-test. \* = p-value < 0.05.

The sensitivity of HUVECs and iLECs to the five drugs does not correlate with protein expression patterns. For example, expression of ALAD, the target of SA, and GCLC, the target of BS, is higher in quiescent HUVECs, but only SA leads to decreased migration (Suppl. Fig. 5). Compared to HUVECs, iLECs have an increased expression of Complex I proteins (NDUFS1, NDUFV2), but migration is not affected in iLECs treated with rotenone for 5 days (Suppl. Fig. 5). G6PD expression is similar in proliferating and quiescent HUVECs and around 20% decreased in quiescent iLECs; however, G6PDi does not impair migration in either cell line (Suppl. Fig. 5).

Further, we assessed whether the differential migratory responses of HUVECs and iLECs to SA and Rotenone treatments are also reflected in angiogenesis. To this end, we performed a sprouting assay, treating the spheroids for 6 days with SA and Rotenone before measuring the total sprout length<sup>69</sup>. SA decreases the total sprout length of HUVECs by 75%, Rotenone by almost 85% (Fig. 4D). SA does not significantly reduce the total sprout length of iLECs, while Rotenone completely diminishes sprouting of iLECs (Fig. 4D).

Proliferating HUVECs are more robust than iLECs to perturbations in redox and NO pathways, but rather rely on balanced ROS levels and heme availability for migration and sprouting. We wondered if balanced ROS levels or heme availability are the necessary factors for HUVECs and iLECs to migrate and sprout. To shed light upon this, we supplemented SA- and Rotenone-treated HUVECs and iLECs with diethylamine NONOate, a NO donor, or separately with dimethylthiourea (DMTU), a hydroxyl radical scavenger. NONOate and DMTU rescue SA-induced migratory defects in HUVECs and promote migration of SA-treated iLECs in the short- and long-term (Fig. 4E and 4F). NONOate does not rescue Rotenone-induced migratory effects in HUVECs but boosts migration rate of short-term Rotenone-treated iLECs by around

60% (Fig. 4E). DMTU slightly increases migration rate of HUVECs treated with Rotenone for 12 hours after the scratch was made (Fig. 4F). Additionally, when DMTU and Rotenone are added to iLECs after the scratch was made, there is a 2-fold increase in migration rate, and a non-significant 40% increase when DMTU is added to iLECs treated for 5 days with Rotenone (Fig. 4F). Interestingly, NONOate alone significantly increases migration rate of HUVECs (+20%) and iLECs (+40%) when treated for 5 days before the scratch assay, but not when treated right after the scratch was made (Fig. 4G), potentially through activation of cGMP-Rho GTPase signalling that exerts its effect on migration only in the long-term<sup>70</sup>. DMTU, on the other hand, increases migration rate of iLECs significantly only when the cells are treated right after scratching (Fig. 4G). We further tested whether DMTU or NONOate supplementation could rescue sprouting defects caused by Rotenone. We find that neither DMTU nor NONOate are able to rescue sprouting defects in Rotenone-treated iLECs (Fig. 4H). DMTU even further reduces total sprout length in Rotenone-treated HUVECs (Fig. 4H). NONOate, however, increases the total sprout length of Rotenone-treated HUVECs by around 2-fold (Fig. 4H).

Taken together, migrating and sprouting HUVECs are more dependent than iLECs on adequate heme availability for NO production. In contrast, iLECs are more sensitive to elevated ROS levels when migrating and proper Complex I activity seems to be crucial for sprouting beyond elevated ROS levels. These results confirm and back up the proteomics and metabolomics results, in which increased intermediates levels in heme biosynthesis only in HUVECs and a stronger enrichment of the electron transport chain in iLECs proposed a cell type-specific dependence on these two pathways.

### **Correct balance of glutamate and $\alpha$ -ketoglutarate levels is crucial for migration and sprouting of iLECs and sprouting of HUVECs**

Recent studies showed that glutamine-dependent asparagine synthesis and anaplerosis is critical for proliferation and, partly, also for migration of HUVECs<sup>20,71</sup>. In our metabolomics analysis, we observed a much stronger decrease of glutamate metabolism intermediates in quiescent vs proliferating HUVECs (FDR =  $1.3 \times 10^{-5}$ ) compared to quiescent vs proliferating iLECs (FDR = 0.04) (Fig. 2D). To assess whether normal cell functions of HUVECs and iLECs are similarly dependent on

glutamate and glutamine metabolism, we included the two drugs CB-839, a glutaminase (GLS1) inhibitor, and R162, a glutamate dehydrogenase (GLUD1) inhibitor, in our inhibition screen (Fig. 5A). Due to higher glutamine uptake and stronger reduction of glutamate metabolism intermediates in quiescent HUVECs, we expected higher susceptibility of HUVECs to perturbations with these drugs, especially in migration, since the cells start migration from a quiescent state. CB-839 and R162 do not affect proliferation of HUVECs and iLECs (Fig. 5B). Migration of HUVECs and iLECs is not impaired by CB-839, in fact migration is slightly increased (Fig. 5C). To our surprise, we observed a 60% decrease in migration of long-term R162-treated iLECs, and only a non-significant 16% decrease of migration in HUVECs (Fig. 5C).

Addition of cell-permeable dimethyl- $\alpha$ -ketoglutarate (DMaKG) to replenish the TCA cycle increases migration of R162-treated iLECs by 2-fold but decreases migration of HUVECs by another 10%; however, in both cases the changes are not significant (Fig. 5D). Surprisingly, DMaKG alone decreases migration of iLECs by around 80%, but only by 30% in short-term treated HUVECs (Fig. 5D). In accordance with the migration results, CB-839 slightly increases total sprout length of HUVECs and iLECs (Fig. 5E). Interestingly, R162 reduces total sprout length of HUVECs and iLECs by around 30%, even though there was no effect of R162 on migration of HUVECs (Fig. 5E). Furthermore, DMaKG supplementation does not rescue R162-induced sprouting defects but even leads to a 70% decrease of total sprout length in HUVECs and iLECs (Fig. 5E). These results suggest that iLECs have either a lower capacity to metabolize excess glutamate than HUVECs or they are more dependent on fully functioning GLUD1 and hence glutamate-derived carbon flow into TCA cycle for migration (Fig. 6). Moreover, the sprouting assay results indicate a role of glutamate metabolism on angiogenesis beyond its isolated effect on EC migration.

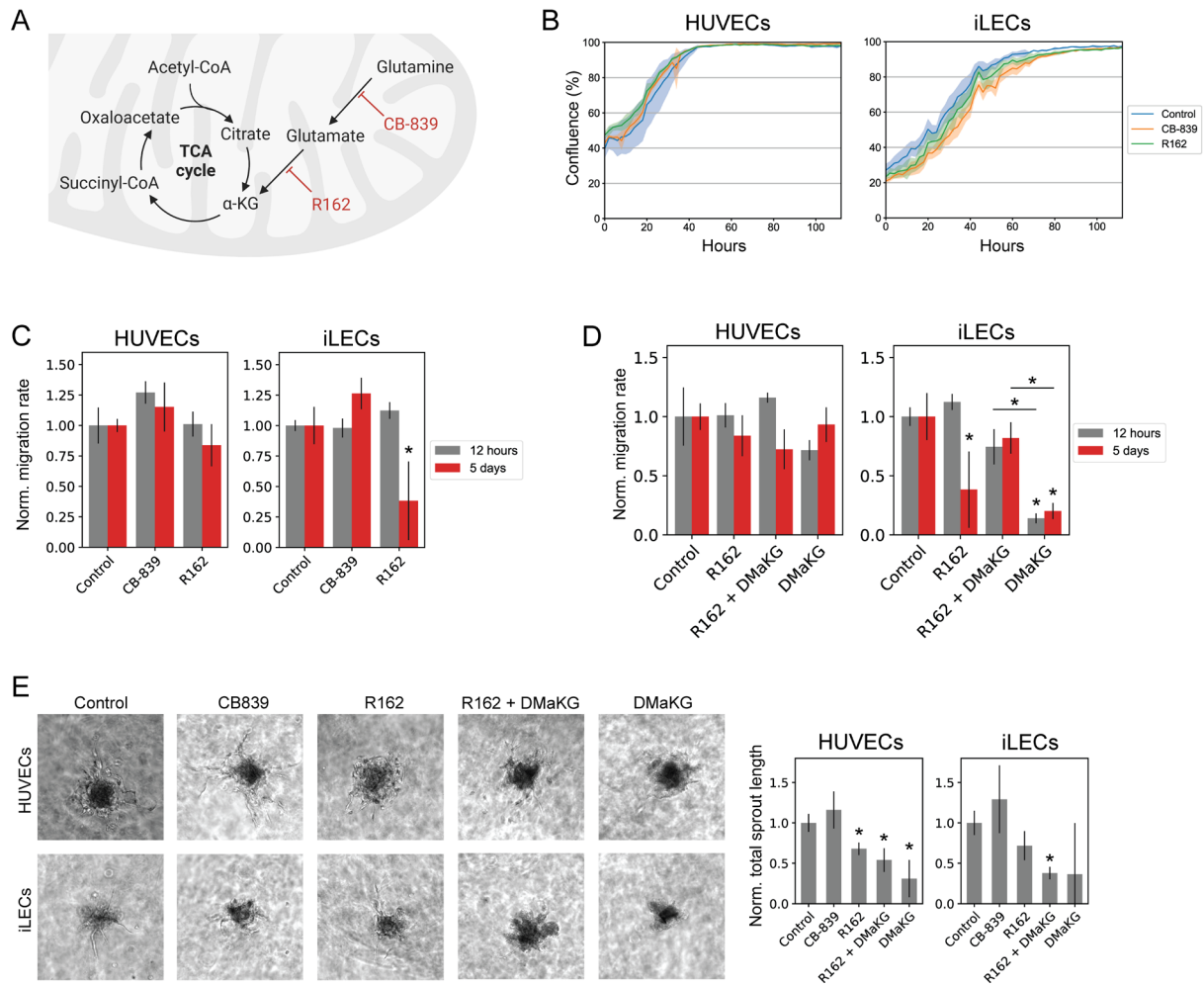


**Figure 5. Correct balance of glutamate and  $\alpha$ -ketoglutarate levels is crucial for migration and sprouting of iLECs and sprouting of HUVECs.**

- (A) Schematic overview of the targets of CB-839 and R162.
- (B) Growth curves of HUVECs and iLECs treated with CB-839 and R162.
- (C) Migration rates of CB839- and R162-treated HUVECs and iLECs, normalized to the respective control. 5 days corresponds to samples that were already treated with drugs 5 days prior to the scratch assay, 12 hours to samples that were treated with drugs only right after scratch generation. Error bars denote standard deviation.  $n = 3$  replicates.  $p$ -values were determined using a two-tailed Student's  $t$ -test. \* =  $p$ -value  $< 0.05$ .
- (D) Migration rates of HUVECs and iLECs treated with R162 and dimethyl  $\alpha$ -ketoglutarate (DMaKG).
- (E) Representative pictures of vessel sprouting assay and total sprout length normalized to the respective control of HUVECs and iLECs treated with CB839, R162, R162 + DMaKG and DMaKG. Error bars denote standard deviation.  $n = 3$  replicates.  $p$ -values were determined using a two-tailed Student's  $t$ -test. \* =  $p$ -value  $< 0.05$ .

## Discussion

Here, taking a multi-omics approach, we characterized the molecular patterns underlying the identities and quiescence induction dynamics of four different EC types

to create a resource to better study and understand EC biology. Using a data-driven analysis approach, we found that FAO and TCA cycle/mitochondrial respiration are the two top enriched pathways associated with LEC identities, even before other signalling pathways like VEGF signalling. Both metabolic pathways have known roles in lymphangiogenesis but it still underscores the crucial role of metabolism in maintenance of LEC identities<sup>16,29</sup>. Such a strong enrichment of metabolic pathways on the proteome level was not observed in BECs. Moreover, we clearly show that metabolic pathways are formative for LEC and BEC identities and states. While all cell lines had similar growth and quiescence induction rates and phenotypes, the underlying metabolic patterns are diverse and reflected in cell type-specific uptake and secretion of metabolites and an intracellular metabolic and proteomic reorganization. We found that all EC types secrete lactate and take up ascorbate in proliferation and quiescence, but uptake of glucose and amino acids varies between cell types and states, strongly suggesting distinct metabolic patterns that support specific functions of the EC types. Intracellular metabolomics analysis further identified 63 metabolites and 51 metabolic pathways that changed between quiescence and proliferation in at least one of the cell lines, supporting the case of EC-specific metabolic adaptations. These results are in line with proteomics data; although, altered protein expression only partly explains changes in metabolite abundances. Nevertheless, we identify a core metabolic signature at the protein-level for quiescence in all EC types, which includes downregulation of nucleotide metabolism and upregulation of FAO and BCAA catabolism. These findings support reports about the relevant role of FAO for quiescence maintenance in HUVECs and propose that FAO is a universal metabolic driver of EC quiescence maintenance. In addition, the observed, increased expression of BCAA catabolism proteins suggests that BCAA catabolism might have a relevant role in quiescence maintenance in ECs as described previously for hematopoietic stem cells<sup>15,45,72</sup>.

Our data provides further evidence that ECs from different tissues and vascular beds are metabolically distinct and that metabolic rewiring in quiescence is driven by the needs of each individual EC type to meet and support their specific functions<sup>22–24</sup>. Indeed, HUVECs and iLECs exhibit a range of phenotypic alterations in response to targeted inhibition of metabolism. In our inhibitor screen, we observed differential sensitivity to inhibition of nucleotide and folate metabolism, fatty acid synthesis, TCA cycle, ROS and NO metabolism and glutamate metabolism. Some anti-proliferative

drugs targeting nucleotide and folate metabolism have an inhibitory effect on proliferation and migration of iLECs and HUVECs, but with various magnitudes. FASN was previously reported to be crucial for proliferation and vessel sprouting of HUVECs by preventing accumulation of malonyl-CoA<sup>19</sup>. Proliferation and migration of HUVECs and iLECs are impaired by FASN inhibition, indicating a conserved role of a fully functioning FASN in angiogenesis of blood and lymphatic vessels. MPC blockage reduces proliferation of HUVECs but not iLECs, and thus suggests that glycolysis-derived pyruvate, besides acetate from FAO, functions as an additional source fuelling TCA cycle and subsequent nucleotide precursors biosynthesis<sup>17</sup>. Decreased proliferation could also explain why short-term UK5099 treatment reduces migration of HUVECs but not iLECs. Interestingly, MPC inhibition over 5 days prior to the scratch assay impairs migration of HUVECs and iLECs, possibly by perturbing transition into or maintenance of quiescence, suggesting that ECs need to establish a fully functional quiescent state to be prepared for migration.

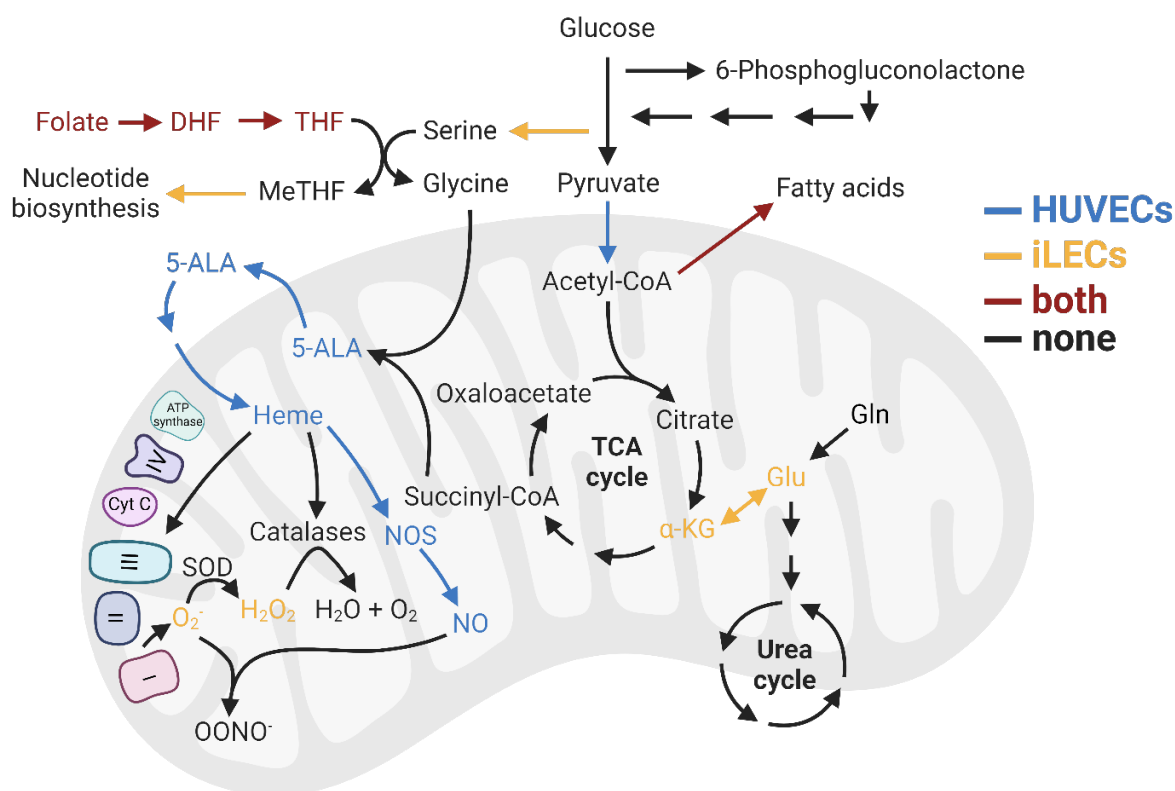


**Figure 6. Schematic overview of HUVEC- and iLEC-specific dependencies on metabolic pathways/reactions for migration**



One of the most striking differences between HUVECs and iLECs is HUVECs dependence on heme. Our inhibition screen confirmed the findings of the metabolomics screen that HUVECs, but not iLECs, rely on heme biosynthesis metabolism; possibly, to ensure sufficient levels of heme as co-factor for NOS to produce NO that is crucial for migration of HUVECs. Yet, NONOate supplementation alone promotes migration of iLECs, which underlines the general important role of NO on migration<sup>59,60</sup>. The effect of NO levels on vessel sprouting is a bit less clear. NONOate fails to rescue migratory effects caused by Rotenone, but sprouting defects of Rotenone-treated HUVECs are partly rescued by NONOate. This could have multiple reasons. First, sprouting is a more complex mechanism than migration, considerably more factors play a role in mediating sprouting (e.g. extracellular cues<sup>73</sup>) and thus, the increased levels of NO might influence factors that boost sprouting but not migration. Second, elevated superoxide levels through Rotenone treatment may have a stronger detrimental effect on sprouting than migration and NONOate addition might attenuate these effects by lowering superoxide levels.

We observed a similar increase of complexity from migration to sprouting in R162- and DMaKG-treated iLECs and HUVECs. Treatment with the GLUD1 inhibitor R162 diminishes migration significantly in iLECs, but only after long-term treatment. Surprisingly, DMaKG supplementation also reduces migration of iLECs. R162, through GLUD1 inhibition, and DMaKG, through negative feedback regulation of GLUD1, potentially lead to toxic intracellular glutamate accumulation or iLECs are specifically sensitive to inhibition of GLUD1 through subsequent impaired malate-aspartate shuttle activity<sup>74–76</sup>. Metabolic flux analysis could be employed in future experiments to assess how metabolic fluxes are rewired when GLUD1 is inhibited in both cell types. Furthermore, both R162 and DMaKG impair sprouting of HUVECs and iLECs. This suggests an effect of glutamate metabolism on (lymph)angiogenesis beyond its isolated effect on EC migration. Previous reports propose that overactivation of ionotropic glutamate receptors, such as NMDA, results in decreased tube network formation and increased vascular permeability in brain BECs and HUVECs<sup>77,78</sup>. Possibly, increased glutamate levels are cleared by increased secretion of glutamate, which leads to higher auto- and paracrine activation of glutamate receptors, resulting in impaired sprout formation.

With the presented work, we contribute to the understanding of how metabolism governs various cellular states and functions of EC types from different tissues and

vascular beds. Furthermore, we provide evidence that certain metabolic pathways play distinct roles in establishing and maintaining a cellular state or function of HUVECs and iLECs, possibly because nutrient and oxygen availability varies greatly in the microenvironments of different ECs and have a direct influence on their metabolic lifestyle. The fact that we captured the metabolic peculiarities of ECs and that we were able to reproduce some *in vivo* findings in our *in vitro* screen shows how important further *in vitro* studies are to expand the understanding of the role of metabolism in mediating and maintaining EC specialization and function.

## **Materials and Methods**

### **Cell culture**

Human umbilical vein endothelial cells were purchased from Lonza (cat. no. C2519A), human dermal blood endothelial cells (cat. no. C-12211) and human dermal lymphatic endothelial cells (cat. no. C-12216) from PromoCell. Intestinal lymphatic endothelial cells are a kind gift from Tatiana Petrova from the University of Lausanne. All endothelial cells were cultured in T-75 cell culture flasks (Thermo Fisher Scientific, cat. no. 156472) in Endothelial Cell Growth Medium-2 (EGM-2) (BulletKit, Lonza, cat. no. CC-3162). EGM2 was made from Endothelial Cell Basal Medium-2 (EBM2), with added endothelial supplements including 2% fetal bovine serum (FBS) (v/v), hydrocortisone, VEGF, human FGF, R3-IGF-1, ascorbic acid, human EGF, glutaraldehyde GA-1000, and heparin. Additionally, we added 10mg/ml ciprofloxacin (Sigma-Aldrich, cat. no. 17850). After the first passage, regular FBS in the culture medium was replaced by dialyzed FBS (dFBS, Sigma-Aldrich, cat. no. F0392). Experiments were performed until passage six. For metabolomics, proteomics and phenotype experiments, cells were seeded at a density of 20'000 cells/cm<sup>2</sup> in a mixed medium (MM). MM consists of 50% EGM2 (with dFBS) and 50% Medium 199 (Gibco, cat. no. 22340020) supplemented with 20% dFBS, 1% penicillin/streptomycin (P/S, Gibco, cat. no. 15140122), 2mM glutamine (Gibco, cat. no. 25030081) and 0.4% (v/v) endothelial cell growth supplement (PromoCell, cat. no. C-39215).

### **Quiescence induction and cell cycle analysis**

ECs were grown for 10 days to assess fractions of proliferating and quiescent cells at each day. The fraction was determined by EdU incorporation into DNA using the EdU Flow Cytometry Kit 488 from baseclick (Sigma-Aldrich, cat. no. BCK-FC488-100)<sup>79</sup>. Briefly, EdU was added at a concentration of 10 $\mu$ M 24 hours prior to trypsinization and cell fixation with 4% PFA to label the cells. Using a click-it reaction, 6-FAM was attached to EdU and EdU incorporation analysed using a BD LSRFortessa Cell Analyzer with a 488nm laser for excitation and a 530/30 emission filter. Flow cytometry data was analysed with Flowing Software 2.5.1 from Turku Bioscience.

## Proteomics

Proteomics sample preparation protocol was adapted from <sup>80</sup> and <sup>81</sup>. In brief, cells were grown in 1.5ml mixed medium in 6-well plates as described above. After removal of medium and washing of cells with PBS, cells were lysed in lysis buffer (8M urea buffer) and subsequently sonicated, centrifuged and supernatants transferred into fresh tubes for protein reduction with DTT and alkylation with iodoacetamide. Supernatants were incubated for 25min at 50°C with 5mM DTT and after cooling down to room temperature, iodoacetamide to 15mM final concentration was added and the mixture incubated for 30min at RT in the dark. An additional 5mM DTT was used to quench unreacted iodoacetamide for 15min at RT in the dark. Protein concentration was determined by BCA assay. Samples were then diluted 1:8 with 100mM HEPES, pH 8.5, to reduce the concentration of urea to 1M. Trypsin was added to the diluted samples to reach a 100:1 sample:trypsin (w/w) ratio and the mix incubated at 37°C overnight on a thermomixer. To stop trypsin digestion, samples were acidified with TFA to 0.4% (vol/vol) to reach a pH around 3. Before MS measurements, samples were desalted using Pierce C18 spin columns (Thermo Scientific, cat. no. 89870).

Peptides were analyzed online by liquid chromatography-tandem mass spectrometry (LC-MS/MS). Online reversed phase chromatography was performed using a Vanquish Neo UPLC system (Thermo Scientific, Sunnyvale) equipped with a heated column compartment set to 50 °C. Mobile Phase A consisted of 0.1% formic acid (FA) in water, while Mobile Phase B was 80% acetonitrile in water and 0.1% FA. Peptides (~1  $\mu$ g) were loaded onto a C18 analytical column (500 mm, 75  $\mu$ m inner diameter), packed in-house with 1.8  $\mu$ m ReproSil-Pur C18 beads (Dr. Maisch, Ammerbuch, Germany) fritted with Kasil, keeping constant pressure of 600 bar or a

maximum flow rate of 1  $\mu\text{l}/\text{min}$ . After sample loading, the chromatographic gradient was run at 0.3  $\mu\text{l}/\text{min}$  and consisted of a ramp from 0 to 43% Mobile Phase B in 70 min, followed by a wash at 100% Solution B in 9 min total, and a final re-equilibration step of 3 column volumes (total run time 90 min).

Peptides from each sample were analysed on an Orbitrap HF-X mass spectrometer (Thermo Fisher Scientific, San Jose, CA) using an overlapping window data-independent analysis (DIA) pattern described by Searle et al<sup>82</sup>, consisting of a precursor scan followed by DIA windows. Briefly, precursor scans were recorded over a 390-1010 m/z window, using a resolution setting of 120,000, an automatic gain control (AGC) target of  $1\text{e}6$  and a maximum injection time of 60 ms. The RF of the ion funnel was set at 40% of maximum. A total of 150 DIA windows were quadrupole selected with an 8 m/z isolation window from 400.43 m/z to 1000.7 m/z and fragmented by higher-energy collisional dissociation, HCD, (NCE=30, AGC target of  $1\text{e}6$ , maximum injection time 60 ms), with data recorded in centroid mode. Data was collected using a resolution setting of 15,000, a loop count of 75 and a default precursor charge state of +3. Peptides were introduced into the mass spectrometer through a 10  $\mu\text{m}$  tapered pulled tip emitter (Fossil Ion Tech) via a custom nano-electrospray ionization source, supplied with a spray voltage of 1.6 kV. The instrument transfer capillary temperature was held at 275  $^{\circ}\text{C}$ .

All Thermo RAW files were converted to mzML format using the ProteoWizard package<sup>83</sup> (version 3.0.2315). Vendor-specific peak picking was selected as the first filter and demultiplexing with a 10ppm window was used for handling the overlapping data collection window scheme. Processed mzML files were then searched using DIA-NN<sup>84</sup> (version 1.8) and the UniProt Homo sapiens proteome (UP000005640, June 15 2021) as the FASTA file for a “library-free” deep neural network-based search approach. Data was searched using deep learning-based spectra and retention time as described by Demichev et al, with trypsin as the protease, and allowing for 2 missed cleavages, with N-terminal methionine cleavage, and cysteine carbamidomethylation. Peptide length was allowed to range from 7-30 amino acids with a precursor charge state range from +1 to +4, a precursor range of 300-1800 m/z and a fragment ion range of 200-1800 m/z. Data was processed to a 1% precursor-level false discovery rate (FDR) with mass accuracy, MS1 accuracy, and match between runs set to the software default settings. A single-pass mode neural network classifier was used with protein

groups inferred from the input Homo sapiens FASTA file. Protein quantities were normalized by delayed normalization and maximal peptide ratio extraction (maxLFQ)<sup>85</sup>.

### **Intracellular metabolomics**

Cells were grown in 1.5ml mixed medium in 6-well plates as described above. Every 24 hours, the medium was removed from the wells and cells were washed with pre-warmed wash buffer, made of freshly prepared 75 mM ammonium carbonate in nanopure water, adjusted to pH 7.4 using 10% acetic acid. After washing the cells, metabolites were extracted with ice-cold extraction buffer, containing 40% (v/v) methanol, 40% (v/v) acetonitrile and 20% (v/v) nanopure water for 1 hour at -20°C. Cells were detached from the wells using a cell lifter, transferred into tubes and centrifuged. Supernatants (metabolic extracts) were stored at -80°C until measurement. Untargeted metabolomics of metabolic extracts was performed by flow injection analysis–time-of-flight mass spectrometry on an Agilent 6550 Q-TOF mass spectrometer as previously described<sup>46</sup>. Measurements were performed in negative ionization mode, and spectra were recorded from a mass/charge ratio of 50 to 1000. Ions were annotated based on their measured mass using reference compounds from the Human Metabolome Database (HMDB 4.0), with a tolerance of 1 mDa. Data analysis was performed with an in-house developed pipeline based on Matlab (The MathWorks). Samples were normalized within each cell-type by normalization of the mean ion intensity to account for the cell number differences at sampling. Differential analysis was performed using a Student's t test and significance was corrected for multiple hypothesis testing with the Benjamini-Hochberg method, and an adjusted p-value < 0.05 was considered significant. Metabolic pathway enrichment was done using pathway definitions from HMDB, using a p-value cut-off of 0.05 and a log<sub>2</sub>(fold-change (FC)) cut-off of 0.25. Significance of enrichments was corrected for multiple hypothesis testing by the Benjamini-Hochberg method, and an adjusted p-value of < 0.05 was considered significant.

### **Extracellular metabolomics**

Cells were grown in 1.5ml mixed medium in 6-well plates as described above. Every 24 hours, the medium was replaced with fresh medium. Supernatant samples were taken 0 hours, 2 hours, 22 hours and 24 hours after medium exchange. Supernatant samples were diluted 1:50 with nanopure water before metabolomics measurement.

Untargeted metabolomics of supernatant samples was performed by flow injection analysis–time-of-flight mass spectrometry on an Agilent 6520 Q-TOF mass spectrometer as described above. Ions were annotated based on their measured mass using reference compounds from the Human Metabolome Database (HMDB 4.0), with a tolerance of 3 mDa. Within each day, samples were normalized to the first time point and linear regression applied to determine the uptake or secretion rate in normalized ion intensity per hour.

## **Validation experiments**

For conditions with pharmacological perturbations, we used IC<sub>50</sub> concentrations of inhibitors previously noted for HUVECs or other mammalian cell lines (Table 2)<sup>54,56,58,86–94</sup>. The drugs or supplements listed below were added to mixed medium at the indicated concentration, and the medium was sterile filtered through a filter with 0.2µm pore size. Medium with drugs was refreshed after 2 days and prepared freshly for each experiment. For drugs dissolved in DMSO, a control condition medium with equal concentration of DMSO was prepared.

## **Phenotypic characterizations**

Phenotype was assessed using three characteristics: response of cells to drug treatment in proliferation, migration, and quiescence:

### **Proliferation**

To determine the effect of drug compounds on EC proliferation, iLECs and HUVECs were seeded in 96-well plates at 20'000 cells/cm<sup>2</sup> in mixed medium on day zero. Cells were left to attach for four to six hours, after which the medium was exchanged with drug-containing medium. Cell growth was determined using an Incucyte S3 Live-Cell Analysis instrument.

**Table 2. Drugs used in the validation experiments.**

Compound name	Source and cat. no.	Concentration
UK5099	Sigma-Aldrich, PZ0160	40 $\mu$ M
G6PDi-1	Sigma-Aldrich, SML2980	0.07 $\mu$ M
Rotenone	Sigma-Aldrich, R8875	0.5 $\mu$ M
CB-839	Lucerna-Chem, 10-4556	23nM
R162	Sigma-Aldrich, 5380980001	23 $\mu$ M
Succinyl acetone (SA)	Sigma-Aldrich, D1415	18 $\mu$ M
Diaminohydroxypyrimidine	Fisher Scientific, 11474757	300 $\mu$ M
Buthionin sulfoximin	Sigma-Aldrich, B2515	2 $\mu$ M
ABH hydrochloride	Sigma-Aldrich, SML1466	0.14 $\mu$ M
Methotrexate	Sigma-Aldrich, PHR1396	100 $\mu$ M
C75	MedChemExpress, HY-12364	35 $\mu$ M
Dimethyl fumarate	Sigma-Aldrich, 242926	25 $\mu$ M
Pemetrexed	Sigma-Aldrich, PHR1596	200nM
5-Fluorouracil	Sigma-Aldrich F8423	10 $\mu$ M
Paclitaxel	Selleckchem, S1150	0.1pM
N $\omega$ -Nitro-L-Arginin (L-NNA)	Sigma-Aldrich, N5501	1mM
DEA-NONOate (NONOate)	Sigma-Aldrich, D184	100 $\mu$ M
N,N'-Dimethylthiourea (DMTU)	Sigma-Aldrich, D188700	10mM
Dimethyl-a-ketoglutarate	Sigma-Aldrich, 349631	1mM

### Migration assays

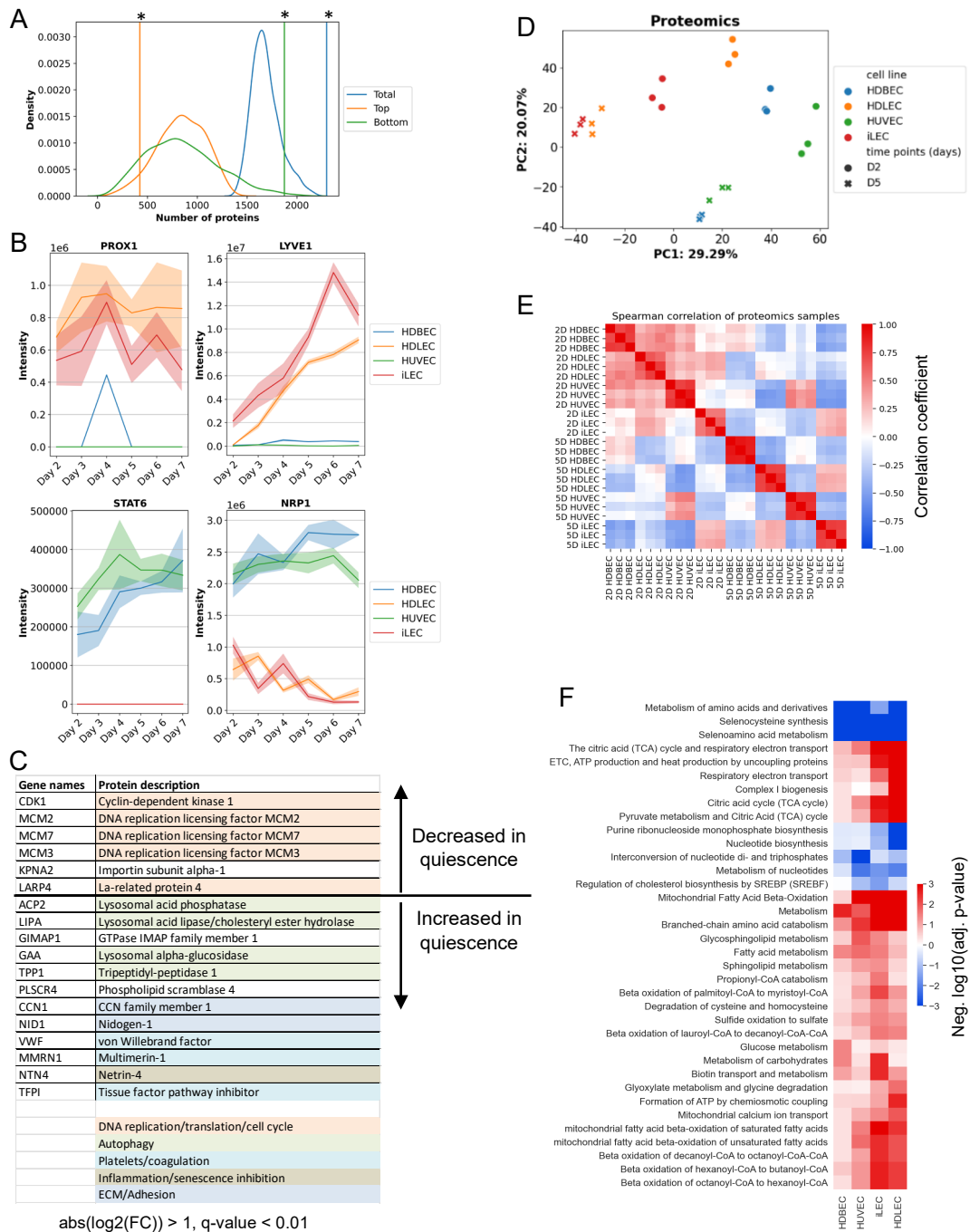
iLECs and HUVECs were seeded in 96-well plates at 20'000 cells/cm<sup>2</sup> and grown for five days with or without drugs, in order to reach contact-inhibited quiescence. On day five, a scratch wound was inflicted on the confluent cell layer in each well using the tip of a 20 $\mu$ l pipette. Medium with drugs was then immediately added to cells which had been grown to contact-inhibition with drugs, respectively newly added to cells which had been grown to quiescence without drugs to capture the effects of chronic and acute drug exposure on migration. The scratch in each well was imaged for 48 hours using an Incucyte S3 Live-Cell Analysis instrument. Migration rate was determined by measuring the width of the scratch at 0 and 12 hours using Fiji ImageJ and calculating the distance that was closed by cells in 12 hours.

### Vessel sprouting assays

Vessel sprouting assays were performed as previously described<sup>69</sup>. Methocel solution was prepared by dissolving 1.2% methyl cellulose (Sigma-Aldrich, cat. no. M0512) in basal medium 199 and stirring the solution at 4% overnight, followed by centrifugation at  $3500 \times g$  for 3h at 4°C. Collagen solution was prepared at the time of the experiment from 3.75mg/ml PureCol collagen (Sigma-Aldrich, cat. no. 5006) in 0.1% acetic acid. The collagen solution was mixed 8:1 with mixed medium, after which pH was adjusted with 0.2M NaOH and 1M HEPES. Spheroids were generated according to the same published protocol by suspending HUVECs or iLECs in mixed medium with 20% Methocel solution to 16'000 cells/ml. From the cell suspension, droplets of 25µl were pipetted onto the lid of a petri dish. The droplets were incubated hanging upside-down for 24h at 37°C to allow for the formation of spheroids. After 24h, spheroids were collected by gently washing them off the petri dish lid with medium. Spheroids were then centrifuged for 5min at 100 x g and carefully resuspended in Methocel solution with 20% FBS and 0.2% Penicillin/Streptomycin. The cell suspension was then gently mixed 1:1 with the collagen solution and distributed over wells of a 48-well plate. The plate was incubated for 30min to allow gelation, after which spheroids were stimulated with mixed medium containing 350ng/ml human VEGF-165 recombinant protein (ThermoFisher, cat. no. PHC9391), for a final concentration of 50ng/ml in the gel. Depending on the condition, drug compounds were added to the medium at 7x of the desired final concentration in the gel. Spheroids gels were imaged by brightfield microscopy after 72 hours at 40x magnification. Sprouts were defined by visual inspection and measured in length using Fiji ImageJ.

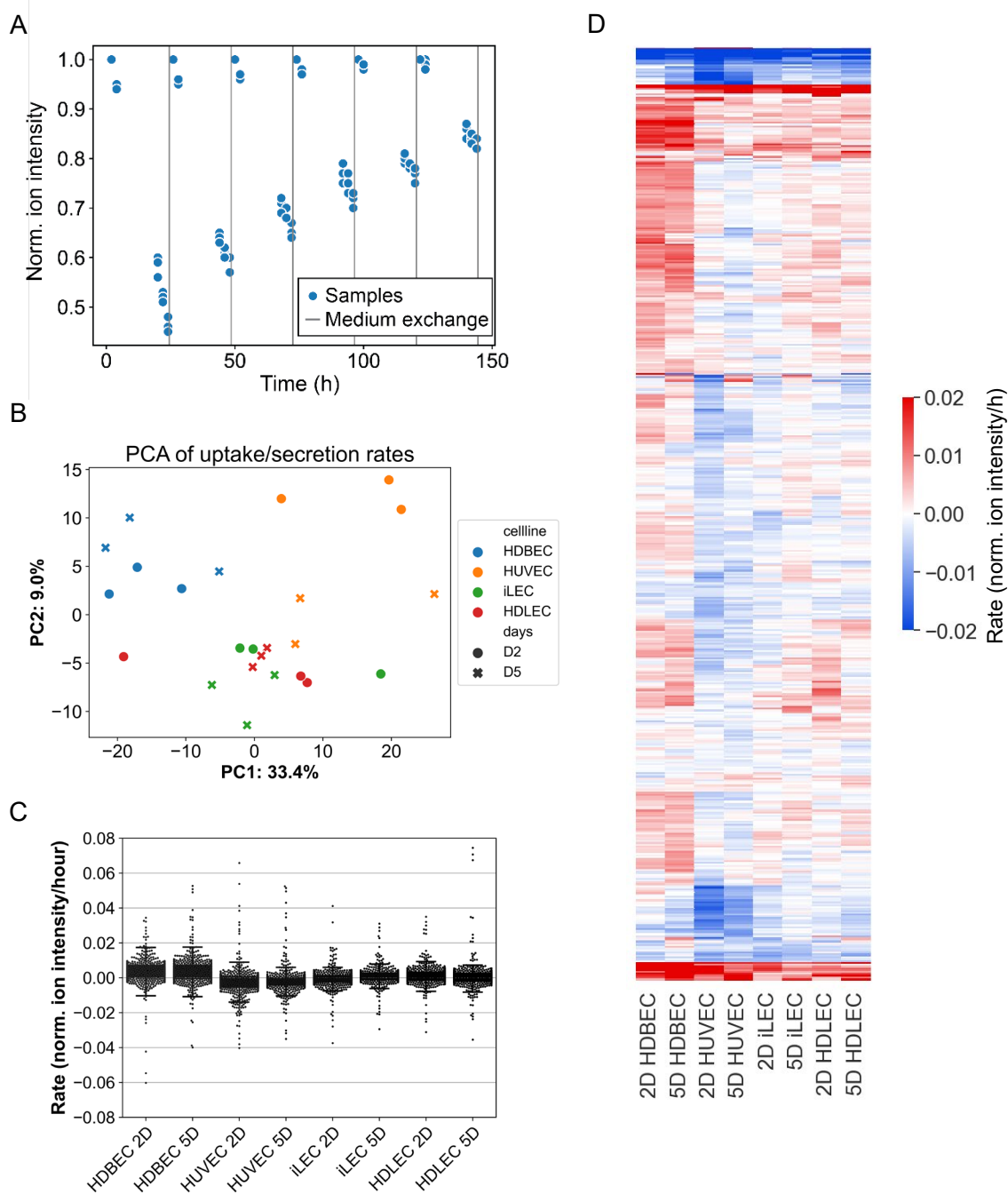


## Supplementary Material



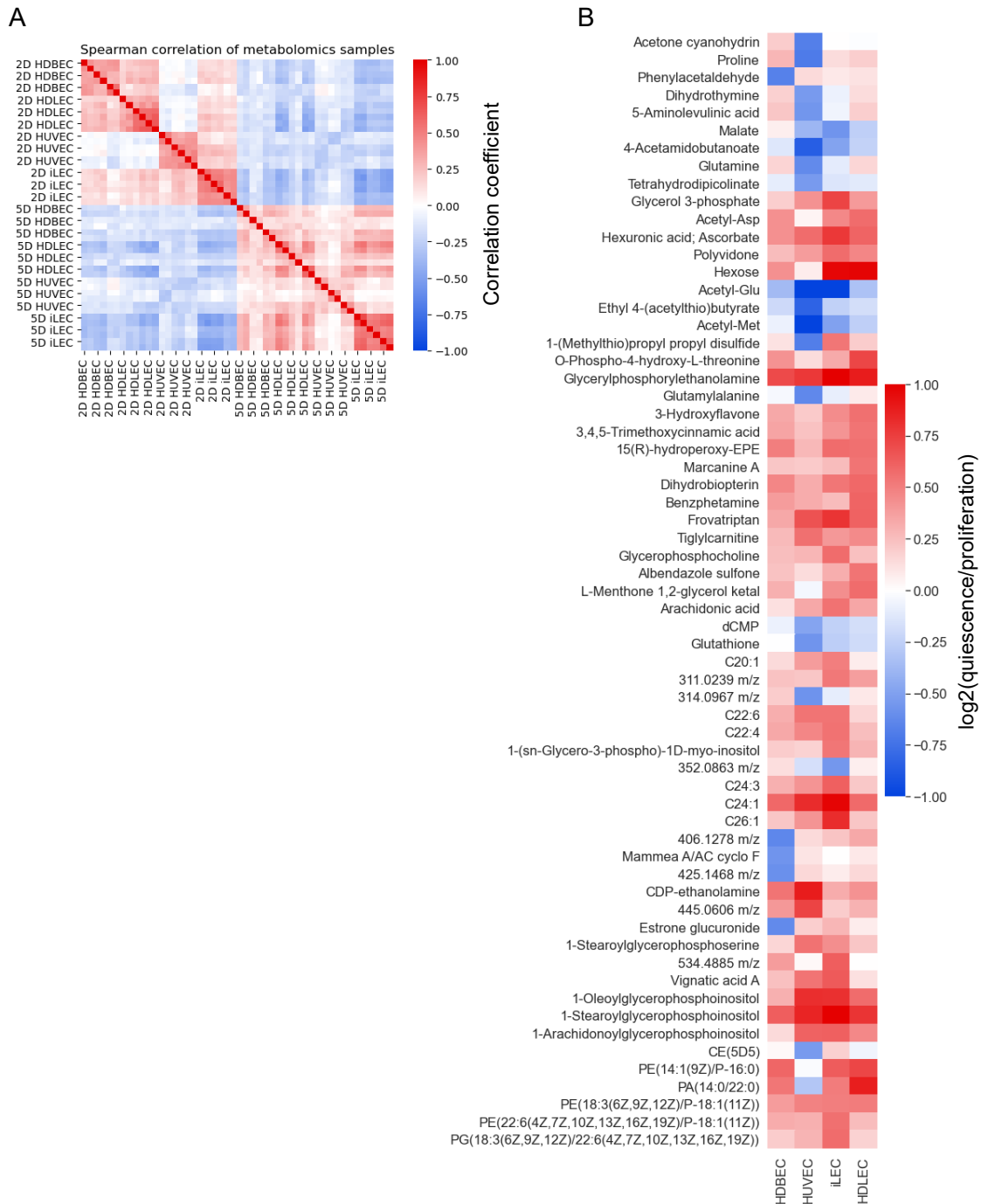
Supplementary Figure 1. Proteomic patterns underlying EC identities and states.

- (A) Permutation test to check whether the number of proteins passing the LV1 threshold is random. The curves depict the distributions of the top 10%, bottom 10% and combined numbers. The vertical lines depict the actual values. p-values were determined using a permutation test. \* = p-value < 0.05.
- (B) Expression levels of LEC markers PROX1 and LYVE1 and BEC markers STAT6 and NRP1.
- (C) Core protein expression changes. Proteins that pass a threshold of  $\text{abs}(\log_2(\text{quiescence/proliferation})) > 1$  and q-value < 0.01 in all cell lines. The colors indicate the process the proteins are involved in.
- (D) Principle component analysis of day 2 (proliferating) and day 5 (quiescent) proteomics samples.
- (E) Spearman correlation of z-scored proteomics data.
- (F) Pathway enrichment analysis of proteomics data of quiescence (day 5) vs proliferation (day 2) samples, hierarchically clustered. Negative values correspond to decreased enrichments in quiescence, positive values to increased enrichments in quiescence.



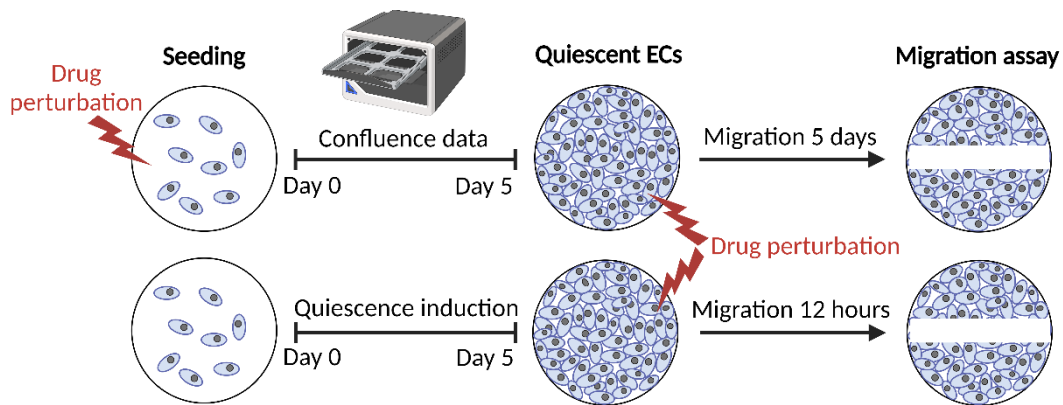
**Supplementary Figure 2. Overview of analysis and results of extracellular metabolomics data.**

- (A) Overview of the experimental workflow.
- (B) PCA of z-scored uptake and secretion rate of each cell line in proliferation (D2) and quiescence (D5).
- (C) Overview of uptake and secretion rates of all 521 extracellular metabolites measured. Each dot represents a metabolite. Negative rate corresponds to uptake, positive rates to secretion of metabolites.
- (D) Hierarchical clustered metabolite uptake and secretion rates of all 521 extracellular metabolites measured.

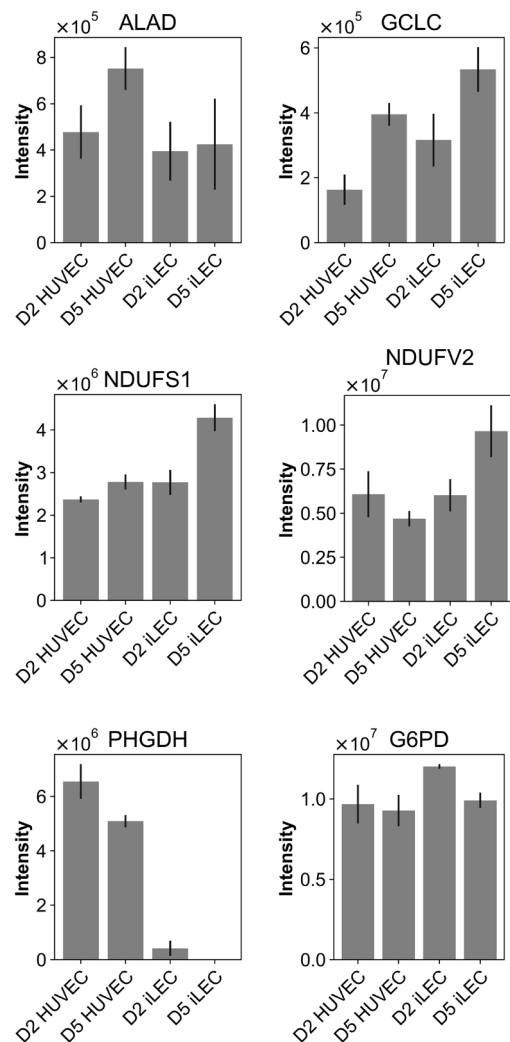


**Supplementary Figure 3. Intracellular metabolomics patterns.**

- (A) Hierarchically clustered Spearman's correlations of z-scored intracellular metabolomics data.
- (B) Overview of metabolites that are changed between quiescence vs proliferation in at least one cell line, passing a threshold of  $abs(\log_2(\text{qsc vs prolif})) > 0.5$  and adj. p-value  $< 0.05$ .



**Supplementary Figure 4. Overview of the functional validation experiments.**



**Supplementary Figure 5.** Expression levels of aminolevulinic acid dehydratase (ALAD, target of SA), glutamate cysteine ligase (GCLC, target of BS), NADH-ubiquinone oxidoreductase 75 kDa subunit (NDUFS1, Complex I, target of rotenone), NADH dehydrogenase [ubiquinone] flavoprotein 2 (NDUFV2, complex I, target of rotenone), D-3-phosphoglycerate dehydrogenase (PHGDH, target of DF) and glucose-6-phosphate 1-dehydrogenase (G6PD, target of G6PDI).

**Supplementary Table 1:** Untargeted proteomics dataset, normalized intensities & results of PLS-DA

**Supplementary Table 2:** Differential analysis of D5 vs D2 samples & pathway enrichment analysis

**Supplementary Table 3:** Extracellular metabolomics dataset, normalized intensities

**Supplementary Table 4:** Intracellular metabolomics dataset, normalized intensities & differential analysis of D5 vs D2 samples & pathway enrichment analysis

All Supplementary Tables can be requested from Stephan Durot, [durot@imsb.biol.ethz.ch](mailto:durot@imsb.biol.ethz.ch).

## References

1. Carmeliet, P. Angiogenesis in health and disease. *Nat. Med.* **9**, 653–660 (2003).
2. Aspelund, A., Robciuc, M. R., Karaman, S., Makinen, T. & Alitalo, K. Lymphatic System in Cardiovascular Medicine. *Circ. Res.* **118**, 515–530 (2016).
3. Adams, R. H. & Alitalo, K. Molecular regulation of angiogenesis and lymphangiogenesis. *Nat. Rev. Mol. Cell Biol.* **8**, 464–478 (2007).
4. De Bock, K., Georgiadou, M. & Carmeliet, P. Role of endothelial cell metabolism in vessel sprouting. *Cell Metab.* **18**, 634–647 (2013).
5. Cao, R. *et al.* Collaborative interplay between FGF-2 and VEGF-C promotes lymphangiogenesis and metastasis. *Proc. Natl. Acad. Sci. U. S. A.* **109**, 15894–15899 (2012).
6. Eelen, G. *et al.* Endothelial Cell Metabolism. *Physiol. Rev.* **98**, 3–58 (2017).
7. Morfoisse, F. & Noel, A. Lymphatic and blood systems: Identical or fraternal twins? *Int. J. Biochem. Cell Biol.* **114**, 105562 (2019).
8. Grada, A. A. & Phillips, T. J. Lymphedema: Pathophysiology and clinical manifestations. *J. Am. Acad. Dermatol.* **77**, 1009–1020 (2017).
9. Yu, P. *et al.* FGF-dependent metabolic control of vascular development. *Nature* **545**, 224–241 (2017).
10. Wilhelm, K. *et al.* FOXO1 couples metabolic activity and growth state in the vascular endothelium. *Nature* **529**, 216–220 (2016).
11. García-Caballero, M. *et al.* Role and therapeutic potential of dietary ketone bodies in lymph vessel growth. *Nat. Metab.* **1**, 666–675 (2019).
12. Ricard, N., Bailly, S., Guignabert, C. & Simons, M. The quiescent endothelium: signalling pathways regulating organ-specific endothelial normalcy. *Nat. Rev. Cardiol.* **18**, 565–580 (2021).
13. Dumas, S. J., García-Caballero, M. & Carmeliet, P. Metabolic Signatures of Distinct Endothelial Phenotypes. *Trends Endocrinol. Metab.* **31**, 580–595 (2020).
14. Teuwen, L. A., Geldhof, V. & Carmeliet, P. How glucose, glutamine and fatty acid metabolism shape blood and lymph vessel development. *Dev. Biol.* **447**, 90–102 (2019).
15. Kalucka, J. *et al.* Quiescent Endothelial Cells Upregulate Fatty Acid  $\beta$ -Oxidation for

- Vasculoprotection via Redox Homeostasis. *Cell Metab.* **28**, 881-894.e13 (2018).
16. Wong, B. W. *et al.* The role of fatty acid  $\beta$ -oxidation in lymphangiogenesis. *Nature* **542**, 49–54 (2017).
  17. Schoors, S. *et al.* Fatty acid carbon is essential for dNTP synthesis in endothelial cells. *Nature* **520**, 192–197 (2015).
  18. Andrade, J. *et al.* Control of endothelial quiescence by FOXO-regulated metabolites. *Nat. Cell Biol.* **23**, 413–423 (2021).
  19. Bruning, U. *et al.* Impairment of Angiogenesis by Fatty Acid Synthase Inhibition Involves mTOR Malonylation. *Cell Metab.* **28**, 866-880.e15 (2018).
  20. Kim, B., Li, J., Jang, C. & Arany, Z. Glutamine fuels proliferation but not migration of endothelial cells. *EMBO J.* **36**, 2321–2333 (2017).
  21. Eelen, G. *et al.* Role of glutamine synthetase in angiogenesis beyond glutamine synthesis. *Nature* vol. 561 (2018).
  22. Kalucka, J. *et al.* Single-Cell Transcriptome Atlas of Murine Endothelial Cells. *Cell* **180**, 764-779.e20 (2020).
  23. Paik, D. T. *et al.* Single-Cell RNA Sequencing Unveils Unique Transcriptomic Signatures of Organ-Specific Endothelial Cells. *Circulation* **142**, 1848–1862 (2020).
  24. Li, Q. *et al.* Single-cell transcriptome profiling reveals vascular endothelial cell heterogeneity in human skin. *Theranostics* **11**, 6461–6476 (2021).
  25. Wilting, J. *et al.* The transcription factor Prox1 is a marker for lymphatic endothelial cells in normal and diseased human tissues. *FASEB J.* **16**, 1271–1273 (2002).
  26. Podgrabinska, S. *et al.* Molecular characterization of lymphatic endothelial cells. *Proc. Natl. Acad. Sci. U. S. A.* **99**, 16069–16074 (2002).
  27. Gao, P., Ren, G., Liang, J. & Liu, J. STAT6 Upregulates NRP1 Expression in Endothelial Cells and Promotes Angiogenesis. *Front. Oncol.* **12**, 1–13 (2022).
  28. Fabregat, A. *et al.* The Reactome Pathway Knowledgebase. *Nucleic Acids Res.* **46**, D649–D655 (2018).
  29. Ma, W. *et al.* Mitochondrial respiration controls the Prox1-Vegfr3 feedback loop during lymphatic endothelial cell fate specification and maintenance. 1–17 (2021).

30. Santamaría, D. *et al.* Cdk1 is sufficient to drive the mammalian cell cycle. *Nature* **448**, 811–815 (2007).
31. Petryk, N. *et al.* MCM2 promotes symmetric inheritance of modified histones during DNA replication. *Science (80-. )*. **361**, 1389–1392 (2018).
32. Madine, M. A., Khoo, C. Y., Mills, A. D. & Laskey, R. A. MCM3 complex required for cell cycle regulation of DNA replication in vertebrate cells. *Nature* **375**, 421–424 (1995).
33. Tsao, C. C., Geisen, C. & Abraham, R. T. Interaction between human MCM7 and Rad17 proteins is required for replication checkpoint signaling. *EMBO J.* **23**, 4660–4669 (2004).
34. Küspert, M. *et al.* LARP4B is an AU-rich sequence associated factor that promotes mRNA accumulation and translation. *Rna* **21**, 1294–1305 (2015).
35. Kim, K. H., Won, J. H., Cheng, N. & Lau, L. F. The matricellular protein CCN1 in tissue injury repair. *J. Cell Commun. Signal.* **12**, 273–279 (2018).
36. Cheng, P. *et al.* Nidogen1-enriched extracellular vesicles accelerate angiogenesis and bone regeneration by targeting Myosin-10 to regulate endothelial cell adhesion. *Bioact. Mater.* **12**, 185–197 (2022).
37. Nightingale, T. & Cutler, D. The secretion of von Willebrand factor from endothelial cells; an increasingly complicated story. *J. Thromb. Haemost.* **11**, 192–201 (2013).
38. Leatherdale, A. *et al.* Multimerin 1 supports platelet function in vivo and binds to specific GPAGPOGPX motifs in fibrillar collagens that enhance platelet adhesion. *J. Thromb. Haemost.* **19**, 547–561 (2021).
39. Maroney, S. A. & Mast, A. E. New insights into the biology of tissue factor pathway inhibitor. *J. Thromb. Haemost.* **13**, S200–S207 (2015).
40. Fu, H., Zhao, D., Sun, L., Huang, Y. & Ma, X. Identification of autophagy-related biomarker and analysis of immune infiltrates in oral carcinoma. *J Clin Lab Anal.* (2022).
41. Grijalva, A., Xu, X. & Ferrante, A. W. Autophagy is dispensable for macrophage-mediated lipid homeostasis in adipose tissue. *Diabetes* **65**, 967–980 (2016).
42. Li, Z. *et al.* GAA deficiency promotes angiogenesis through upregulation of Rac1 induced by autophagy disorder. *Biochim. Biophys. Acta - Mol. Cell Res.* **1868**, 1–14 (2021).
43. Smith, P. K., Sen, M. G., Fisher, P. R. & Annesley, S. J. Modelling of neuronal ceroid lipofuscinosis type 2 in dictyostelium discoideum suggests that cytopathological outcomes result from altered TOR signalling. *Cells* **8**, 1–22 (2019).



44. Zhang, H. *et al.* Netrin-4 expression by human endothelial cells inhibits endothelial inflammation and senescence. *Int. J. Biochem. Cell Biol.* **134**, 105960 (2021).
45. Liu, X. *et al.* PPM1K Regulates Hematopoiesis and Leukemogenesis through CDC20-Mediated Ubiquitination of MEIS1 and p21. *Cell Rep.* **23**, 1461–1475 (2018).
46. Fuhrer, T., Heer, D., Begemann, B. & Zamboni, N. High-Throughput, Accurate Mass Metabolome Profiling of Cellular Extracts by Flow Injection–Time-of-Flight Mass Spectrometry. *Anal. Chem.* **83**, 7074–7080 (2011).
47. Falkenberg, K. D., Rohlenova, K., Luo, Y. & Carmeliet, P. The metabolic engine of endothelial cells. *Nat. Metab.* **1**, 937–946 (2019).
48. Lemons, J. M. S. *et al.* Quiescent fibroblasts exhibit high metabolic activity. *PLoS Biol.* **8**, (2010).
49. Coloff, J. L. *et al.* Differential Glutamate Metabolism in Proliferating and Quiescent Mammary Epithelial Cells. *Cell Metab.* **23**, 867–880 (2016).
50. Liang, C. C., Park, A. Y. & Guan, J. L. In vitro scratch assay: A convenient and inexpensive method for analysis of cell migration in vitro. *Nat. Protoc.* **2**, 329–333 (2007).
51. Bruning, U. *et al.* Impairment of Angiogenesis by Fatty Acid Synthase Inhibition Involves mTOR Malonylation. *Cell Metab.* **28**, 866-880.e15 (2018).
52. Zecchin, A., Kalucka, J., Dubois, C. & Carmeliet, P. How endothelial cells adapt their metabolism to form vessels in tumors. *Front. Immunol.* **8**, (2017).
53. Petrelli, F. *et al.* Mitochondrial pyruvate metabolism regulates the activation of quiescent adult neural stem cells. *bioRxiv* 2022.05.31.494137 (2022).
54. Ocaña, C. *et al.* The anti-angiogenic compound dimethyl fumarate inhibits the serine synthesis pathway and increases glycolysis in endothelial cells. *bioRxiv* (2021).
55. Sassa, S. & Kappas, A. Hereditary tyrosinemia and the heme biosynthetic pathway. Profound inhibition of  $\delta$ -aminolevulinic acid dehydratase activity by succinylacetone. *J. Clin. Invest.* **71**, 625–634 (1983).
56. Nishizawa, S. *et al.* Low tumor glutathione level as a sensitivity marker for glutamate-cysteine ligase inhibitors. *Oncol. Lett.* **15**, 8735–8743 (2018).
57. Li, N. *et al.* Mitochondrial complex I inhibitor rotenone induces apoptosis through enhancing mitochondrial reactive oxygen species production. *J. Biol. Chem.* **278**, 8516–8525 (2003).

58. Ghergurovich, J. M. *et al.* A small molecule G6PD inhibitor reveals immune dependence on pentose phosphate pathway. *Nat. Chem. Biol.* **16**, 731–739 (2020).
59. Murohara, T. *et al.* Endothelial Cell Migration. *Arter. Thromb Vasc Biol.* 1156–1161 (1999).
60. Cooke, J. P. & Losordo, D. W. Nitric oxide and angiogenesis. *Circulation* **105**, 2133–2135 (2002).
61. Brieger, K., Schiavone, S., Miller, F. J. & Krause, K. H. Reactive oxygen species: From health to disease. *Swiss Med. Wkly.* **142**, 1–14 (2012).
62. Kohen, R. & Nyska, A. Oxidation of biological systems: Oxidative stress phenomena, antioxidants, redox reactions, and methods for their quantification. *Toxicol. Pathol.* **30**, 620–650 (2002).
63. Förstermann, U. & Münzel, T. Endothelial nitric oxide synthase in vascular disease: From marvel to menace. *Circulation* **113**, 1708–1714 (2006).
64. Taniyama, Y. & Griendling, K. K. Reactive Oxygen Species in the Vasculature: Molecular and Cellular Mechanisms. *Hypertension* **42**, 1075–1081 (2003).
65. Santoro, M. M. Fashioning blood vessels by ROS signalling and metabolism. *Semin. Cell Dev. Biol.* **80**, 35–42 (2018).
66. Kuroki, M. *et al.* Reactive oxygen intermediates increase vascular endothelial growth factor expression in vitro and in vivo. *J. Clin. Invest.* **98**, 1667–1675 (1996).
67. Vandekerke, S. *et al.* Serine Synthesis via PHGDH Is Essential for Heme Production in Endothelial Cells. *Cell Metab.* **28**, 573–587.e13 (2018).
68. Jiang, P. *et al.* P53 regulates biosynthesis through direct inactivation of glucose-6-phosphate dehydrogenase. *Nat. Cell Biol.* **13**, 310–316 (2011).
69. Tetzlaff, F. & Fischer, A. Human Endothelial Cell Spheroid-based Sprouting Angiogenesis Assay in Collagen. *Bio-Protocol* **8**, 1–10 (2018).
70. Zhan, R. *et al.* Nitric oxide promotes epidermal stem cell migration via cGMP-Rho GTPase signalling. *Sci. Rep.* **6**, 1–12 (2016).
71. Huang, H. *et al.* Role of glutamine and interlinked asparagine metabolism in vessel formation. *EMBO J.* **36**, 2334–2352 (2017).
72. Knobloch, M. *et al.* A Fatty Acid Oxidation-Dependent Metabolic Shift Regulates Adult Neural Stem Cell Activity. *Cell Rep.* **20**, 2144–2155 (2017).

73. Wang, W. Y., Lin, D., Jarman, E. H., Polacheck, W. J. & Baker, B. M. Functional angiogenesis requires microenvironmental cues balancing endothelial cell migration and proliferation. *Lab Chip* **20**, 1153–1166 (2020).
74. Parfenova, H. *et al.* Glutamate induces oxidative stress and apoptosis in cerebral vascular endothelial cells: Contributions of HO-1 and HO-2 to cytoprotection. *Am. J. Physiol. - Cell Physiol.* **290**, 1399–1410 (2006).
75. Miura, K., Ishii, T., Sugita, Y. & Bannai, S. Cystine uptake and glutathione level in endothelial cells exposed to oxidative stress. *Am. J. Physiol. - Cell Physiol.* **262**, (1992).
76. Soro-Arnáiz, I. *et al.* GLUD1 dictates muscle stem cell differentiation by controlling mitochondrial glutamate levels. *bioRxiv* (2023).
77. Vazana, U. *et al.* Glutamate-mediated blood–brain barrier opening: Implications for neuroprotection and drug delivery. *J. Neurosci.* **36**, 7727–7739 (2016).
78. Sailem, H. Z. & Al Haj Zen, A. Morphological landscape of endothelial cell networks reveals a functional role of glutamate receptors in angiogenesis. *Sci. Rep.* **10**, 1–14 (2020).
79. Salic, A. & Mitchison, T. J. A chemical method for fast and sensitive detection of DNA synthesis in vivo. *Proc. Natl. Acad. Sci. U. S. A.* **105**, 2415–2420 (2008).
80. Weekes, M. P. *et al.* Quantitative temporal viromics: An approach to investigate host-pathogen interaction. *Cell* **157**, 1460–1472 (2014).
81. Villén, J. & Gygi, S. P. The SCX\_IMAC enrichment approach for global phosphorylation. *Nat. Protoc.* **3**, 1630–1638 (2008).
82. Searle, B. C. *et al.* Chromatogram libraries improve peptide detection and quantification by data independent acquisition mass spectrometry. *Nat. Commun.* **9**, (2018).
83. Chambers, M. C. *et al.* A cross-platform toolkit for mass spectrometry and proteomics. *Nat. Biotechnol.* **30**, 918–920 (2012).
84. Demichev, V., Messner, C. B., Vernardis, S. I., Lilley, K. S. & Ralser, M. DIA-NN: neural networks and interference correction enable deep proteome coverage in high throughput. *Nat. Methods* **17**, 41–44 (2020).
85. Cox, J. *et al.* Accurate proteome-wide label-free quantification by delayed normalization and maximal peptide ratio extraction, termed MaxLFQ. *Mol. Cell. Proteomics* **13**, 2513–2526 (2014).
86. Focaccetti, C. *et al.* Effects of 5-fluorouracil on morphology, cell cycle, proliferation, apoptosis,

- autophagy and ros production in endothelial cells and cardiomyocytes. *PLoS One* **10**, 1–25 (2015).
87. Liu, T. *et al.* Sequence-dependent synergistic cytotoxicity of icotinib and pemetrexed in human lung cancer cell lines in vitro and in vivo. *J. Exp. Clin. Cancer Res.* **38**, 1–15 (2019).
88. Wang, D. *et al.* Hypoxia induces lactate secretion and glycolytic efflux by downregulating mitochondrial pyruvate carrier levels in human umbilical vein endothelial cells. *Mol. Med. Rep.* **18**, 1710–1717 (2018).
89. Mader, B. J. *et al.* Rotenone inhibits autophagic flux prior to inducing cell death. *ACS Chem. Neurosci.* **3**, 1063–1072 (2012).
90. Gross, M. I. *et al.* Antitumor activity of the glutaminase inhibitor CB-839 in triple-negative breast cancer. *Mol. Cancer Ther.* **13**, 890–901 (2014).
91. Jin, L. *et al.* Glutamate Dehydrogenase 1 Signals through Antioxidant Glutathione Peroxidase 1 to Regulate Redox Homeostasis and Tumor Growth. *Cancer Cell* **27**, 257–270 (2015).
92. Costantini, D. L., Villani, D. F., Vallis, K. A. & Reilly, R. M. Methotrexate, paclitaxel, and doxorubicin radiosensitize HER2-amplified human breast cancer cells to the auger electron-emitting radiotherapeutic agent <sup>111</sup>In-NLS-trastuzumab. *J. Nucl. Med.* **51**, 477–483 (2010).
93. Heller, R. *et al.* L-ascorbic acid potentiates endothelial nitric oxide synthesis via a chemical stabilization of tetrahydrobiopterin. *J. Biol. Chem.* **276**, 40–47 (2001).
94. Rae, C., Haberkorn, U., Babich, J. W. & Mairs, R. J. Inhibition of fatty acid synthase sensitizes prostate cancer cells to radiotherapy. *Radiat. Res.* **184**, 482–493 (2015).



## Chapter 4

### **Systematic analysis of transcription factor activity patterns that underlie endothelial cell identities and states**

Stephan Durot<sup>1</sup>, Nicola Zamboni<sup>1</sup>

<sup>1</sup> Institute of Molecular Systems Biology, ETH Zürich, Otto-Stern-Weg 3, 8093 Zürich, Switzerland

Stephan Durot designed the study, conducted all computational analyses and data visualizations and wrote the chapter. Nicola Zamboni helped designing the study, supervised and contributed to the writing.

## Abstract

Development and maintenance of endothelial cell (EC) identities and states is tightly controlled by transcription factors (TFs) that regulate the expression of defined sets of genes driving these processes. Furthermore, TFs coordinate metabolic activities of ECs to drive differentiation and growth states. Vascular-related diseases are direct consequences of disturbances in the transcriptional regulation system in ECs and demonstrate the need to comprehensively understand the TF activity patterns that underlie EC identities and states. To address this need, we performed TF activity inference with a dataset of 7894 quantified proteins in four different EC types, two from the blood (BECs) and two from the lymphatic system (LECs), over a period of 6 days, for which we previously showed that the cells are first proliferating and then transition into quiescence. The resulted TF activity patterns show cell type- and state specific behaviour, indicating the effect of the origin and needs of each cell type. However, we were also able to extract TFs whose activities are fundamentally different between BECs and LECs, including well-known markers of LEC and BEC identities. In addition, we correlated TF activities with expression patterns of 14 enzymes that were targets of pharmacological inhibition and propose two new TFs that potentially regulate expression of enzymes necessary for functioning migration in HUVECs and iLECs.

## Introduction

Cellular homeostasis and functions require tightly controlled gene expression patterns in order to be established and maintained correctly<sup>1-3</sup>. Gene expression patterns are regulated through transcription factors (TFs), which enhance or suppress transcription of defined sets of genes<sup>1-4</sup>. Activities of specific TFs are influenced by multiple extra- and intracellular factors, such as growth signals or the bioenergetic and metabolic state of the cell, and they often work in concert, organised in gene regulatory networks<sup>1-4</sup>. TFs are key players in development and maintenance of cellular identities and tissues, including endothelial cell differentiation and vascular development<sup>5,6</sup>. Numerous TFs have been described to orchestrate the formation and maintenance of blood endothelial cell (BEC) and lymphatic endothelial cell (LEC) identities and consequently blood and lymphatic vessel development and integrity<sup>5-7</sup>. Development of BECs is mainly controlled by GATA2, ETV2 and members of the HESR (Hey1, Hey2), FOX

(FOXC1, FOXC2) and SOX (SOX7, SOX18) family of transcription factors<sup>5</sup>. LECs develop from venous BECs through an interplay of SOX18, NR2F2 and the master regulator of LEC identity, PROX1<sup>8</sup>.

Transcriptional regulation is also essential to maintain metabolic homeostasis, to adapt to changing environments or forming cellular identities<sup>9–11</sup>. For example, PROX1 rewires cellular metabolism to increase acetyl-CoA production, which is then used to acetylate histones of target genes through PROX1-p300 interaction, leading to expression of lymphangiogenesis-promoting genes<sup>11</sup>. Moreover, in ECs, it has been shown that the forkhead box O transcription factor FOXO1 controls growth states in ECs by regulating metabolic activity and production of signalling metabolites that mediate quiescence<sup>12,13</sup>. Conversely, a study by Ma *et al.* demonstrated that mitochondrial respiration controls PROX1 expression, proposing that not only TFs regulate metabolism but that metabolic cues can modulate TF expression and subsequent downstream consequences<sup>14</sup>. Disturbances in these fine-tuned regulatory processes lead to various vasculature-related diseases<sup>5,7</sup>. For instance, mutations in TFs relevant for LEC maturation and maintenance cause lymphatic malformations or primary lymphedema and mutations in mechanosensitive TFs in BECs support atherosclerosis formation<sup>7,15,16</sup>.

In chapter 2, we applied untargeted proteomics and metabolomics to comprehensively characterize the molecular patterns that define identities and states of two blood and two lymphatic EC types (human dermal blood endothelial cells (HDBECs), human umbilical vein endothelial cells (HUVECs), human dermal lymphatic endothelial cells (HDLECs) and intestinal lymphatic endothelial cells (iLECs)). The studied ECs exhibited distinct and general proteomic and metabolic patterns in quiescence and proliferation. In further functional studies we showed that migrating HUVECs rely on heme biosynthesis for NO production and that unbalanced glutamate and  $\alpha$ -ketoglutarate levels lead to migratory defects in iLECs. To deepen our knowledge of transcriptional regulation of EC identities and to examine the TF patterns that drive the different metabolic peculiarities in ECs, we used the untargeted proteomics dataset to infer transcription factor activities. TFs are generally present in low numbers in cells, which hinders their identification in untargeted proteomics measurements<sup>17</sup>. However, statistical methods can be applied to infer transcription factor activities based on the expression patterns of their targets. Here, we created a TF activities dataset using Dorothea, a curation of human TF regulons and decoupler,



an collection of computational methods to infer TF activities<sup>18,19</sup>. We extracted fundamental differences in TF activities patterns between LECs and BECs, which contained well-known markers of LEC and BEC identities. Furthermore, we observed that some TFs are more active in one specific cell type and propose two TFs that might regulate expression of two enzymes in HUVECs and iLECs, respectively, that are needed for migration.

## Results

### Transcription factor activity inference exhibits cell type- and state-specific patterns

In chapter 3, we observed diverse proteomic and metabolic patterns underlying different endothelial identities and states. We could show that these patterns support normal cellular functions, like migration, of HUVECs and iLECs, such as heme biosynthesis for appropriate nitric oxide (NO) levels in HUVECs and  $\alpha$ -ketoglutarate-glutamate balance in iLECs. Expression of enzymes, as well as cellular identities and states, are tightly controlled by gene regulatory networks and signalling pathways. Thus, to better understand how these patterns emerge, we set out to use computational methods to infer transcription factor (TF) activities using the proteomics dataset generated in the previous chapters.

Gene regulatory networks are networks that contain information about TF-target gene interactions. Dorothea is a repository of TF-target interactions containing information about 1541 human TFs and their targets<sup>18</sup>. TF-target interactions in Dorothea are assigned a confidence level, depending on the level of evidence for the respective TF-target interactions. The confidence levels reach from manually curated repositories (A), ChIP-seq binding data (B) to in silico prediction of TF binding on gene promoters (C) and reverse-engineered regulons from large gene expression data sets (D), with decreasing level of confidence from A to D. We used the TF-target interaction network with confidence levels A, B and C to infer TF activities in the four endothelial cell types HUVEC, HDLEC, HDBEC and iLEC using decoupler (Fig. 1A)<sup>19</sup>. The used TF-target network consisted of 32'275 TF-target pairs, with increasing number of TF-target pairs from confidence level A to C (Suppl. Fig. 1A). To infer TF activities, we

applied the consensus method in decoupler, which was shown to be the top performing method in the original publication<sup>19</sup>. The resulting dataset contained the Z-scored activities of 263 TFs across all samples (Fig. 1A, Suppl. Fig. 1B, Suppl. Table 1).

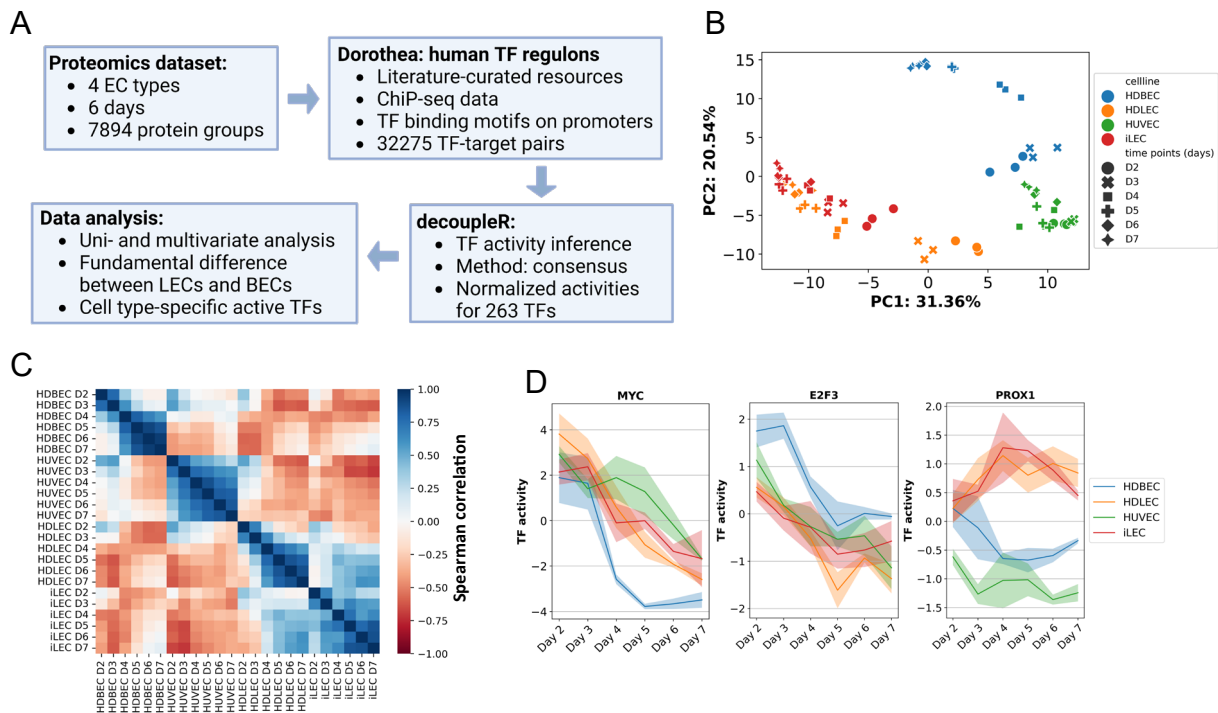


**Figure 1. Transcription factor activity inference exhibits cell type- and state-specific patterns.**

- Overview of TF activities inference workflow.
- Principal component analysis of inferred TF activities.
- Spearman's correlation between all samples using the mean activities of the three replicates for each sample.
- Temporal TF activity patterns of the proliferation-associated TFs MYC and E2F3 and the master regulator of LEC identity, PROX1.

Principal component analysis and Spearman's correlation revealed that TF activity patterns are different between lymphatic ECs, HUVECs and HDBECs (Fig. 1B, 1C). We checked whether we could observe expected activity patterns of certain TFs to ensure the validity of the dataset. Indeed, MYC, a TF controlling proliferation of mammalian cells, and E2F3, controlling proliferation in endothelial cells, become less active over time, when cells undergo transition from proliferation to quiescence (Fig. 1D)<sup>20,21</sup>. Additionally, the master regulator of LEC identity, PROX1, is active in HDLECs and iLECs but not in HDBECs and HUVECs (Fig. 1D)<sup>22</sup>. PROX1 activity is in line with the expression pattern of PROX1, namely being expressed in HDLECs and iLECs but not in HDBECs and HUVECs (Suppl. Fig. 1C). We wondered how similar inferred TF activity patterns and expression patterns of TFs are overall in our dataset. From the 263 inferred TF activities, 71 were detected in the proteomics measurements (Suppl.

Fig. 1D). TF activities and intensities correlate poorly, most TFs have Spearman's correlation coefficients between -0.5 and 0.5 (Suppl. Fig. 1E). The LEC marker PROX1 is the exception with a correlation coefficient of 0.8. This suggests that the activity of TFs is not only dependent on their expression levels but also on other factors, like activation through extra- and intracellular signals, post-translational and -transcriptional regulation or the interaction of TFs with other TFs or co-activators<sup>23</sup>.

## **Transcription factor networks fundamentally differentiate blood and lymphatic endothelial cells**

HDLECs and iLECs have similar TF activity patterns and can be discriminated against HUVECs and HDBECs among a combination of the first and second principal component from the principal component analysis (Fig. 1B). To further distill fundamental TF activity differences between blood and lymphatic endothelial cells, we performed a partial least squares discriminant analysis (PLS-DA) (Fig. 2A). By categorizing distinct cell types and encompassing all their states, we can investigate the overarching TF activity patterns that define BECs and LECs independently of their specific states. There was a clear distinction between BECs and LECs among the first component of the PLS-DA. To identify TFs contributing significantly to the first component of the PLS-DA, we employed a permutation method. This approach allowed us to generate lists of active TFs associated with BECs and LECs. 38 and 28 TFs were associated with LECs and BECs, respectively, with a 10% cutoff (Fig. 2B). We wondered whether the lists we generated were not just random or biased by the previous computational analyses that depended on expression patterns and the assigned TF-target pairs. To that end, we conducted a permutation test to determine the distribution of randomly assigned TFs in the top and bottom 10%, and in the total number of TFs passing the 10% thresholds (Suppl. Fig. 2A). The numbers of TFs in our lists were significantly higher than in the lists from the permutation assay and thus not random. Additionally, we checked whether having a specific weight in the first component is influenced by the number of targets, which was also not the case (Suppl. Fig. 2B). Moreover, the TF list associated with LECs included the LEC marker PROX1, demonstrating that we capture cell type-specific markers.

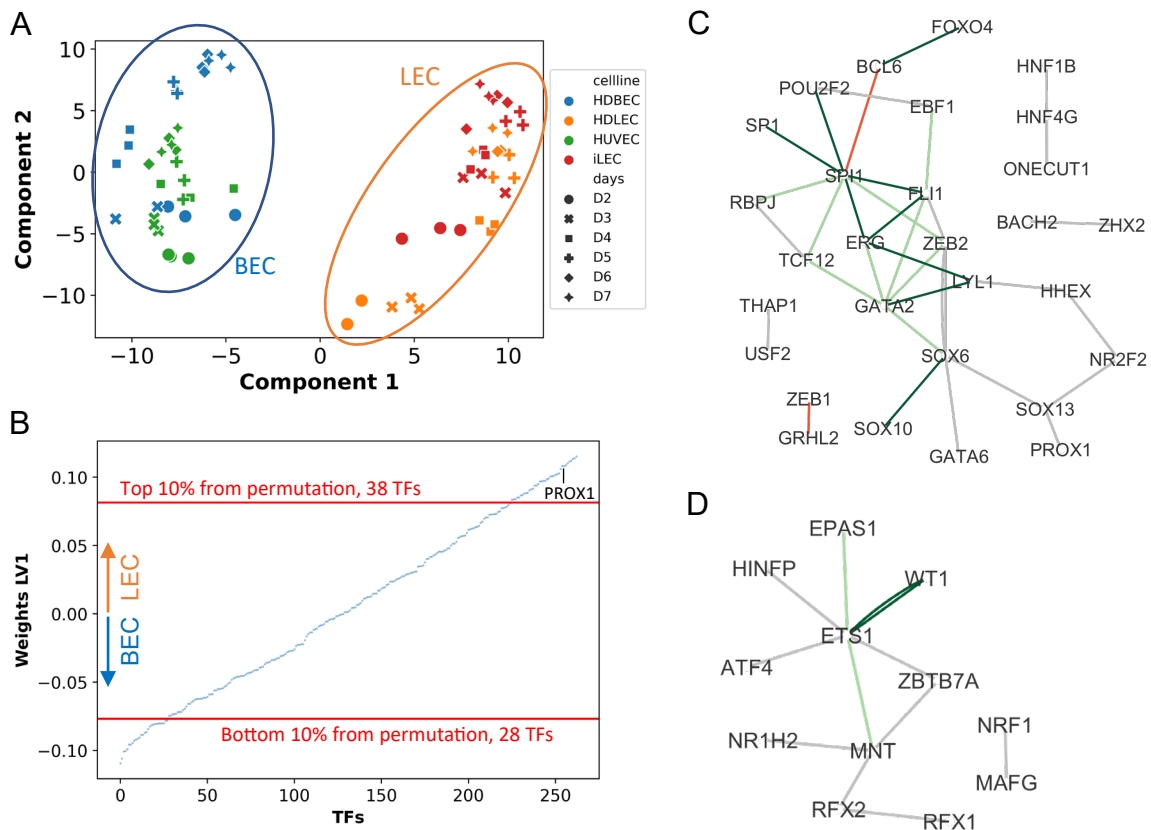


**Figure 2. Transcription factor networks fundamentally differentiate blood and lymphatic endothelial cells.**

- (A) Partial least squares discriminant analysis (PLS-DA) of the TF activities dataset showing the discrimination between LECs and BECs among component 1.
- (B) Weights of the first component of the PLS-DA. Each TF has a weight that corresponds to its cell type-related information. A permutation approach was applied to determine the 10% and 90% percentile, associated with BEC and LEC identity, respectively.
- (C) TF-interaction network of TFs associated with LEC identity. Dark green edges correspond to confidence level A, positive interactions (activation), red edges to confidence level A, negative interactions (repression), light green to confidence level B, positive interactions (activation) and grey to confidence level C interactions.
- (D) TF-interaction network of TFs associated with BEC identity. Same meaning of colors of the edges as in (C).

The expression of TFs is also regulated by TFs<sup>24</sup>. Out of the 32'275 TF-target pairs in the network we used, 1760 were TF-TF pairs. We extracted TF-TF pairs that contain TFs that are present in the TFs lists associated with either LECs or BECs to create LEC- and BEC-specific TF interaction networks. The TF interaction networks consisted of 35 and 12 TF-TF pairs for LECs and BECs, respectively (Fig. 2C, 2D). The networks contained known TFs and interactions that play a role in LEC and BEC development and maintenance and could therefore be used as sources to find novel TF-TF interactions important in these processes. For example, the four TFs GATA2, LYL1, HHEX and NR2F2 were all associated with LEC identity and were connected in the TF-TF interaction network. Interestingly, all four TFs are involved in development or maintenance of LECs through modulating VEGFC/FLT4/PROX1 signalling and

expression (HHEX, GATA2, NR2F2) or the expression of Angiopoietin-2 (LYL1, GATA2)<sup>25–28</sup>. On the other hand, the BEC-associated TFs WT1, ETS1 and EPAS1, connected in the TF-TF interaction network, are involved in proliferation, migration and angiogenesis of BECs by regulating VEGFA, VEGFR1 and Angiopoietin-1 expression and signalling<sup>29–31</sup>. Furthermore, the LEC- and BEC-associated TF lists cannot only be used to find new regulators or interactions supporting EC development and maintenance but also how metabolic pathways defining EC identities are regulated. In the previous chapter, we found that mitochondrial fatty acid beta-oxidation and TCA cycle/OXPHOS discriminate LEC from BEC identities. Hepatic nuclear factor 1 $\beta$  (HNF1B), controlling mitochondrial respiration in renal tubular cells, and hepatic nuclear factor 4 $\gamma$  (HNF4G), regulating fatty acid beta-oxidation in intestinal stem cells of mice, were connected and associated with LECs, suggesting that these two factors might also play a role in regulating metabolic processes that are tightly connected with LEC identity maintenance, or to support the previously described feedback loop between mitochondrial respiration and PROX1-VEGFR3 that controls LEC identity<sup>14,32,33</sup>. Furthermore, we observed HUVEC-specific vulnerability to decreased NO levels in the last chapter, and interestingly, several TFs that are involved in regulation of NO metabolism or that are regulated by NO are associated with BEC identities, such as ATF2, TCF7L2 and ETS1 (Suppl. Fig. 3)<sup>34–36</sup>. This underscores the crucial role of NO in BEC but not LEC homeostasis, either through regulation of eNOS (endothelial nitric oxide synthase) expression or the signalling properties of NO that leads to expression or activation of certain TFs. In summary, the LEC- and BEC-associated lists of TF activities we extracted from our inferred TF activity dataset contain TFs and their interactions known to regulate LEC and BEC development and maintenance and can serve as resources for the discovery of novel TFs or TF interactions involved in these processes.

### **Cell type-specific active TFs correlate well with enzymes essential for normal cellular functions**

We next wondered whether there are cell type- and state-specific TF activity patterns that are dependent on the role of the respective cell type in its hosting tissue. Hierarchically clustering of TF activities indicated diverse TF activities in the different cell types and states (Fig. 3A). We first employed a 2-way-ANOVA to determine which TFs explain the temporal or cell type-dependent variance in the dataset (Suppl. Fig.

4A). Instead of combining LECs and BECs in the analysis, as in the PLS-DA, all the four cell types were assigned individually to the samples so that we could get TF patterns that are specific for one cell type. The TF with the strongest impact on temporal variance was E2F4 (Suppl. Fig. 4A, 3B). In all four cell types, there was a steady decrease of E2F4 activity from proliferation at day 2 to quiescence at days 5 to 7. E2F4 has previously been reported to be required for cardiomyocyte proliferation and it also regulates expression of thymidylate synthase (TYMS), an enzyme involved in nucleotide biosynthesis<sup>37,38</sup>. Not surprisingly, we observed a similar decrease of TYMS when cells enter quiescence (Suppl. Fig. 4B). On the other hand, the TF defining cell lines variance the strongest was HHEX (Suppl. Fig. 4A, 3B). HHEX had also the second highest weight in the PLS-DA. One of HHEX's targets, TLE1, is a transcriptional corepressor with unknown function in LECs. Its expression was constantly higher in LECs compared to BECs and might hint towards a role in LEC development or maintenance (Suppl. Fig. 4B). We also captured cell type-specific patterns, such as increased activity of SREBF1 (also known as SREBP1) and expression of its target acetyl-CoA carboxylase 1 (ACACA) in HDBECs (Suppl. Fig. 4A, 3B).

Even though the 2-way-ANOVA helped us to understand the extend of cell type- and state-specific TF activity patterns, we additionally applied a model selection-like approach to receive lists with cell type-specific active or inactive TFs. For each TF in all four cell types, we calculated different parameters like mean activity, peak activity at specific days and the slope. Arbitrary labels were then assigned to each TF in every cell type and the list of labels compared between the cell types to find unique and overlapping active TFs (Fig. 3B). With this approach, we were able to create lists that contain 14, 15, 16 and 23 active TFs for HUVECs, HDLECs, iLECs and HDBECs, respectively. The only overlap between cell types were 4 TFs that were generally active in iLECs and HDLECs, namely CTCFL, HHEX, POU2F2 and ZEB2, and were also in the LEC-associated TF list from the PLS-DA.

In the previous chapter, we observed cell type-specific metabolic vulnerabilities of HUVECs and iLECs when treated with enzyme inhibitory drugs. For example, inhibition of GLUD1 decreased migration in iLECs but not HUVECs, and ALAD inhibition led to migratory defects in HUVECs only. GLUD1 expression is 1.5- to 2-fold

higher in iLECs compared to HUVECs at each time point and might hint towards higher dependence of iLECs on sufficient GLUD1 availability and activity (Suppl. Fig. 5A).

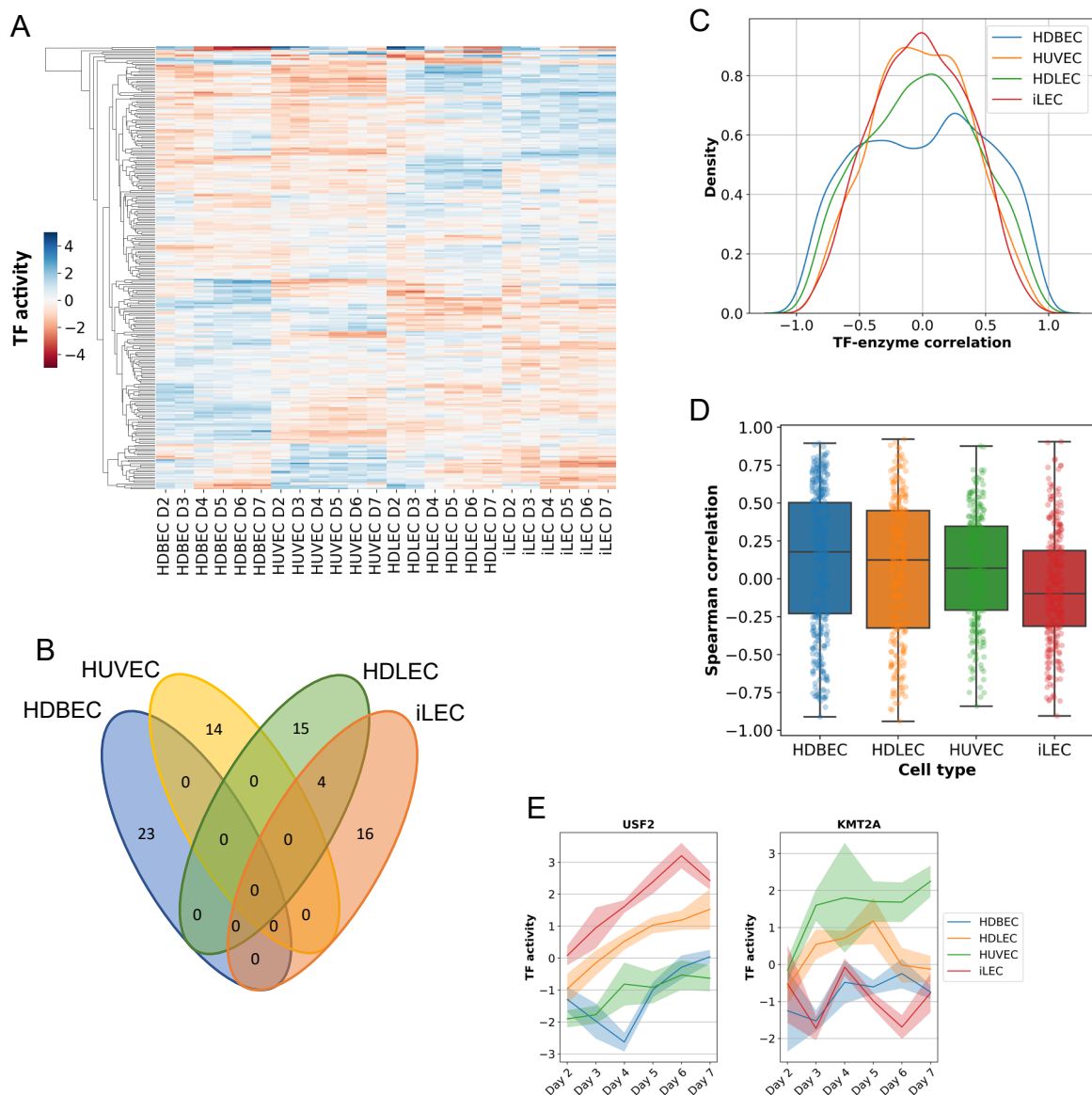


**Figure 3. Cell type-specific active TFs correlate with enzymes essential for normal cellular functions.**

- Hierarchical clustering among the 263 TF activities illustrates diverse activity patterns between the EC types.
- Number of active TFs in each or multiple cell types.
- Spearman's correlation between all TFs with the 14 enzyme targets from the validation experiments in the previous chapter.
- Spearman's correlation between cell type-specific active TFs with the 14 enzyme targets from the validation experiments in the previous chapter.
- Temporal TF activity patterns of USF2 and KMT2A, that are specifically highly active in iLECs and HUVECs, respectively.

The same could hold true for ALAD and HUVECs since we observed 50% higher expression in quiescent HUVECs compared to iLECs (Suppl. Fig. 5A). To find potential novel transcriptional regulators of the enzymes that were targeted in the validation

screen in chapter 2, we correlated the expression levels of 7894 proteins from the proteomics dataset with the activity of all 263 TFs (Suppl. Fig. 5B). From all correlations, we selected the correlations that include the 14 enzymes we targeted in the validation screen of chapter 2 (Fig. 3C, Suppl. Table 2). A strong negative correlation coefficient means a repressing relationship between TF and enzyme, a positive correlation coefficient an activating relationship. The direction of the relationship, TF-enzyme or enzyme-TF, is, however, not possible to determine. Nevertheless, this approach helped us to confine the space of potential novel regulators.

First, we wanted to assess if the TF-target pairs with confidence level A in the Dorothea network positively correlate. Surprisingly, this was not the case for many of the 16 TFs that are supposed to upregulate expression of their targets (Suppl. Fig. 5C). Some TF-target pairs were even highly anti-correlating, for example ESR1-TYMS in HDBECs ( $\rho = -0.96$ ) and HDLECs ( $\rho = -0.88$ ). On the other hand, a TF-target pair that was in the top 25% in each cell type is SREBF1-FASN (fatty acid synthase) (Suppl. Fig. 5D). SREBF1 has been shown to upregulate FASN expression in different cancer cell lines, but not in endothelial cells so far<sup>39</sup>. Only one TF-target pair (ATF3-GCLC) had a negative confidence level A, meaning that either the TF suppresses expression of the enzyme or vice versa. But the lowest correlation coefficient had TP53-TYMS in all four cell types, reaching from -0.85 in HUVECs to -0.54 in iLECs. Interestingly, this is a case in which the enzyme regulates TF expression, namely TYMS downregulating P53 expression, and the result suggests that this mechanism may also be present in ECs (Suppl. Fig. 4B, 5E)<sup>40</sup>.

Next, we selected TF-enzyme pairs for each cell type that included TFs which were active in one cell type specifically (Fig. 3D). The TF-enzyme pairs with confidence levels A or B that correlated the strongest were SREBF1-FASN in HDBECs ( $\rho = 0.82$ ), E2F1-TYMS in HUVECs ( $\rho = 0.87$ ), NFE2-GCLC (glutamate-cysteine ligase catalytic subunit) in HDLECs ( $\rho = 0.74$ ) and HNF4A-GCLC in iLECs ( $\rho = 0.55$ ). The top correlating TF-enzyme pairs over all confidence levels were SMAD3-G6PD (glucose-6-phosphate 1-dehydrogenase) in HDBECs ( $\rho = 0.89$ ), KMT2A-ALAD in HUVECs ( $\rho = 0.88$ ), PRDM14-GLUD1 in HDLECs ( $\rho = 0.90$ ) and USF2-GLUD1 in iLECs ( $\rho = 0.90$ ). These four top correlating TF-enzyme pairs were also amongst the top 0.5% of all TF-protein correlations. From these top correlating TF-enzyme pairs, only SMAD3-G6PD



is mentioned in literature, with SMAD3 being involved in downregulation of PFKFB3 and subsequent shunting of glucose into the pentose phosphate pathway, reflected by increased expression of G6PD in CD4<sup>+</sup> T cells<sup>41</sup>. However, the upregulation of G6PD could only be an indirect effect and not mediated by SMAD3. ALAD and GLUD1, the targets of the top correlating TF-enzyme pairs in HUVECs, HDLECs and iLECs, were subject of pharmacological inhibition in the previous chapter and upon inhibition of ALAD and GLUD1, HUVECs and iLECs exhibited impaired migration capacity. Thus, KMT2A and USF2 are potential novel cell type-specific TFs regulating key enzymes that are essential for migration in HUVECs and iLECs, respectively (Fig. 3E). To summarize, we extracted cell type-specific active TFs and correlated them with protein intensities, resulting in a comprehensive dataset of potentially novel TF-target interactions that are involved in the formation or maintenance of specific EC identities and states. For example, the dataset contains highly correlating TF-target pairs that were known to be formative for a distinct phenotype in other cell types, or cell type-specific active TFs that highly correlate with enzymes that were shown to be necessary for migration of HUVECs and iLECs.

## Discussion

We observed diverse molecular patterns underlying EC identities and states in the previous chapters. In this chapter, we aimed to infer activities of transcription factors across the various EC types and states and to examine the transcription factor (TF) activity patterns that underlie and potentially define the EC identities and states. To that end, we used the untargeted proteomics dataset, which includes the quantities of 7894 proteins in four endothelial cell types over 6 days from proliferation to quiescence, and inferred TF activities with a previously published computational method, decoupler, that uses human TF regulons derived from Dorothea<sup>18,19</sup>. We found that HDBECs, HUVECs and LECs are clearly separated by the inferred activity patterns of 263 TFs. Unlike HDBECs and HUVECs, HDLECs and iLECs have very similar patterns, which likely arise from the similar proteomic patterns observed in chapter 2, hence biasing the inference of TF activities. Even though HDBECs and HUVECs are both blood-derived endothelial cells, their origin seems to have a profound effect on transcriptional activities and thus protein expression patterns. For example, KMT2A, which is

especially active in HUVECs but not in HDBECs, plays an important role in embryonic development<sup>42</sup>. HUVECs form the umbilical vein and are thus a vital part of embryonic development as well<sup>43</sup>. KMT2A might be therefore one of the transcriptional regulators ensuring normal HUVEC function, which consequently forms a functioning umbilical vein. On the other hand, we see clear patterns when it comes to some TFs involved in proliferation or markers of LECs. MYC and E2F3 both decrease clearly over time in all four EC types due to a reorganization of transcriptional regulation that underlies the transition from proliferation to quiescence. Furthermore, the LEC marker PROX1 is active in HDLECs and iLECs but not BECs. Both results show that TF activity inference is a useful tool to uncover and investigate novel cellular identity- and state-shaping TF activity patterns.

Using PLS-DA and permutation tests, we were able to unveil fundamental TF activities differences between LECs and BECs, which enabled us to create a resource of potential transcriptional regulators and their interactions shaping EC identities. Besides PROX1, there are 37 more TFs, whose activities are associated with LEC identity and 28 TFs that are associated with BEC identity. Some of these TFs were described previously to be involved in LEC and BEC development and maintenance<sup>25-27,29</sup>. It is important to note that this list is not final, and more TFs or TF-TF interactions are most likely involved in these processes. Furthermore, the activity of some TFs might even be ambiguous *in vivo*, depending on the developmental stage of ECs or where they reside, not only on a global level, i.e. lymphatic or blood vessels, but also on a more local level, such as capillaries, collecting vessels or around valves<sup>23</sup>. For example, ETV4 is associated with iLECs in our screen but was shown previously to regulate Angiopoietin-1 signalling in HUVECs<sup>29</sup>. Moreover, GATA2 was predicted to be highly active in iLECs and HDLECs, especially in quiescence, and the expression of LYVE1 was high in both, iLECs and HDLECs, in our screen. In contrast, González-Loyola *et al.* measured increased LYVE1 transcript levels in capillary LECs and of GATA2 in valve LECs<sup>44</sup>. This suggests that the LECs in our experimental setup may represent a combination of LECs from various vascular locations, including capillaries, collecting vessels, and valves. Alternatively, it is possible that they have undergone a loss of vessel-specific molecular patterns while retaining tissue-specific patterns when cultured *in vitro*. In addition to the TFs differentiating LECs and BECs, we observed cell type-specific active TFs, supporting the case of tissue-dependent activities. This could also explain the discrepancy between the list of TFs associated to LECs and

BECs and the cell type-specific active TFs. In the PLS-DA, the samples were only assigned to be either BECs or LECs, which can lead to slightly different results between the PLS-DA and the model selection approach. For example, USF2 is one of the 38 TFs defining LECs in the PLS-DA, but its activity is constantly higher in iLECs compared to HDLECs. Nevertheless, the applied workflow helps to understand fundamental differences between LECs and BECs and to find cell type-specific TF activity patterns.

TFs play a pivotal role in the regulation of mammalian cellular metabolism<sup>9</sup>. The most prominent example in ECs is the control of the differentiation into and maintenance of LECs by PROX1<sup>11</sup>. Other TFs, such as FOXO1, regulate metabolic activity in response to growth states<sup>12,13</sup>. Conversely, it was shown that mitochondrial respiration controls PROX1 expression, proposing that not only TFs regulate metabolism but that metabolic cues can modulate TF expression and subsequent downstream consequences<sup>14</sup>. We therefore performed Spearman's correlation analysis to find potential novel TF-metabolism connections. Interestingly, the top correlating TF-enzyme pairs of cell type-specific active TFs in HUVECs and iLECs include enzymes that were shown in chapter 3 to be important for migration. The correlation analysis does not tell us something about cause and consequence, namely the direction of regulation. That's why it is important to functionally validate these findings. A possible validation experiment would be knock-downs of TFs, followed by growth and migration rate measurements and qPCR to determine the transcript levels of the potential TF targets. If we observe a similar phenotype as in the drug perturbation experiments and lower mRNA levels of the target, the TF indeed regulates the expression levels of the target enzyme. If the mRNA levels of the target enzymes are unaltered and the phenotype is like the perturbation experiments, then the inversed case could be the case, in which the enzyme regulates TF expression.

In this study, we generated lists of TFs defining LEC and BEC identity and potentially novel TF-enzyme interactions. We concentrated our efforts on the fundamental differences between LECs and BECs and to find TF activity patterns that underlie the metabolic peculiarities observed in chapter 3. However, the proteomics and TF activities datasets could additionally be used in the future to examine the correlation between TF activities and all proteins. For example, USF2, which is highly active in quiescent LECs, and the serine protease HTRA2 have the third highest

correlation between TFs and proteins in iLECs of all the 2'076'122 TF-protein pairs. HTRA2 is known for its role in maintaining mitochondrial integrity and quality control and therefore USF2-mediated regulation of HTRA2 might be an important piece of maintaining a healthy quiescent state in LECs<sup>45,46</sup>. Another way to use the datasets is to focus on the proteins that are not part of the TF-target network from Dorothea. These proteins do not contribute in any way to the outcome of the computational analysis. Hence, the correlation of TF activities with these proteins is completely unbiased and could be used to find new TF-protein interactions.

## Materials and Methods

### Proteomics dataset

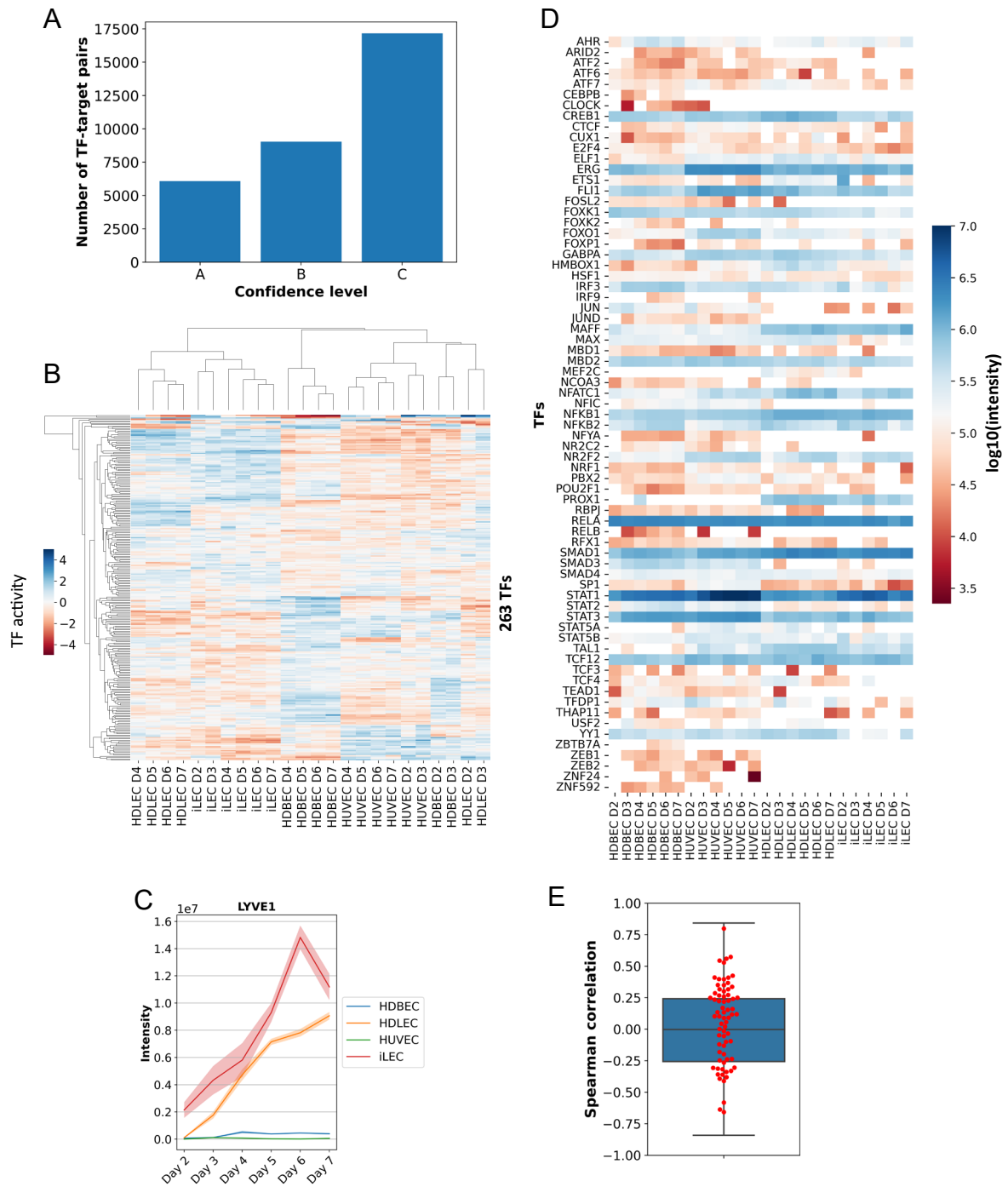
We used the proteomics dataset generated in chapter 1. In brief, we seeded the four EC types at 20'000 cells/cm<sup>2</sup> in triplicates and extracted proteins each 24 hours from day 2 until day 7 post-seeding, reduced, alkylated and trypsinized the proteins using a protocol adapted from <sup>47</sup> and <sup>48</sup>. After C18 desalting, the peptides were analysed by liquid chromatography-tandem mass spectrometry (LC-MS/MS) on a Vanquish Neo UPLC system (Thermo Scientific, Sunnyvale) coupled to an Orbitrap HF-X mass spectrometer (Thermo Fisher Scientific, San Jose, CA). The LC gradient had a total run time of 90min, ramping from 100% mobile phase A (0.1% formic acid (FA) in water) and 0% mobile phase B (80% acetonitrile in water with 0.1% FA) to 43% mobile phase B in 70min, followed by a wash at 100% mobile phase B for 9min and final re-equilibration. Peptide spectra were generated using an overlapping window data-independent analysis (DIA) pattern<sup>49</sup>. Thermo RAW files were converted to mzML format using the ProteoWizard package (version 3.0.2315)<sup>50</sup>. Processed mzML files were searched using DIA-NN (version 1.8) and peptide intensities selected at a 1% precursor-level false discovery rate<sup>51</sup>. The resulting protein quantities were normalized by delayed normalization and maximal peptide ratio extraction (maxLFQ)<sup>52</sup>.

### TF activity inference and data analysis

The TF network to infer TF activities was created using Dorothea<sup>18</sup>. We used all human TF-target pairs with confidence levels A (manually curated repositories), B (ChIP-seq

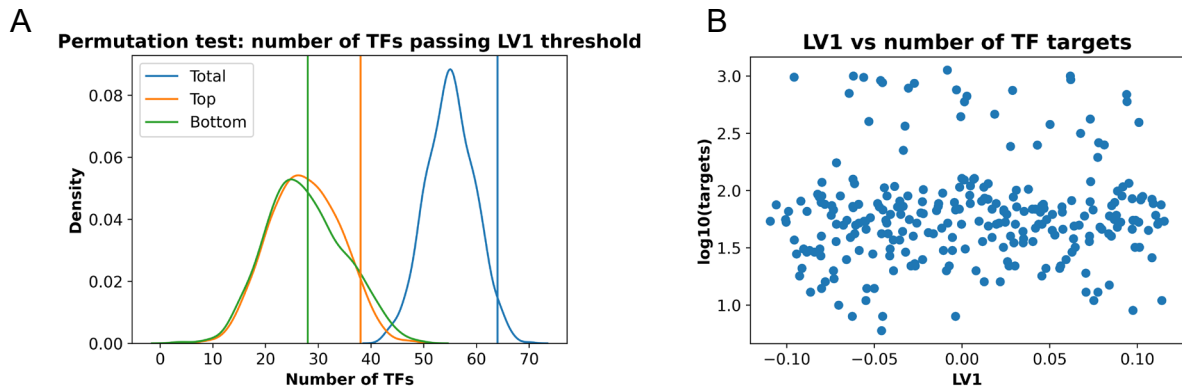
binding data) and C (in silico prediction of TF binding on gene promoters). The TF network was subjected to decoupler in order to infer TF activities using the consensus method<sup>19</sup>. TF activities inference and all subsequent statistical analyses were performed using Python 3.11.3. TF interaction networks plots were created in Cytoscape (Version 3.10). The workflow scheme was created using BioRender.

## Supplementary Material



**Supplementary Figure 1. Transcription factor activity inference exhibits cell type- and state-specific patterns.**

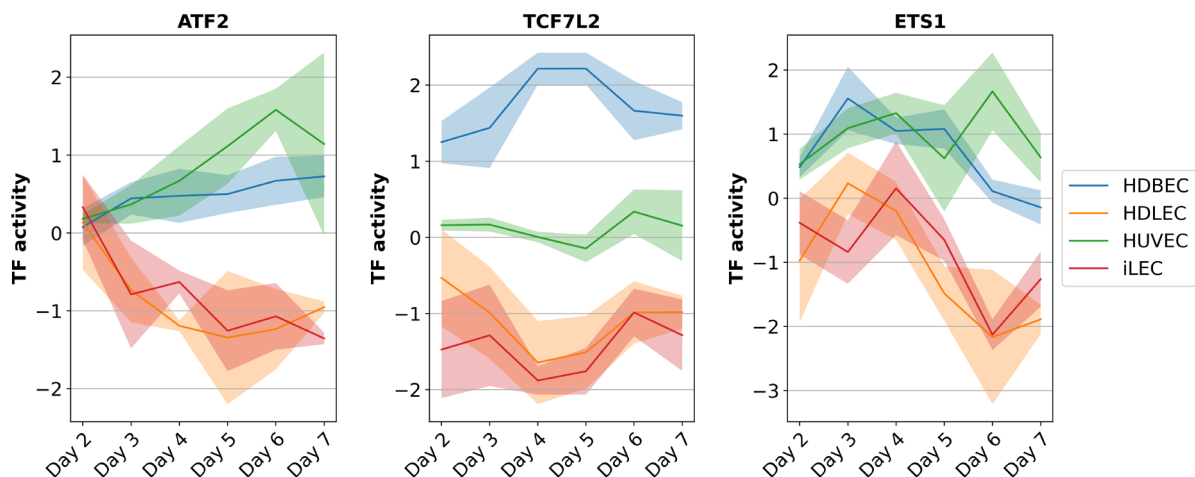
- Number of TF-target pairs with confidence levels A, B or C in the TF-target network derived from Dorothea.
- Hierarchical clustering of inferred TF activities.
- Measured protein intensity of PROX1.
- Intensities of 71 TFs that are found in the proteomics dataset.
- Distribution of Spearman's correlation coefficients between intensities and activities of the 71 TFs.



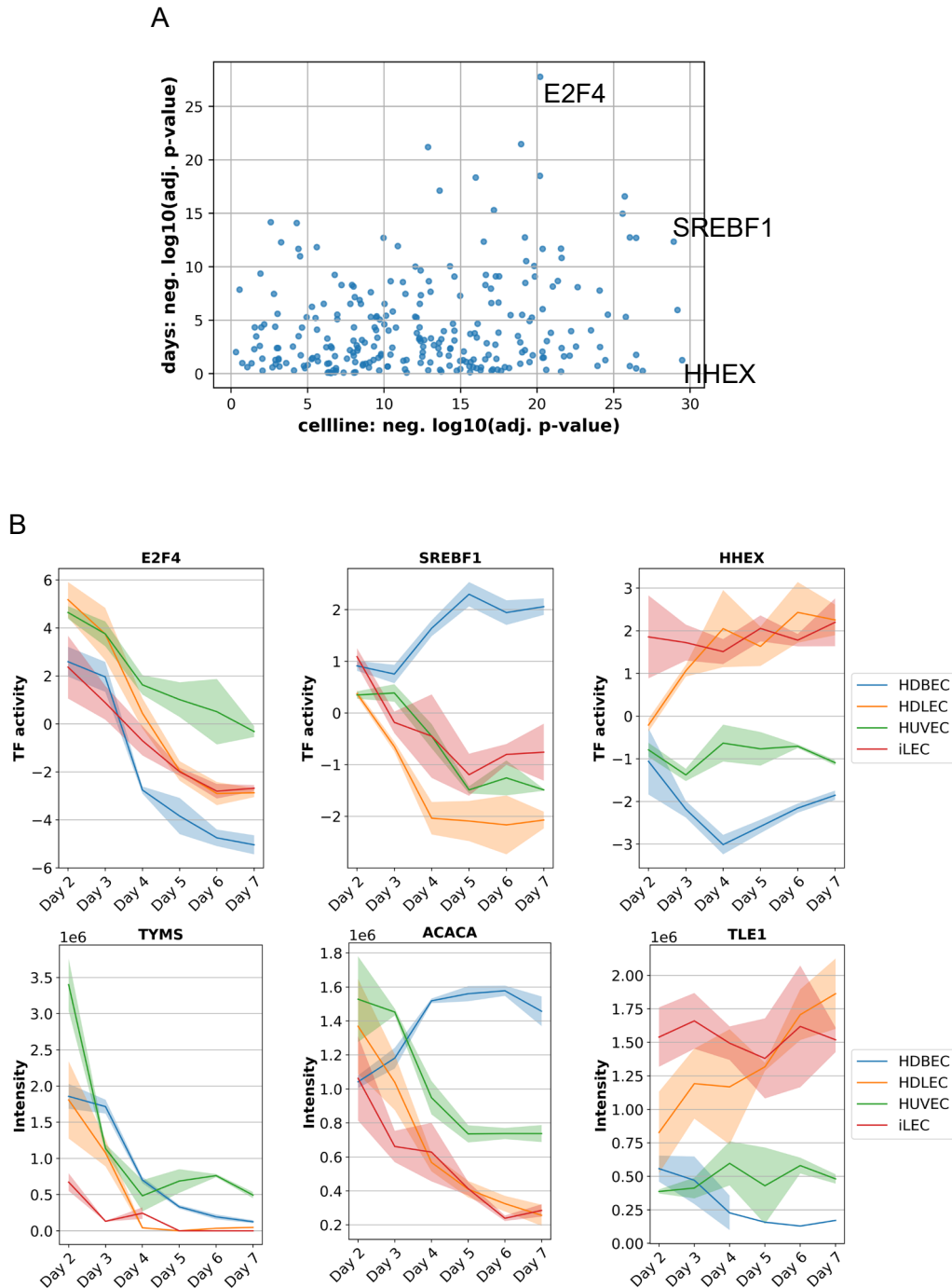
**Supplementary Figure 2. LEC- and BEC-associated TF lists are not random or biased by number of TF targets.**

(A) Permutation test with the weights defining the first component of the PLS-DA. The threshold for the 10 and 90 percentiles were used in a permutation test, in which cell type labels were randomly assigned to the samples and calculated how many TFs would pass the thresholds. The distributions depict the number of TFs passing the thresholds in the permutation test (total = the sum of top and bottom 10%), the vertical lines are the true numbers of TFs passing the 10 and 90 percentile and the sum of both. The p-values of the difference of each true number compared to the mean of the distribution were all below 5% (calculated with a permutation test), indicating that the number of TFs in the LEC- and BEC-associated lists are not random.

(B) Number of targets for each TFs, sorted by the weight on the first component of the PLS-DA.



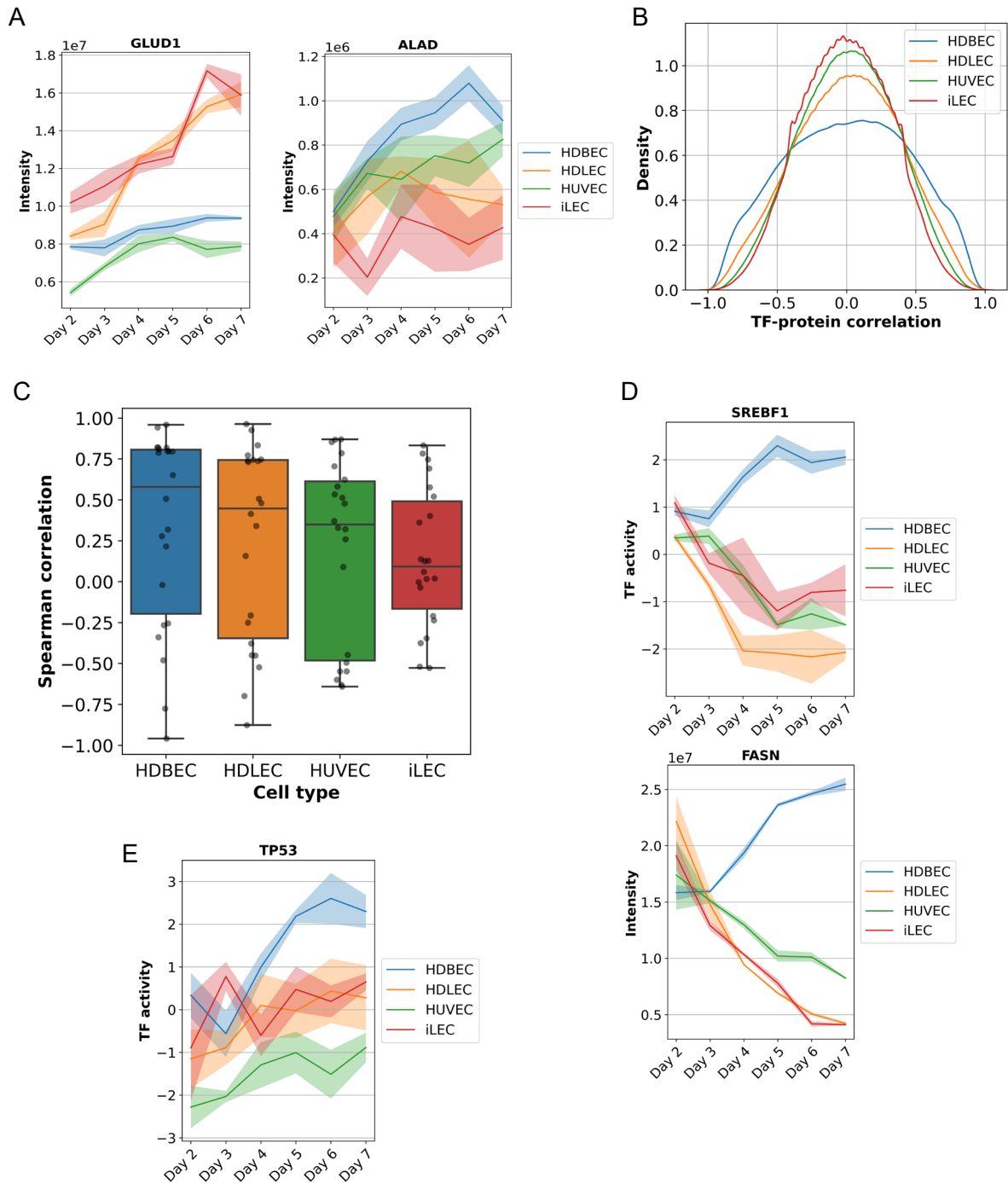
**Supplementary Figure 3. Activities of BEC-associated TFs that either regulate NO metabolism (ATF2, TCF7L2) or are regulated by NO signaling (ETS1).**



**Supplementary Figure 4. 2-way-ANOVA of all TFs to find TFs that have cell type- or state-specific patterns.**

- (A) Overview of the TFs that drive the variance between cell types or over time. The higher the neg. log<sub>10</sub>(adj. p-value), the stronger the effect of the TF on the variance.
- (B) Activities of three TFs that explain temporal variance (E2F4), cell line variance (HHEX) or both (SREBF1), and one of their targets with confidence level A (E2F4-TYMS and SREBF1-ACACA) or B (HHEX-TLE1).





**Supplementary Figure 5. Cell type-specific active TFs correlate with enzymes essential for normal cellular functions.**

- (A) Intensities of GLUD1 and ALAD, two enzymes needed for proper migration of iLECs and HUVECs, respectively.
- (B) Spearman's correlation between all TFs and all 7894 proteins.
- (C) Spearman's correlation of TF-target pairs, with targets from the validation experiment in chapter 2 and TF-target pairs with a positive confidence level A (activating) in the Dorothea network.
- (D) Temporal activity patterns of SREBF1 and intensity patterns of its target FASN.
- (E) Temporal activity pattern of TP53.

## References

1. Spitz, F. & Furlong, E. E. M. Transcription factors: From enhancer binding to developmental control. *Nat. Rev. Genet.* **13**, 613–626 (2012).
2. Mitsis, T. *et al.* Transcription factors and evolution: An integral part of gene expression (Review). *World Acad. Sci. J.* **2**, 3–8 (2020).
3. Lee, T. I. & Young, R. A. Transcriptional regulation and its misregulation in disease. *Cell* **152**, 1237–1251 (2013).
4. Weidemüller, P., Kholmatov, M., Petsalaki, E. & Zaugg, J. B. Transcription factors: Bridge between cell signaling and gene regulation. *Proteomics* **21**, 1–14 (2021).
5. Park, C., Kim, T. M. & Malik, A. B. Transcriptional regulation of endothelial cell and vascular development. *Circ. Res.* **112**, 1380–1400 (2013).
6. De Val, S. & Black, B. L. Transcriptional Control of Endothelial Cell Development. *Dev. Cell* **16**, 180–195 (2009).
7. Schulte-Merker, S., Sabine, A. & Petrova, T. V. Lymphatic vascular morphogenesis in development, physiology, and disease. *J. Cell Biol.* **193**, 607–618 (2011).
8. Ducoli, L. & Detmar, M. Beyond PROX1: transcriptional, epigenetic, and noncoding RNA regulation of lymphatic identity and function. *Dev. Cell* **56**, 406–426 (2021).
9. Desvergne, B., Michalik, L. & Wahli, W. Transcriptional regulation of metabolism. *Physiol. Rev.* **86**, 465–514 (2006).
10. Scholtes, C. & Giguère, V. Transcriptional control of energy metabolism by nuclear receptors. *Nat. Rev. Mol. Cell Biol.* **23**, 750–770 (2022).
11. Wong, B. W. *et al.* The role of fatty acid  $\beta$ -oxidation in lymphangiogenesis. *Nature* **542**, 49–54 (2017).
12. Wilhelm, K. *et al.* FOXO1 couples metabolic activity and growth state in the vascular endothelium. *Nature* **529**, 216–220 (2016).
13. Andrade, J. *et al.* Control of endothelial quiescence by FOXO-regulated metabolites. *Nat. Cell Biol.* **23**, 413–423 (2021).
14. Ma, W. *et al.* Mitochondrial respiration controls the Prox1-Vegfr3 feedback loop during lymphatic endothelial cell fate specification and maintenance. 1–17 (2021).
15. Paolacci, S. *et al.* Genetic testing for lymphatic malformations with or without primary lymphedema. **2**, 5–9 (2018).
16. Niu, N., Xu, S., Xu, Y., Little, P. J. & Jin, Z. G. Targeting Mechanosensitive Transcription Factors in Atherosclerosis. *Trends Pharmacol. Sci.* **40**, 253–266 (2019).

17. Milo, R., Jorgensen, P., Moran, U., Weber, G. & Springer, M. BioNumbers The database of key numbers in molecular and cell biology. *Nucleic Acids Res.* **38**, 750–753 (2009).
18. Garcia-Alonso, L., Holland, C. H., Ibrahim, M. M., Turei, D. & Saez-Rodriguez, J. Benchmark and integration of resources for the estimation of human transcription factor activities. *Genome Res.* **29**, 1363–1375 (2019).
19. Badia-I-Mompel, P. *et al.* decoupleR: ensemble of computational methods to infer biological activities from omics data. *Bioinforma. Adv.* **2**, 1–3 (2022).
20. Bretones, G., Delgado, M. D. & León, J. Myc and cell cycle control. *Biochim. Biophys. Acta - Gene Regul. Mech.* **1849**, 506–516 (2015).
21. Zhou, J. *et al.* Contrasting roles of E2F2 and E2F3 in endothelial cell growth and ischemic angiogenesis. *J. Mol. Cell. Cardiol.* **60**, 68–71 (2013).
22. Wilting, J. *et al.* The transcription factor Prox1 is a marker for lymphatic endothelial cells in normal and diseased human tissues. *FASEB J.* **16**, 1271–1273 (2002).
23. Sonawane, A. R. *et al.* Understanding Tissue-Specific Gene Regulation. *Cell Rep.* **21**, 1077–1088 (2017).
24. Göös, H. *et al.* Human transcription factor protein interaction networks. *Nat. Commun.* **13**, 1–16 (2022).
25. Kazenwadel, J. *et al.* GATA2 is required for lymphatic vessel valve development and maintenance. *J. Clin. Invest.* **125**, 2979–2994 (2015).
26. Deleuze, V. *et al.* Angiopoietin-2 is a direct transcriptional target of tal1, lyl1 and lmo2 in endothelial cells. *PLoS One* **7**, (2012).
27. Gauvrit, S. *et al.* HHEX is a transcriptional regulator of the VEGFC/FLT4/PROX1 signaling axis during vascular development. *Nat. Commun.* **9**, (2018).
28. Aranguren, X. L. *et al.* Transcription factor COUP-TFII is indispensable for venous and lymphatic development in zebrafish and *Xenopus laevis*. *Biochem. Biophys. Res. Commun.* **410**, 121–126 (2011).
29. Harel, S. *et al.* ETS1, ELK1, and ETV4 Transcription Factors Regulate Angiopoietin-1 Signaling and the Angiogenic Response in Endothelial Cells. *Front. Physiol.* **12**, 1–14 (2021).
30. Wagner, N., Michiels, J. F., Schedl, A. & Wagner, K. D. The Wilms' tumour suppressor WT1 is involved in endothelial cell proliferation and migration: Expression in tumour vessels in vivo. *Oncogene* **27**, 3662–3672 (2008).
31. Takeda, N. *et al.* Endothelial PAS domain protein 1 gene promotes angiogenesis through the transactivation of both vascular endothelial growth factor and its receptor, Flt-1. *Circ. Res.* **95**, 146–153 (2004).

32. Casemayou, A. *et al.* Hepatocyte nuclear factor-1b controls mitochondrial respiration in renal tubular cells. *J. Am. Soc. Nephrol.* **28**, 3205–3217 (2017).
33. Chen, L. *et al.* HNF4 Regulates Fatty Acid Oxidation and Is Required for Renewal of Intestinal Stem Cells in Mice. *Gastroenterology* **158**, 985-999.e9 (2020).
34. Niwano, K. *et al.* Competitive binding of CREB and ATF2 to cAMP/ATF responsive element regulates eNOS gene expression in endothelial cells. *Arterioscler. Thromb. Vasc. Biol.* **26**, 1036–1042 (2006).
35. Cintra, R. *et al.* TCF7L2 polymorphism is associated with low nitric oxide release, endothelial dysfunction and enhanced inflammatory response after myocardial infarction. *BBA Clin.* **5**, 159–165 (2016).
36. Shimizu, S. *et al.* Stimulation of in vitro angiogenesis by nitric oxide through the induction of transcription factor ETS-1. *Int. J. Biochem. Cell Biol.* **36**, 114–122 (2004).
37. Van Amerongen, M. J., Diehl, F., Novoyatleva, T., Patra, C. & Engel, F. B. E2F4 is required for cardiomyocyte proliferation. *Cardiovasc. Res.* **86**, 92–102 (2010).
38. Sowers, R. *et al.* mRNA expression levels of E2F transcription factors correlate with dihydrofolate reductase, reduced folate carrier, and thymidylate synthase mRNA expression in osteosarcoma. *Mol. Cancer Ther.* **2**, 535–541 (2003).
39. Cheng, C., Geng, F., Cheng, X. & Guo, D. Lipid metabolism reprogramming and its potential targets in cancer. *Cancer Commun.* **38**, 49–54 (2018).
40. Ju, J., Pedersen-Lane, J., Maley, F. & Chu, E. Regulation of p53 expression by thymidylate synthase. *Proc. Natl. Acad. Sci. U. S. A.* **96**, 3769–3774 (1999).
41. Erlandsson, M. C. *et al.* Survivin promotes a glycolytic switch in CD4+ T cells by suppressing the transcription of PFKFB3 in rheumatoid arthritis. *iScience* **25**, (2022).
42. Castiglioni, S. *et al.* KMT2A: Umbrella Gene for Multiple Diseases. *Genes (Basel)*. **13**, (2022).
43. Reckelhoff, J. F., Lamarca, B., Garovic, V. D. & Alexander, B. T. Human Umbilical Venous Endothelial Cells: Early Predictors of Cardiovascular Risk in Offspring?: What Is Known and What More Needs to Be Investigated? *Hypertension* **74**, 32–34 (2019).
44. González-Loyola, A. *et al.* FOXC2 controls adult lymphatic endothelial specialization, function, and gut lymphatic barrier preventing multiorgan failure. *Sci. Adv.* **7**, (2021).
45. Vande Walle, L., Lamkanfi, M. & Vandenabeele, P. The mitochondrial serine protease HtrA2/Omi: An overview. *Cell Death Differ.* **15**, 453–460 (2008).
46. Chakraborty, A., Bose, R. & Bose, K. Unraveling the Dichotomy of Enigmatic Serine Protease HtrA2. *Front. Mol. Biosci.* **9**, 1–8 (2022).
47. Weekes, M. P. *et al.* Quantitative temporal viromics: An approach to investigate host-pathogen

- interaction. *Cell* **157**, 1460–1472 (2014).
48. Villén, J. & Gygi, S. P. The SCXAC enrichment approach for global phosphorylation. *Nat. Protoc.* **3**, 1630–1638 (2008).
  49. Searle, B. C. *et al.* Chromatogram libraries improve peptide detection and quantification by data independent acquisition mass spectrometry. *Nat. Commun.* **9**, (2018).
  50. Chambers, M. C. *et al.* A cross-platform toolkit for mass spectrometry and proteomics. *Nat. Biotechnol.* **30**, 918–920 (2012).
  51. Demichev, V., Messner, C. B., Vernardis, S. I., Lilley, K. S. & Ralser, M. DIA-NN: neural networks and interference correction enable deep proteome coverage in high throughput. *Nat. Methods* **17**, 41–44 (2020).
  52. Cox, J. *et al.* Accurate proteome-wide label-free quantification by delayed normalization and maximal peptide ratio extraction, termed MaxLFQ. *Mol. Cell. Proteomics* **13**, 2513–2526 (2014).



## **Concluding Remarks**

## Generation of a multi-omics dataset to study molecular patterns in different EC types and growth states

The objective of this work was to generate a systematic description of the dynamic molecular patterns that underlie or even underpin EC identities and states. To that end, we first aimed to develop an experimental workflow that would allow us to systematically analyse the molecular patterns underlying proliferative and quiescent states in four endothelial cell types. We were inspired by previous studies that showed strong induction of quiescence through contact inhibition and mitogen reduction, which proved to be superior to activation of Notch<sup>1,2</sup>. In this setup, ECs were seeded at the same density and grown for 10 days in the same vessel with a medium that had reduced amount of growth factors. This approach led to a strong induction of quiescence in all four EC types tested, but especially in LECs with up to 98% quiescent cells after 5 days. The strong induction of quiescence is underpinned by the reduced expression of the proliferation markers MKI67 and PCNA<sup>3,4</sup>. *In vivo*, quiescent ECs start to migrate and proliferate upon external stimulation to form novel vessels. We wondered whether quiescent ECs in our *in vitro* assay were able to proliferate after the strong quiescence induction. We therefore reseeded iLECs, which have the highest fraction of quiescent cells after 10 days and monitored growth and the fraction of quiescent cells after reseeded. Indeed, reseeded quiescent iLECs immediately resumed growth and the fraction of quiescent cells 48h post-reseeding was almost at the same level as in the proliferation-to-quiescence setup. Although the growth and quiescence induction dynamics were similar for all EC types, we observed that BECs partly grew into 3D *in vitro*. This goes in line with the slightly higher expression of MKI67 and PCNA after day 5 in HDBECs and HUVECs, potentially indicating that BECs have stronger intrinsic proliferation signals than LECs.

Next, we used the experimental setup to collect extracellular metabolome and intracellular metabolome and proteome samples every 24 hours. Uptake and secretion of certain metabolites by a cell usually correlate with the metabolic activity of the cell and thus analysis of the extracellular metabolome is a first indicator of the extent of metabolic variability between EC types. The mass spectrometry-based measurements of extracellular metabolites from each cell type were performed at different days, which led to temporal batch effects. We consequently corrected with a moving median-based temporal drift normalization. This is a simple and gentle, yet effective method to correct



for temporal drifts without reducing the biological variance. The same temporal batch effects were observed in the intracellular metabolomics dataset. On top of the moving median-based normalization, we applied a mean normalization to account for biomass differences that arise from the varying number of cells the intracellular metabolomes were extracted from. Our chosen normalization approach for extra- and intracellular metabolomics data indeed reduced the temporal drift between the cell types and still conserved the biological variability between the samples. On the phenotype level, we observed that reseeded quiescent iLECs immediately resumed growth and most cells are proliferating again 48 hours post-reseeding. In line with that, the dynamic metabolic patterns observed in the transition from proliferation to quiescence are inversed when quiescent iLECs were reseeded, which confirms that either approach, proliferation to quiescence or quiescence to proliferation, is suitable to study the temporal dynamics of metabolism in the transition from one state to another.

Lastly, we performed untargeted proteomics, which resulted in a dataset that contains 7894 protein groups. For proteomics we used maxLFQ normalization, a previously published normalization method, that results in comparable quantities of proteins across cell types and days<sup>5</sup>. A big advantage of untargeted proteomics datasets is the ability to assess the presence of marker proteins, which confirms that cells have an expected identity or phenotype. For example, we clearly observe the presence of the LEC marker proteins LYVE1 and PROX1 in HDLECs and iLECs and the presence of STAT6, a BEC marker, in HDBECs and HUVECs. Furthermore, the proliferation markers PCNA and MKI67, which is frequently used in fluorescence-assisted cell analysis assays to determine proliferation, have the highest expression after 2 to 3 days in all cell types, confirming the results of the cell cycle state analysis we performed to determine the fractions of quiescent and proliferating cells. The cell type-specific markers also proved useful when we were assessing whether we should impute missing values in our dataset. Data imputation is a standard procedure in transcriptomics and sequencing, but using marker proteins as examples, we showed that random forest-based data imputation in our proteomics dataset leads to intensities that are biologically incorrect, for example imputed intensities of PROX1 in BECs. Thus, we stuck to our original dataset for further analysis.

In summary, we developed an experimental workflow in which the four EC types tested are first proliferating and then transition into quiescence. Untargeted metabolomics and proteomics measurements done with samples taken every 24 hours

allow us to study the dynamic molecular patterns that define EC types and states. The advantage of applying the same experimental procedure to the four EC types is the possibility for unbiased extraction of distinct and general molecular features and thus assess the molecular diversity amongst different EC types.

## **Endothelial cell lines identities and states are defined by distinct proteomic signatures**

In the second part, we analysed in detail the molecular patterns that underlie EC identities and states. There are two main strategies to analyse multi-omics datasets that contain metabolomics and proteomics data: knowledge-based methods that map metabolic and proteomic patterns onto a predefined network to generate mechanistic hypotheses and data-driven methods that require less prior knowledge and use statistical analyses or neural nets for predictions and hypothesis generation<sup>6</sup>. Knowledge-based methods often require absolute quantities to generate mechanistic insights and are therefore not well suited for our semi-quantitative datasets.

We therefore chose a data-driven approach and used in a first step partial least squares discriminant analysis (PLS-DA) on the proteomics dataset to decipher the general differences between LECs and BECs on a proteome level (Figure 1). Surprisingly, we found that FAO and TCA cycle/mitochondrial respiration are the two top enriched pathways using the list of proteins that are associated with LEC identities, even before other signalling pathways like VEGF or Rho GTPase signalling. Both metabolic pathways have known roles in lymphangiogenesis but it still underscores the crucial role of metabolism in maintenance of LEC identities. Such a strong enrichment of metabolic pathways was not observed in BECs.

All time points from each cell type were included in the PLS-DA, thus neglecting the temporal protein expression patterns. Consequently, in a second step, we moved forward with day 2 and day 5 post-seeding time points to further explore the proteomic patterns that underlie different growth states. These two time points represent the samples that contain the highest fraction of proliferating and quiescent cells, respectively. Besides core proteomic changes in processes well-known to be involved in cellular quiescence or vessel formation, such as downregulated DNA replication and upregulated extracellular matrix organisation, we found enrichments in a total of 291 very diverse pathways, which indicates extensive molecular adaptations that follow or

drive quiescence induction (Figure 1). The enrichments dataset is a vast resource for further investigations on their role in quiescence formation and maintenance, but this is beyond the scope of this thesis. However, we also found enrichments of proteins in 36 metabolic pathways across all cell types, and we moved forward with in-depth analysis of the altered metabolic pathways.

HDBECs have generally the weakest enrichments of specific metabolic pathways compared to the other three EC types. Yet, there is a strong enrichment of metabolism itself, which includes proteins in all metabolic pathways, and intra- and extracellular metabolomics show that quiescent and proliferating HDBECs have different metabolic patterns. This suggests that HDBECs have weaker, but still widespread metabolic adaptations. In line with the results from the PLS-DA, quiescent iLECs and HDLECs have the strongest enrichment in TCA cycle and mitochondrial respiration, once more confirming the crucial role of these two pathways in LEC homeostasis. Enrichment of FAO in quiescence across all cell types, to a lesser extent in HDBECs though, suggests that the previously described, essential role of FAO for redox homeostasis in HUVECs is a general feature of endothelial quiescence<sup>2</sup>. However, whether FAO is more important for redox homeostasis or for keeping up a lymphatic identity in LECs needs further investigation. We also observed enrichment of branched-chain amino acid (BCAA) catabolism, sphingolipid metabolism and glyoxylate metabolism and glycine degradation. BCAA catabolism and sphingolipid metabolism have previously been described to be involved in regulation of quiescence and self-renewal of hematopoietic stem cells, suggesting that they act in the same way in quiescent ECs<sup>7,8</sup>. Glyoxylate metabolism involves the degradation of hydroxyproline from collagen, a major extracellular matrix constituent, and glyoxylate metabolism is potentially upregulated in quiescent ECs in order to dynamically build and modify collagen for vessel homeostasis<sup>9</sup>. These three metabolic pathways are promising targets for future investigations of their role in EC quiescence formation and maintenance.

## **Distinct metabolic programs underlie quiescence induction and maintenance processes across different EC types**

Although our assessment of protein expression patterns revealed variances in metabolic pathways among different EC types, the implications of these patterns for metabolite levels and the metabolic activity of these four EC types remained uncertain.

Consequently, as a first step, we investigated the overall metabolic activity of these four cell lines by assessing the uptake and secretion rates of extracellular metabolites. Overall, the uptake and secretion rates do not support the case for a general decrease of metabolic activity in quiescent ECs. In fact, we found that all EC types secrete lactate and take up ascorbate in proliferation and quiescence, but uptake of glucose and amino acids varies between cell types and states, strongly suggesting distinct metabolic patterns that support specific functions of the EC types, as it was observed previously in fibroblasts and epithelial cells (Figure 1)<sup>1,10</sup>. One striking difference is the uptake of glucose and secretion of lactate across cell types and states, which is an indicator for the glycolytic activity. Proliferating HUVECs have the highest uptake rate of glucose and second highest secretion rate of lactate, suggesting that the glycolytic activity is the highest in proliferating HUVECs amongst all ECs. In line with previous research, the glycolytic activity of quiescent HUVECs is lower<sup>11,12</sup>. This reduction of glycolytic flux from proliferation to quiescence is also observed in iLECs, but not in HDLECs and HDBECs. HDLECs seem to have a stable glycolytic flux in proliferation and quiescence, while HDBECs do not take up glucose in proliferation at all. This is surprising and it is not completely clear why they do not take up glucose and what they use to generate energy from. In the proteomics data, we observed upregulation of glucose metabolism in quiescent HDBECs, which suggests that HDBECs indeed increase glycolysis in quiescence. Even more surprising is that, additionally to the lacking glucose uptake, HDBECs secrete many amino acids in proliferation and quiescence, including glutamine. One possible carbon source could be lipids or fatty acids from the medium. However, this needs further investigation, for example by employing tracer studies to follow the route of carbons through the metabolic network.

Intracellular metabolomics exhibits a similar picture of distinct metabolic patterns in the tested EC types. We identified 63 metabolites and 51 metabolic pathways that are significantly changed between quiescence and proliferation in at least one cell type. On the metabolite level, in combination with the extracellular metabolomics results, some of these findings could point towards cell type-specific or tissue-specific demands and roles of individual ECs. For example, quiescent HUVECs have the highest uptake rate of glutamine but still a significant decrease of intracellular glutamine pools, suggesting a HUVEC-specific high demand for glutamine in quiescence. Furthermore, quiescent HDLECs and HDBECs have elevated intracellular proline pools even though they have increased secretion rates of proline in quiescence,

possibly indicating a supporting role in collagen homeostasis in the skin that is formed by the surrounding tissue rather than cellular identity<sup>13,14</sup>.

On the pathway level, the patterns are very diverse and more difficult to interpret. Increased levels of intermediates in a pathway could mean that the flux through the pathway is reduced and thus the pools of the intermediates increased, however, this holds only true if the flux into the pathway stays constant. On the other hand, decreased levels of intermediates could arise from higher flux through a pathway, assuming that there is a constant flux into the pathway. For example, there are increased levels of intermediates in glycolysis in quiescent HUVECs, even though we assumed decreased glycolytic flux from the extracellular metabolomics data. Also, there is increased expression of TCA cycle enzymes in quiescent cells, but we observed generally increased pools of TCA cycle intermediates. Moreover, intracellular metabolic patterns can only be partially attributed to changes in the expression of proteins involved in these pathways. This suggests that these patterns are not solely influenced by variations in protein expression levels. Additional regulators of metabolic fluxes, such as allosteric regulation, post-translational modifications, or other mechanisms likely play a significant role in formation of metabolic patterns. Nevertheless, we hypothesize that different EC types may rely on distinct metabolic pathways to support cellular programs and the most straightforward way to examine this hypothesis is through experimental validation.

## **Pharmacological inhibitors identify HUVEC- and iLEC-specific metabolic program susceptibilities**

To do so, we chose a panel of 14 metabolic drugs and assessed their effect on growth, migration and sprouting capacity of iLECs and HUVECs, as representatives from lymphatic and blood ECs, respectively. Overall, HUVECs and iLECs exhibit a range of phenotypic alterations in response to targeted inhibition of metabolism, for example in nucleotide and folate metabolism, fatty acid synthesis, TCA cycle, ROS and NO metabolism and glutamate metabolism (Figure 1). While interpretation of impaired proliferation upon pharmacological inhibition is rather straightforward, interpretation of impaired migration and sprouting is more complex. The results, particularly those drugs targeting ROS and NO metabolism, suggest that some cellular processes, be it balanced ROS generation, NAD<sup>+</sup> regeneration, adequate NO pools, or another process, do not necessarily play similarly important roles in the regulation of migration

and sprouting. This might be due to the complex interplay of different states needed to perform migration and sprouting. In migration assays, the cells are first quiescent, and then start to migrate and proliferate after applying a scratch. And in sprouting, there is a complex interplay between migrating tip cells, proliferating stalk cells and quiescent phalanx cells. Perturbations of any of these states can lead to impaired phenotypes and elucidating which state (quiescent, migrating, proliferating) or cell type (tip, stalk or phalanx) contributes to the impaired phenotypes is difficult. One possibility is to account for the effect of the drug on proliferation alone. For example, Rotenone impairs proliferation of iLECs but not HUVECs, and decreases migration rate of long- and short-term treated HUVECs and only short-term treated iLECs. Short-term treated iLECs do not have time to adjust to elevated ROS levels and the impaired proliferation upon Rotenone treatment might therefore impact the outcome of the migration assay. This suggests that Rotenone, hence increased ROS levels, has an adverse effect on proliferation of iLECs and on migration of HUVECs.

More conclusive is the adverse effect of Succinylacetone on migration and sprouting of HUVECs. Succinylacetone inhibits heme biosynthesis and we could show that the lack of NO production by eNOS, in which heme acts as co-factor, is detrimental for HUVEC migration and sprouting, but not for iLECs. This recapitulates previous findings of the essential role of NO as signalling molecule regulating angiogenesis and the vascular tone<sup>15-18</sup>. It also suggests that NO plays a minor role in lymphangiogenesis. Another intriguing observation is impaired migration of iLECs but not HUVECs upon inhibition of glutamate dehydrogenase (GLUD1) by R162 and upon  $\alpha$ -ketoglutarate supplementation. We hypothesize that GLUD1 inhibition, either through R162 or a negative feedback regulation by elevated  $\alpha$ -ketoglutarate levels, leads to toxic intracellular accumulation of glutamate in iLECs and that HUVECs have higher capacity to metabolize excess glutamate, potentially through increased export of glutamate or the upregulation of transamination enzymes<sup>19,20</sup>. Surprisingly, both R162 and  $\alpha$ -ketoglutarate supplementation impair sprouting of iLECs and HUVECs. This suggests an effect of glutamate metabolism on (lymph)angiogenesis beyond its isolated effect on EC migration. Previous reports propose that overactivation of ionotropic glutamate receptors, such as NMDA, results in decreased tube network formation and increased vascular permeability in brain BECs and HUVECs<sup>21,22</sup>. Possibly, increased glutamate levels are cleared by increased secretion of glutamate, which leads to higher auto- and paracrine activation of glutamate receptors, resulting

in impaired sprout formation. However, the exact cause of the toxic effect of GLUD1 inhibition and  $\alpha$ -ketoglutarate supplementation in migration of iLECs and sprouting of iLECs and HUVECs needs further investigation.

Taken together, even though the interpretation of the validation experiments is sometimes difficult, they are useful tools to assess the differential metabolic susceptibilities of HUVECs and iLECs. And the results clearly show that HUVECs and iLECs have divergent dependencies to metabolic pathways for proliferation, migration and sprouting. Moreover, the validation experiments confirm the findings of the metabolomics and proteomics measurements to some extent. Generally, the metabolomics dataset proved to be a more valuable resource to choose drugs used to study the effect of perturbations in metabolism on phenotype formation and maintenance. For example, HUVEC's dependence on heme for NO production was based on the negative enrichment of heme biosynthesis intermediates in quiescent HUVECs found in the metabolomics dataset. No enrichment of proteins in the heme biosynthesis pathway was observed in the proteomics dataset, although ALAD, the target of Succinylacetone was indeed higher expressed in quiescent HUVECs. This demonstrates that different omics measurements go hand in hand and provide useful insights into a particular molecular level or process in cells. Finally, we argue that the generated proteomics and metabolomics datasets are valid and valuable resources to investigate the role of more metabolic and different molecular, non-metabolic pathways in the formation and maintenance of EC identities and states.

## **Diverse transcription factor activity patterns underlie endothelial cell identities and states**

In the last part, we aimed to systematically explore the diversity of TF activity patterns and whether distinct TFs are potential cell type-specific regulators of enzymes needed for a specific phenotype. To that end, we took advantage of the untargeted proteomics dataset and inferred TF activities with a previously published computational method<sup>23</sup>. The applied method uses abundances of TFs targets to infer the activities of TFs. There are two major advantages using this method: first, TFs are usually low abundant and thus often below or right at the limit of detection of untargeted proteomics approaches. Second, the abundance of a TF does not necessarily correlate with its activity. The applied method has the advantage of being independent of the actual abundances of the TFs by using the abundances of the TFs targets in the inference.

Overall, we were able to infer the activities of 263 TFs. Because of the diversity observed in the proteomics and metabolomics data, we expected similar diversity of TF activity patterns. Indeed, we observed cell type- and state specific TF activities but also general activity patterns that fundamentally differentiate BECs and LECs, including well-known markers of LEC and BEC identities (Figure 1). These general and distinct patterns are likely driven by the identities of the EC types, such as high activity of PROX1 in LECs, but also by the individual needs and roles of the cell types in their residing tissues. TF activities might also help to pinpoint the exact identity of LECs used in the screen. Previous studies displayed differential transcript levels in LECs, including TFs, that are dependent on the locations of the LECs in the lymphatic vasculature, such as in the lymphatic capillaries, collecting vessels or valves<sup>24</sup>. For example, González-Loyola *et al.* measured increased LYVE1 transcript levels in capillary LECs and GATA2 transcript levels in valve LECs. In our screen, LYVE1 levels are generally high in LECs, especially in quiescent LECs, but also GATA2 activity was predicted to be generally high in the tested LECs. This suggests that the LECs in our setup are either a mix of LECs from capillaries, collecting vessels and valves, or that they lose the vessel-specific molecular patterns, yet without losing the tissue and vascular bed-specific patterns when grown *in vitro*. Not all expected patterns of previously reported markers of endothelial identities or states were observed here. For example, we did not observe increased activity of FOXO1 in quiescent ECs, even though FOXO1 is known to be a gatekeeper of endothelial quiescence<sup>25,26</sup>. This is probably due to incomplete data or the predefined networks that were used to infer TF activities and highlights the weakness of computational methods to be dependent on well-defined networks and complete data.

Furthermore, we used the dataset to identify potentially novel interactions between TFs and metabolism through correlation analysis, focusing on enzymes that were shown in the previous chapter to be necessary for certain phenotypes. Notably, the strongest correlating pairs of TFs and enzymes among cell type-specific active TFs in HUVECs and iLECs consist of enzymes, which were demonstrated to be crucial for migration in the previous chapter. It is worth emphasizing that the correlation analysis does not provide insights into causality, specifically the direction of regulation. Therefore, it is necessary to conduct functional validation to confirm these discoveries. In summary, we were able to generate a comprehensive dataset of TF activities across EC types and states, extracted general and distinct patterns and proposed novel TF-



enzyme interactions. However, since we only focused on 14 enzymes in the correlation analysis, there is still a lot to discover in this dataset, as we demonstrated with the USF2-HTRA2 example in iLECs.

## Limitations and outlook

To our knowledge, the presented experimental workflow is one of the most adequate approaches to study different growth states of primary ECs in single culture. Since this setup is only an *in vitro* experiment, the molecular patterns *in vivo* might differ to some extent due to extracellular cues that are not present *in vitro*, i.e. paracrine or cell-cell signalling with surrounding cells like pericytes or shear stress arising from blood and lymph flow<sup>27–29</sup>. One possibility to address the interactions with other cell types in the future would be co-cultures. There are two ways to do so: one is a transwell approach, in which endothelial cells would be grown as a monolayer on and another cell type, like pericytes, below a permeable membrane, and subsequently the metabolome and proteome extracted from the endothelial cells that grow on the membrane for in-depth analysis<sup>30,31</sup>. Another approach could be co-cultures with GFP-tagged ECs, which enables fluorescent-assisted sorting afterwards to extract only the metabolome and proteome from ECs<sup>32</sup>. This approach is more suitable for experiments in which proteins or RNA is extracted, but less for metabolomics since the sorting process can have a profound effect on metabolite levels<sup>33</sup>. In order to study the consequences of blood and lymph flow on phenotypes and molecular patterns, microfluidic systems could be employed<sup>34–36</sup>. In brief, ECs are subjected to different types of flow in microfluidic chambers, which imitate normal or disturbed blood and lymph flow. For example, a study by Sabine *et al.* showed that oscillatory shear stress, as it occurs around the valves in lymphatic vessels, triggers widespread up- and downregulation of gene expression as well as FOXC2-regulated growth and motility arrest, which protects vessel integrity<sup>36</sup>. Accordingly, we propose that employing co-cultures or microfluidics devices on different EC types in future experiments would add an additional layer of information, thereby integrating the effect of extracellular cues on the cell type-specific and general molecular patterns.

In this work, we validated the findings of the untargeted proteomics and metabolomics measurements in a functional screen using pharmacological inhibitors. Nevertheless, if we want to deepen our understanding of intracellular metabolic fluxes and their regulation in ECs, further measurements that would result in absolute

concentrations or metabolic flux analysis would be necessary. The determined semi-quantitative levels of metabolites only allow us to make relative comparisons between cell types and states but do not inform us about the absolute concentrations of metabolites in the respective cell types and states. This sometimes impairs the comparison with previous studies, in which the absolute concentrations of intracellular or taken up/secreted metabolites were measured. Additionally, knowledge-based modelling methods depend on absolute metabolite concentrations, which means that quantitative measurements would be necessary for the development of models that generate mechanistic insights. Furthermore, the observed relative changes in metabolite levels are not fully informative about the intracellular fluxes. Metabolic flux analysis is an approach to experimentally quantify the integrated responses of metabolic networks and would therefore shed further light on the extent and strength of intracellular fluxes between EC types and states<sup>37</sup>.

We performed data-driven analysis only on one dataset (proteomics and metabolomics) at a time. Nowadays, more sophisticated algorithms for data integration are available and promise to be valuable tools for hypothesis generation from multi-omics data. We tried out many available algorithms and methods to integrate and/or visualize proteomics and metabolomics data, such as GAM, metabolic network segmentation (MNS), cosmos or joint pathway enrichment analysis in MetaboAnalyst<sup>38-41</sup>. Often, these methods work as a starting point in providing an overview of the data (GAM) but did not lead to conclusive results due to different reasons. For example, GAM generates subgraphs of the metabolic network that are the most changing subnetworks between two conditions. Depending on the chosen thresholds, these subnetworks are quite messy and difficult to interpret. Cosmos uses prior knowledge to extract co-regulated metabolites and proteins, but only results in few subnetworks in our case, which does not reflect the diversity we observed in the data. And joint pathway enrichment analysis relies on lists of proteins and metabolites that are up- or downregulated, which is not reasonable to do because as we discussed earlier, we cannot assume whether upregulated protein levels lead to lower metabolite levels or vice versa. Because of these limitations, we performed the data analysis separately on the two datasets. However, in the future, more tools might be published that could be used to integrate proteomics and metabolomics data and help to generate further hypotheses.

The applied validation screen with pharmacological inhibition is a straightforward and useful approach to determine cell type-specific metabolic vulnerabilities. Nevertheless, there are some limitations and improvements that could be made. First, we compare iLECs with HUVECs and it is not too surprising that we observe cell type-specific metabolic dependencies. In a next step, a similar screen with iLECs and HDLECs could be done to show how different two cell types from the same vascular bed but different tissues are when it comes to formation of a phenotype upon pharmacological inhibition, especially since we observe quite similar proteomic and metabolic patterns in iLECs and HDLECs. Furthermore, we only used one drug concentration. A range of drug concentrations could tell us how much more sensitive or resistant one cell type is than the other through the determination of GR50 for proliferation or a similar value for the migration rate and total sprout length. Even though we selected drugs that have only one described target, there might be some off-targets that have not been described yet. Knock-down or knock-out experiments of the targeted enzymes would provide further confirmation that the resulting metabolic pathways are indeed necessary for the formation of a specific phenotype. Also, the findings only suggest that a metabolic pathway is necessary for the formation of a phenotype, but it does not fully imply if it is a driver or a passenger. To address this, supplementation experiments or overexpression of enzymes could be performed. For example, if increased concentrations of a metabolite in the medium or enzyme overexpression enhances migration rate and this effect can be reversed through enzyme inhibition, then this would strongly indicate that the targeted enzyme or the pathway it lies in is a driver of a phenotype. However, driving a phenotype is usually not solely driven by one factor but by an interplay of multiple different molecular features. Nevertheless, our experiments with NONOate suggest for example that NO is indeed a partial driver of migration in iLECs and HUVECs. Furthermore, for some experiments, like the investigation of the role of NO and ROS metabolism, additional measurements could be done in the future, such as quantitative ROS assays or Seahorse assays, to determine if intracellular ROS accumulation and mitochondrial respiration rate are altered after drug interventions and thus play a role in formation of impaired phenotypes.

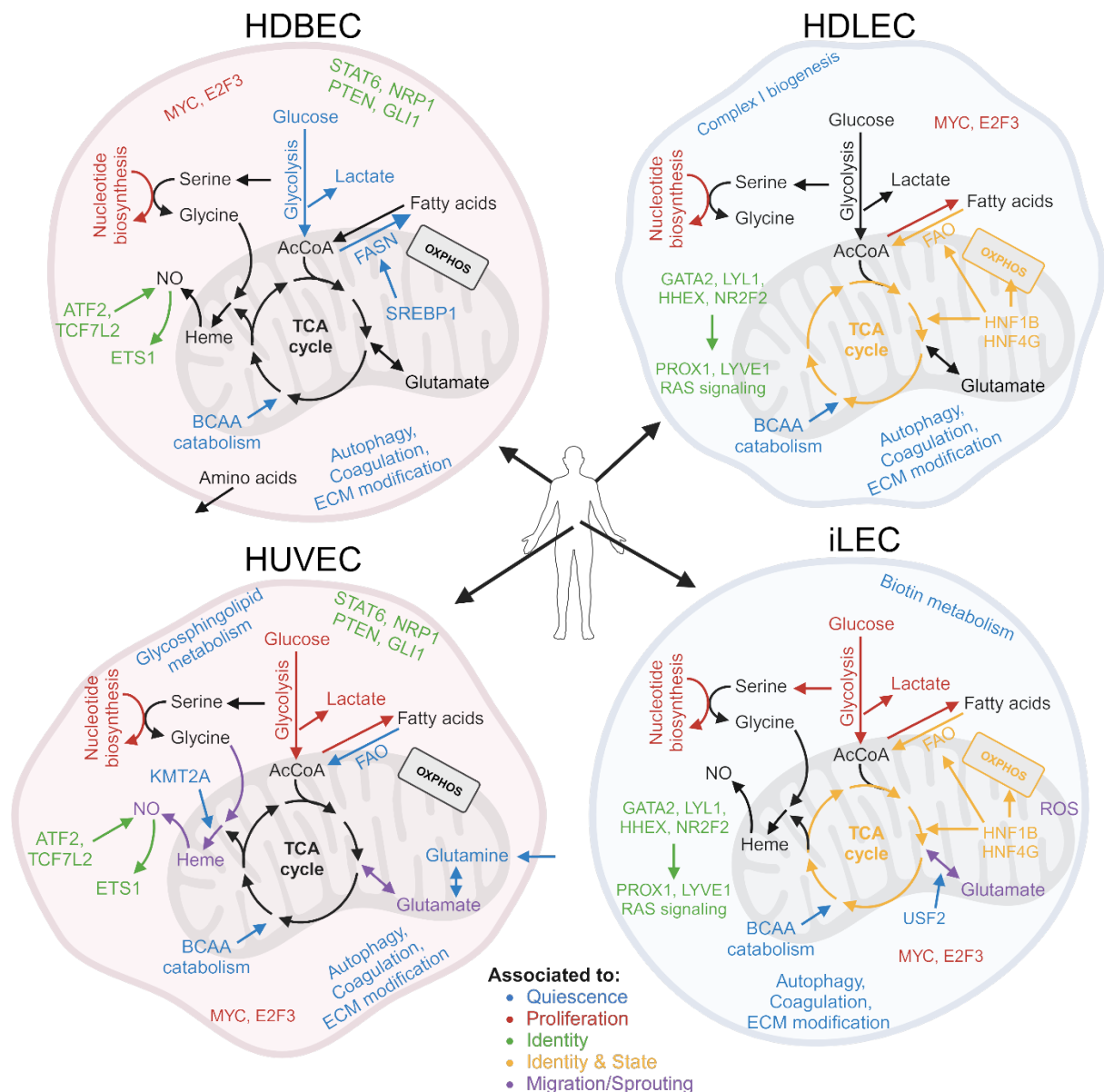


**Figure 1.** Overview of metabolites, proteins, metabolic and signaling pathways and TFs that were formative of, active in or associated with either quiescence, proliferation, identity formation and maintenance, identity and growth state or migration/sprouting in the four EC types tested.

## Implications on further EC research

Our work provides further evidence that ECs from different tissues and vascular beds have distinct molecular patterns that are formative and supportive for certain phenotypes and hence directly impact local tissue homeostasis. For example, secretion of proline in quiescent HDBECs and HDLECs and upregulation of glyoxylate metabolism in quiescent HDLECs suggests an important role of these two EC types in collagen maintenance and modification and thus for skin homeostasis. Additionally,

the validation experiments show that iLECs and HUVECs depend differently on certain metabolites and metabolic pathways to form a specific phenotype. It implies that findings on the molecular level of a specific EC type cannot simply be extrapolated to other EC types, making EC research more complex and tedious. But it also suggests that dysfunctional ECs from specific vascular beds and tissues could be subjected to targeted interventions that do not affect other ECs, as it was shown before with BECs in glioblastoma or LECs in a murine lymphedema model although the systematic effects of the interventions are missing in these publications<sup>42,43</sup>. Moreover, we discussed in the introduction how metabolism could be causative or supportive of vascular diseases, for example of secondary lymphedema. Based on our research, we argue that if the metabolic patterns of ECs from healthy and diseased lymphatic vasculature are studied in-depth, potentially novel interventions that alleviate lymphedema symptoms by only affecting the diseased but not healthy lymphatic vasculature could be developed.

Our validation experiments focused completely on metabolism, pharmacologically inhibiting the activities of 14 enzymes in different metabolic pathways and assessing the effect on phenotype formation and maintenance. The targeted pathways are only a tiny fraction of all molecular pathways or proteins and TFs found to define LEC and BEC identities, proliferation and quiescence or a specific EC type. We therefore think that our proteomics, metabolomics and TF activities datasets have the potential to contribute to the discovery of more molecular factors that are involved in EC homeostasis and might even be future targets in fields such as regenerative medicine by improving vascularization in organoids, or to optimize cell culture media for *in vitro* experiments, as well as the development of therapeutics. For example, there is an enrichment of Ras signaling proteins in LECs, indicating an important role of this signaling pathway in lymphatic identity formation and maintenance specifically. Indeed, it has been shown that Ras signaling regulates lymphatic vessel growth through VEGFR3 expression<sup>44</sup>. On the other hand, PTEN signaling is enriched in BECs and it has been shown before that the PTEN/PI3K pathway governs normal vascular development but also tumor angiogenesis<sup>45</sup>. Signaling pathways that are specific for (lymph)angiogenesis therefore hold the potential to be future targets for clinical interventions aimed at reducing or activating (lymph)angiogenesis, depending on clinical needs<sup>46</sup>.

## References

1. Lemons, J. M. S. *et al.* Quiescent fibroblasts exhibit high metabolic activity. *PLoS Biol.* **8**, (2010).
2. Kalucka, J. *et al.* Quiescent Endothelial Cells Upregulate Fatty Acid  $\beta$ -Oxidation for Vasculoprotection via Redox Homeostasis. *Cell Metab.* **28**, 881-894.e13 (2018).
3. Gerdes, J., Schwab, U., Lemke, H. & Stein, H. Production of a mouse monoclonal antibody (B1N) reactive with a human nuclear antigen associated with cell proliferation. *Int. J. Cancer* **31**, 13–20 (1983).
4. Kelman, Z. PCNA: Structure, functions and interactions. *Oncogene* **14**, 629–640 (1997).
5. Cox, J. *et al.* Accurate proteome-wide label-free quantification by delayed normalization and maximal peptide ratio extraction, termed MaxLFQ. *Mol. Cell. Proteomics* **13**, 2513–2526 (2014).
6. Noor, E., Cherkaoui, S. & Sauer, U. Biological insights through omics data integration. *Curr. Opin. Syst. Biol.* **15**, 39–47 (2019).
7. Liu, X. *et al.* PPM1K Regulates Hematopoiesis and Leukemogenesis through CDC20-Mediated Ubiquitination of MEIS1 and p21. *Cell Rep.* **23**, 1461–1475 (2018).
8. Xie, S. Z. *et al.* Sphingolipid Modulation Activates Proteostasis Programs to Govern Human Hematopoietic Stem Cell Self-Renewal. *Cell Stem Cell* **25**, 639-653.e7 (2019).
9. Knight, J., Jiang, J., Assimos, D. G. & Holmes, R. P. Hydroxyproline ingestion and urinary oxalate and glycolate excretion. *Kidney Int.* **70**, 1929–1934 (2006).
10. Coloff, J. L. *et al.* Differential Glutamate Metabolism in Proliferating and Quiescent Mammary Epithelial Cells. *Cell Metab.* **23**, 867–880 (2016).
11. Wilhelm, K. *et al.* FOXO1 couples metabolic activity and growth state in the vascular endothelium. *Nature* **529**, 216–220 (2016).
12. De Bock, K. *et al.* Role of PFKFB3-driven glycolysis in vessel sprouting. *Cell* **154**, 651–663 (2013).
13. Rohlenova, K. *et al.* Single-Cell RNA Sequencing Maps Endothelial Metabolic Plasticity in Pathological Angiogenesis. *Cell Metab.* **31**, 862-877.e14 (2020).
14. Goveia, J. *et al.* An Integrated Gene Expression Landscape Profiling Approach to Identify Lung Tumor Endothelial Cell Heterogeneity and Angiogenic Candidates. *Cancer Cell* **37**, 21-36.e13 (2020).
15. Murohara, T. *et al.* Endothelial Cell Migration. *Arter. Thromb Vasc Biol.* 1156–1161 (1999).
16. Cooke, J. P. & Losordo, D. W. Nitric oxide and angiogenesis. *Circulation* **105**, 2133–2135 (2002).

17. Förstermann, U. & Münzel, T. Endothelial nitric oxide synthase in vascular disease: From marvel to menace. *Circulation* **113**, 1708–1714 (2006).
18. Förstermann, U. & Sessa, W. C. Nitric oxide synthases: Regulation and function. *Eur. Heart J.* **33**, 829–837 (2012).
19. Parfenova, H. *et al.* Glutamate induces oxidative stress and apoptosis in cerebral vascular endothelial cells: Contributions of HO-1 and HO-2 to cytoprotection. *Am. J. Physiol. - Cell Physiol.* **290**, 1399–1410 (2006).
20. Miura, K., Ishii, T., Sugita, Y. & Bannai, S. Cystine uptake and glutathione level in endothelial cells exposed to oxidative stress. *Am. J. Physiol. - Cell Physiol.* **262**, (1992).
21. Vazana, U. *et al.* Glutamate-mediated blood–brain barrier opening: Implications for neuroprotection and drug delivery. *J. Neurosci.* **36**, 7727–7739 (2016).
22. Sailem, H. Z. & Al Haj Zen, A. Morphological landscape of endothelial cell networks reveals a functional role of glutamate receptors in angiogenesis. *Sci. Rep.* **10**, 1–14 (2020).
23. Badia-I-Mompel, P. *et al.* decoupleR: ensemble of computational methods to infer biological activities from omics data. *Bioinforma. Adv.* **2**, 1–3 (2022).
24. González-Loyola, A. *et al.* FOXC2 controls adult lymphatic endothelial specialization, function, and gut lymphatic barrier preventing multiorgan failure. *Sci. Adv.* **7**, (2021).
25. Wilhelm, K. *et al.* FOXO1 couples metabolic activity and growth state in the vascular endothelium. *Nature* **529**, 216–220 (2016).
26. Andrade, J. *et al.* Control of endothelial quiescence by FOXO-regulated metabolites. *Nat. Cell Biol.* **23**, 413–423 (2021).
27. Chatterjee, S. & Naik, U. P. Pericyte-endothelial cell interaction. *Cell Adh. Migr.* **6**, 157–159 (2012).
28. Sabine, A., Saygili Demir, C. & Petrova, T. V. Endothelial Cell Responses to Biomechanical Forces in Lymphatic Vessels. *Antioxid. Redox Signal.* **25**, 451–465 (2016).
29. Doddaballapur, A. *et al.* Laminar shear stress inhibits endothelial cell metabolism via KLF2-mediated repression of PFKFB3. *Arterioscler. Thromb. Vasc. Biol.* **35**, 137–145 (2015).
30. Goers, L., Freemont, P. & Polizzi, K. M. Co-culture systems and technologies: Taking synthetic biology to the next level. *J. R. Soc. Interface* **11**, (2014).
31. Kämpfer, A. A. M. *et al.* Development of an in vitro co-culture model to mimic the human intestine in healthy and diseased state. *Toxicol. Vitro.* **45**, 31–43 (2017).
32. Casbas-Hernandez, P., Fleming, J. M. & Troester, M. A. Gene expression analysis of in vitro cocultures to study interactions between breast epithelium and stroma. *J. Biomed. Biotechnol.* **2011**, (2011).

33. Binek, A. *et al.* Flow Cytometry Has a Significant Impact on the Cellular Metabolome. *J. Proteome Res.* **18**, 169–181 (2019).
34. Tovar-Lopez, F. *et al.* A microfluidic system for studying the effects of disturbed flow on endothelial cells. *Front. Bioeng. Biotechnol.* **7**, 1–7 (2019).
35. Meng, F. *et al.* In vitro fluidic systems: Applying shear stress on endothelial cells. *Med. Nov. Technol. Devices* **15**, 100143 (2022).
36. Sabine, A. FOXC2 and fluid shear stress stabilize postnatal lymphatic vasculature. *J. Clin. Invest.* **125**, 3861–3877 (2015).
37. Zamboni, N., Fendt, S. M., Rühl, M. & Sauer, U. 13C-based metabolic flux analysis. *Nat. Protoc.* **4**, 878–892 (2009).
38. Sergushichev, A. A. *et al.* GAM: a web-service for integrated transcriptional and metabolic network analysis. *Nucleic Acids Res.* **44**, W194–W200 (2016).
39. Kuehne, A., Mayr, U., Sévin, D. C., Claassen, M. & Zamboni, N. Metabolic network segmentation: A probabilistic graphical modeling approach to identify the sites and sequential order of metabolic regulation from non-targeted metabolomics data. *PLoS Comput. Biol.* **13**, 1–26 (2017).
40. Dugourd, A. *et al.* Causal integration of multi-omics data with prior knowledge to generate mechanistic hypotheses. *Mol. Syst. Biol.* **17**, 1–17 (2021).
41. Xia, J. & Wishart, D. S. Web-based inference of biological patterns, functions and pathways from metabolomic data using MetaboAnalyst. *Nat. Protoc.* **6**, 743–760 (2011).
42. Zhang, D. *et al.* PHGDH-mediated endothelial metabolism drives glioblastoma resistance to chimeric antigen receptor T cell immunotherapy. *Cell Metab.* **35**, 517-534.e8 (2023).
43. García-Caballero, M. *et al.* Role and therapeutic potential of dietary ketone bodies in lymph vessel growth. *Nat. Metab.* **1**, 666–675 (2019).
44. Ichise, T., Yoshida, N. & Ichise, H. H-, N- and Kras cooperatively regulate lymphatic vessel growth by modulating VEGFR3 expression in lymphatic endothelial cells in mice. *Development* **137**, 1003–1013 (2010).
45. Hamada, K. *et al.* The PTEN/PI3K pathway governs normal vascular development and tumor angiogenesis. *Genes Dev.* **19**, 2054–2065 (2005).
46. Bui, K. & Hong, Y. K. Ras Pathways on Prox1 and Lymphangiogenesis: Insights for Therapeutics. *Front. Cardiovasc. Med.* **7**, 1–15 (2020).





## Acknowledgments

This work would not have been possible with the help and support of many people. I would like to thank everyone that contributed and supported me in my PhD journey.

First and foremost, I would like to thank **Prof. Dr. Nicola Zamboni** for his great supervision and the chance to work on this fun project. I am grateful for the interesting discussions we had about my project and science in general, and especially also for the freedom I had to explore new ideas and technologies.

I want to thank **Prof. Dr. Uwe Sauer** for his supervision and support not only during my PhD, but also in the semester and Master's project I conducted in his lab, in which I made my first steps in research.

Big thanks as well to my committee members **Prof. Dr. Tatiana Petrova** and **Prof. Dr. Katrien De Bock** for the fruitful discussions, feedback and advice along the way, but also for the interesting collaborations we had together.

I want to thank all the past and present **Sauer/Zamboni/Zampieri** lab members for the great and fun environment, beers, ping pong games, coffee breaks and scientific discussions. Special thanks to **Duncan** and **Karin (O.)**, which supervised me in my semester and Master's project, for teaching me how to do science and being great supervisors. Also, special thanks to **Peter** for helping me in the last years of my PhD with your expertise and patience, and **Lydia** for your great work in the validation experiments. Furthermore, I would like to thank **Sarah** for the fun first year, in which I hopefully could teach you how to cell culture, but also for the great friendship that developed out of it. And one special thanks goes to **Sammy** for being such a cool neighbor for 4 years in the lab, but also at Schürbungert. A big thanks as well to all the other members of the lab: **Chris (ex-master dungeon companion)**, **Julian, Laurentz, Tomek, Evgeniya, Andi, Vilhelmiina, Doro, Kate, Anna, Vince, Lorenzo, Adriano, Michelle, Abraham** and of course the former lab members: **Karin, Daniela, Tobi, Andrei, Philipp, Mauro, Alexis, Petra, Maren, Pau, Alaa, Mattia** and whoever I forgot.

I would like to thank everyone from the other labs at the institute and the admin team for making IMSB so great, and the friends I made throughout the years at ETH, not only during my PhD but also in my studies.

Finally, I would like to say a big thank you to **my family** for their support in all these years at ETH, danka eu viel mol! And last but not least, my friends from famous Rheintal, thanks for the fun times and support, it's always a pleasure and fun to spend time with you.

## Curriculum Vitae

### Stephan Durot

Schürbungert 14  
8057 Zürich  
+41 79 441 66 75  
stephan.durot@hotmail.com  
04. May 1992  
Nationality: Swiss



### Education

---

- 2019 - Present      **ETH Zürich, Doctor of Science**
- PhD thesis “A systematic analysis of the molecular patterns that define endothelial identities and states” in Prof. Nicola Zamboni’s group at the Institute of Molecular Systems Biology.
- 2017 - 2019      **ETH Zürich, Master of Science in Biology, Major in Systems Biology**
- Master thesis: “Investigation of metabolic adaptive responses in quiescent and proliferating cancer cells upon drug treatment” in Prof. Uwe Sauer’s group at the Institute of Molecular Systems Biology.
- 2012 - 2016      **ETH Zürich, Bachelor of Science in Biology**
- 2011 - 2012      **ISME Sargans, Passarelle**
- 2007 - 2010      **Microsynth AG, Apprenticeship as biology laboratory assistant**

### Working experience

---

- 2019 - Present      **ETH Zürich, Institute of Molecular Systems Biology**
- Research scientist
- 2014 - 2018      **SFS intec**
- Vibratory finishing operator during semester breaks
- 2007 - 2011      **Microsynth AG**
- Biology laboratory assistant

## Further engagements and volunteering

---

2020 - 2022	<b>ETH Zürich, Institute of Molecular Systems Biology</b> , PhD representative
2018	<b>ETH Zürich</b> , teaching assistant of 1 <sup>st</sup> year biology course
2016 - 2017	<b>Spitalregion RWS</b> , civil service in quality management and communication
2015 - 2019	<b>Rheintal Duathlon</b> , organizing committee member
2013 - 2015	<b>VeBiS, biology student association of ETH Zürich</b> , controller

## Conference attendances

---

June 2023	Poster presentation at “Systems Biology of Human Diseases”
February 2023	Poster presentation at the Life Sciences Switzerland (LS2) Annual Meeting
September 2021	Poster presentation at “EMBO/EMBL Symposium: Multiomics to Mechanisms: Challenges in Data Integration”

## Awards

---

February 2023	FEBS Letters poster prize at the LS2 Annual Meeting
---------------	---

## Publications

---

Jeremiah Bernier-Latmani, Cristina Mauri, Rachel Marcone, François Renevey, **Stephan Durot**, Liqun He, Michael Vanlandewijck, et al. “ADAMTS18+ Villus Tip Telocytes Maintain a Polarized VEGFA Signaling Domain and Fenestrations in Nutrient-Absorbing Intestinal Blood Vessels.” *Nature Communications* 13, no. 1 (2022): 1–17.

Sarah Cherkaoui, **Stephan Durot**, Jenna Bradley, Susan Critchlow, Sebastien Dubuis, Mauro Miguel Masiero, Rebekka Wegmann, et al. “A Functional Analysis of 180 Cancer Cell Lines Reveals Conserved Intrinsic Metabolic Programs.” *Molecular Systems Biology* 18, no. 11 (2022): 1–15.

Alejandra González-Loyola, Jeremiah Bernier-Latmani, Irena Roci, Tania Wyss, Jakob Langer, **Stephan Durot**, Olivia Munoz, et al. “C-MAF Coordinates Enterocyte Zonation and Nutrient Uptake Transcriptional Programs.” *Journal of Experimental Medicine* 219, no. 12 (2022).

Alejandra González-Loyola, Esther Bovay, Jaeryung Kim, Tania Wyss Lozano, Amélie Sabine, Francois Renevey, Silvia Arroz-Madeira, Alexis Rapin, Tomasz P. Wypych, Giorgia Rota, **Stephan Durot**, et al. “FOXC2 Controls Adult Lymphatic Endothelial Specialization, Function, and Gut Lymphatic Barrier Preventing Multiorgan Failure.” *Science Advances* 7, no. 29 (2021).

Duncan Holbrook-Smith, **Stephan Durot**, and Uwe Sauer. “High-throughput Metabolomics Predicts Drug–Target Relationships for Eukaryotic Proteins.” *Molecular Systems Biology* 18, no. 2 (2022): 1–16.